General Disclaimer

One or more of the Following Statements may affect this Document

- This document has been reproduced from the best copy furnished by the organizational source. It is being released in the interest of making available as much information as possible.

- This document may contain data, which exceeds the sheet parameters. It was furnished in this condition by the organizational source and is the best copy available.

- This document may contain tone-on-tone or color graphs, charts and/or pictures, which have been reproduced in black and white.

- This document is paginated as submitted by the original source.

- Portions of this document are not fully legible due to the historical nature of some of the material. However, it is the best reproduction available from the original submission.

PURDUE UNIVERSITY

Purdue Research Foundation

Lafayette, Indiana

School of Mechanical Engineering

Heat Transfer Laboratory

Improved Fluid Dynamics Similarity, Analysis and Verification

Final Report - Part II

EFFECTS OF LONGITUDINAL VIBRATION ON DISCHARGE OF LIQUIDS FROM PROPELLANT TANKS

by

E. R. F. Winter and R. J. Schoenhals

Improved Fluid Dynamics Similarity.
Analysis and Verification

Final Report - Part II

EFFECTS OF LONGITUDINAL VIBRATION ON DISCHARGE OF LIQUIDS FROM PROPELLANT TANKS

Submitted by

Heat Transfer Laboratory
School of Mechanical Engineering
Purdue University
Lafayette, Indiana

to

NATIONAL AERONAUTICS AND SPACE ADMINISTRATION
George C. Marshall Space Flight Center
Applied Mechanical Research Branch
Propulsion Division
Propulsion and Vehicle Engineering Laboratory
Huntsville, Alabama

* Period Covered: June 29, 1965 - June 28, 1968

Principal Investigators: E. R. F. Winter and R. J. Schoenhals

Contracting Officer's Representatives: Hugh M. Campbell
William E. Dickson
Carl G. Fritz

Contract Number: NAS 8-20222
Control Number: DCN 1-5-52-01195-01 (IF) & S1 (IF)

Authors: R. W. Griebe
E. I. Griggs
H. Y. Pak
J. A. Pesar
R. J. Schoenhals
L. Wen
E. R. F. Winter
A. C. Wong

October 1968

TABLE OF CONTENTS

Nomenclature

C_c	Contraction coefficient
C_D	Discharge coefficient
D	Container diameter
d	Outlet diameter
F, G	Functions
f	Friction factor
g	Gravitational field
h	Total liquid height
h_L	Head loss
K	Entrance coefficient
L	Tube length
$\dot{m}$	Mass flow rate
P_1, P_2	Pressures, Fig. 1 and 2
ΔP	Pressure drop, $(P_1 - P_2)$
t	Time
V	Discharge velocity
y	Liquid height
β	$\sqrt{(D/d)^4 - 1}$
ν	Kinematic viscosity
ρ	Liquid density

Introduction

Full scale testing of large liquid propellant and oxidizer supply systems can be time consuming, expensive, and in some cases inconvenient. For these reasons it is frequently appropriate that scaled down laboratory models be considered. It might be desirable, for example, to ascertain the performance of a large system in advance of its construction in order to evaluate the soundness of a particular design or to provide concrete evidence of the need for engineering changes if laboratory tests on a model should indicate weaknesses in a tentative design. Where a large scale system has already been built, the ability to predict overall performance is not as important. However, in this situation certain unexpected features of operational behavior in the large system may become evident. If they do, then further study may be required to establish confidence in the existing system or to determine the necessary changes which will eliminate any of these features which are found to be undesirable. In cases such as this it may be more convenient, realistic, and economical to simulate the actual system with a laboratory apparatus of smaller size. There are some occasions when only a portion of a system requires intensive study, and a scaled down laboratory model of an individual system component may allow large numbers of experimental measurements to be obtained rapidly and easily.

In order to exactly duplicate the behavior of a large system with a corresponding laboratory model, it is required that complete similarity be achieved. This can sometimes be accomplished if fairly simple processes are involved. However, the task of attaining complete similarity becomes increasingly difficult when a number of physical phenomena all

Effects of Longitudinal Vibration on Discharge of Liquids from Propellant Tanks[1]

ABSTRACT

A study of liquid discharge from a cylindrical container exposed to longitudinal vibration is described. The experimental results presented reveal the existence of a flow retardation effect due to vibration. The magnitude of this retardation increases with vibrational acceleration level and decreases with both the vibration frequency and with the outlet tube length. Photographs showing some of the more interesting visual observations are given. Possible causes of the flow retardation effects are discussed. These are based on analytically derived results and on evidence provided by the photographs.

---

[1] This section of part II of the final report was presented as a paper by R. J. Schoenhals, E. R. F. Winter, and E. I. Griggs at the 1967 Heat Transfer and Fluid Mechanics Institute, and published in the Proceedings of the 1967 Heat Transfer and Fluid Mechanics Institute, Stanford University Press, 1967, Stanford, California.

occur simultaneously and interact with each other within a single system. In the less complex situations it is important that the similation be made essentially exact in order to maximize the usefulness of the laboratory data. For the more complex cases, where exact simulation may not be attainable, it is important to evaluate the limitations of the laboratory simulation and to formulate a laboratory program which minimizes these limitations as much as possible.

It is clear that the procedures outlined above can be carried out effectively only if the similarity parameters have been obtained and if the relationships between them have been roughly established, perhaps by means of approximate analytical techniques or from previously obtained experimental measurements. The second point is very important if exact similarity cannot be achieved. In this situation similarity should be maintained with respect to those parameters which are dominant, and should be sacrificed only with respect to those parameters which are known to have a minor effect within the range of operation considered. The present investigation was undertaken in order to provide:

1. A better understanding of the similarity relationships associated with some of the fluid dynamics phenomena occurring in propellant and oxidizer supply systems.
2. A basis for obtaining a given amount of needed information from a minimum of similarity experiments conducted with scaled laboratory models.
3. A basis for obtaining maximum information from a given number of similarity experiments conducted with scaled laboratory models.

4. A basis for suggesting improved techniques that may facilitate future similarity investigations whose goals are related to any of the three items above.

This paper describes results obtained from a similarity study of gravity and pressure driven discharge of liquids from propellant supply containers. The similarity parameters derived should be applicable to systems of complex geometry (Fig. 1). For purposes of simplicity, however, the experimental and analytical results were obtained for a simpler geometry (Fig. 2) in order to verify the significance and importance of the similarity parameters, and to establish the validity and limitations associated with the approximate analytical solutions. The experimental and analytical results make it possible to estimate the performance of the more complex systems such as that shown in Fig. 1. Only single phase fluid flow conditions are considered.

Physical Effects Associated With Single Phase Discharge

In this section the major physical effects associated with single phase discharge are discussed briefly, and the problem definition is given for the situations illustrated in Figs. 1 and 2. Forces act on the fluid to produce fluid acceleration during the discharge process. The various kinds of forces, and the corresponding two types of fluid acceleration that result from the action of these forces, are indicated in Table 1.

The boundary forces (forces perpendicular to the walls) are sufficient to prevent the fluid from moving normal to the boundaries, the confining structure being considered rigid. Gravity and the external

pressure drop (from the top to the bottom of the fluid column) contribute to downward acceleration of the fluid column, while viscous forces impede this acceleration. Convective acceleration is associated with the change in velocity of a fluid particle as it travels from a region of one velocity into a region having a different velocity. Thus, convective acceleration can be produced even if the flow is steady. Local acceleration of the fluid is associated with the time varying, or transient, condition of the flow. This acceleration, at any point in the system, is equal to the time rate of change of velocity at that point. The two acceleration contributions, when added together at any particular point in the system, give the actual acceleration of the fluid particle passing through that point at a particular instant of time.

In general, the pressure drop across the system, (P_1-P_2), may vary with time. The effective gravitational field, g, may also vary in accordance with changes in vehicle thrust. If local pressures are low enough cavitation may occur. Surface tension effects may conceivably be important if the system dimensions are small enough. Also, in practical applications the valve setting may vary with time. This, however, amounts to a time varying change in the system geometry and is beyond the scope of this paper. In order to keep the discussion brief, the pressure drop, ΔP, and the gravitational field, g, are taken as constants. Surface tension and variable valve settings are omitted. Phenomena associated with cavitation are not considered. It should be mentioned at this point that similarity studies of other phenomena occurring in propellant supply systems have been reported by a number of investigators. For example, Nein and Thompson [2] have presented similarity results from a study of

cryogenic propellant tank pressurization in which heat and mass transfer were considered.

Similarity Parameters

Application of dimensional analysis to the single phase situation (Figs. 1 and 2) gives rise to the following dimensionless parameters:

$\frac{\dot{m}}{\rho\left(\frac{\pi d^2}{4}\right)\sqrt{2gh}}$, dimensionless mass flow rate

$\frac{t}{\sqrt{2h/g}}$, dimensionless time

$\frac{\Delta P/\rho g}{h}$, ratio of pressure head to initial hydrostatic head

$\frac{d\sqrt{2gh}}{\nu}$, a characteristic Reynolds number

Consideration of these quantities, together with the various combinations of system dimensions (Figs. 1 and 2), results in

$$\frac{\dot{m}}{\rho\left(\frac{\pi d^2}{4}\right)\sqrt{2gh}} = F\left[\frac{t}{\sqrt{2h/g}}, \frac{\Delta P/\rho g}{h}, \frac{d\sqrt{2gh}}{\nu}, \frac{h}{d}, \frac{D}{d}, \frac{L}{d}\right] \qquad (1)$$

This result can also be expressed in terms of the instantaneous liquid height, y, rather than the mass discharge rate, $\dot{m}$, provided that the liquid surface remains planar. This leads to

$$\frac{y}{h} = G\left[\frac{t}{\sqrt{2h/g}}, \frac{\Delta P/\rho g}{h}, \frac{d\sqrt{2gh}}{\nu}, \frac{h}{d}, \frac{D}{d}, \frac{L}{d}\right] \qquad (2)$$

Notice that parameter, $\Delta P/\rho gh$, gives the driving effect due to the external pressure drop relative to that produced by gravity. This similarity parameter, therefore, provides a comparison of two of four types of forces indicated in Table 1. Similarly, the reciprocal of $d\sqrt{2gh}/\nu$ provides a measure of the impeding viscous forces relative to the gravity forces.

Experimental Results in Terms of Similarity Parameters

Discharge experiments were carried out using two different containers having inside diameters of 9" and 18" respectively. The containers were designed so that discharge tubes of various diameters and lengths could be attached. Orifice plates with several different opening diameters were also provided in order to simulate conditions corresponding to discharge tubes having very short lengths. Various external pressure drops were used. This was accomplished by increasing the container air supply pressure, P_1, above atmospheric pressure or by reducing the discharge pressure, P_2, below atmospheric pressure, or by combinations of both. Some of the tests were conducted with no external pressure drop, for the case where $P_1=P_2$. With the arrangement indicated above, all of the dimensionless parameters could be varied one at a time.

Both water and glycerin were used as test fluids so that a large range of Reynolds numbers could be conveniently covered. The containers were made of plexiglass so that the liquid level was clearly visible. Fluid height measurements were obtained by both visual and photographic methods. The visual measurements were made by attaching graduated paper strips to the exterior of the container wall. The zero coordinate was

set at the initial position of the fluid surface, and surface heights were marked at fixed increments of time. This procedure gave a permanent record of the fluid surface height decrease as a function of time.

For the more rapid discharge processes a movie camera was used. The camera was operated at a fixed frame rate. At the exact instant the discharge process was initiated the lighting system was actuated, thus marking the initial frame at which the discharge process was started. Fluid height as a function of time was obtained from the film. This was done by counting the number of frames which were exposed during the period from the initiation of discharge until a particular fluid height of interest was reached. The number of frames exposed was then converted to elapsed time.

Typical experimental results which illustrate the qualitative effects of the various similarity parameters are shown in Fig. 3. Increases in $\Delta P/\rho gh$ produce corresponding increases in the rate of discharge (Fig. 3A). A similar trend occurs with increasing $d\sqrt{2gh}/\nu$ (Fig. 3B), an effect which is associated with a relative reduction in the influence of fluid viscosity. Variations in h/d were found to have a lesser effect within the operating ranges investigated (Fig. 3C). Decreasing the discharge outlet diameter relative to the container diameter (increasing D/d) produces a retardation in the discharge rate (Fig. 3D). Increasing the discharge tube length relative to its diameter (increasing L/d) also produces a retarding influence due to an increase in fluid friction (Fig. 3E). The above remarks and the typical results shown in Fig. 3 briefly summarize the qualitative effects associated with variations in the several similarity parameters. It is reasonable to assume that when (h-L)/d is small, i.e., of the order

of unity or less, the close proximity of the liquid surface to the container exit strongly influences the streamline pattern. In this range variations in h/d affect the discharge rate significantly (see Fig. 3C). For the more practical operating ranges investigated, which are associated with large values of (h-L)/d, variations in h/d produce no significant effect on the discharge rate.

Analysis and Experimental Verification

A number of analyses were carried out which vary in complexity, in the geometry associated with the system being studied, and in the physical effects accounted for. The simplest of these analyses involved application of Bernoulli's equation to an assumed ideal fluid in the absence of an external pressure drop. This kind of physical model accounts for boundary forces, gravity forces, and convective fluid acceleration. But it fails to account for forces due to fluid viscosity and system pressure drop as well as fluid inertia associated with local acceleration (see Table 1). The results obtained, for both liquid height and for mass flow rate, are

$$\sqrt{1 - \left(\frac{d}{D}\right)^4}\left[\frac{\dot{m}}{\rho\left(\frac{\pi d^2}{4}\right)\sqrt{2gh}}\right] = 1 - \left(\frac{1}{\beta}\frac{t}{\sqrt{2h/g}}\right) \qquad (3)$$

$$\frac{Y}{h} = \left[1 - \left(\frac{1}{\beta}\frac{t}{\sqrt{2h/g}}\right)\right]^2 \qquad (4)$$

Since β is defined as $\sqrt{(D/d)^4 - 1}$, the above expressions are consistent with the similarity parameters previously given. Due to the conditions assumed in the derivation, however, $\Delta P/\rho gh$ and $d\sqrt{2gh}/\nu$ do not appear.

L/d and h/d also have no effect on the results according to this highly simplified method of prediction.

The additional physical effects in Table 1, not accounted for by the physical model described above, were introduced one at a time to obtain predictions of the relative influence of each of these effects. In reality the local fluid acceleration dominates over convective acceleration during the initial portion of the discharge since the discharge rate is zero at the very start of the process. During this period the inertia associated with the fluid local acceleration produces a retarding effect. The time duration of this period is small, however, and its effect on the overall discharge process is very slight unless the discharge diameter becomes sizeable relative to the container diameter. This is illustrated in Fig. 4, which contains results determined by incorporating the local acceleration effect into the simplified physical model described above. With L/d=0, the corresponding equation of motion for the fluid, from which these results were calculated, is

$$\frac{d^2\left(\frac{y}{h}\right)}{d\left(\frac{1}{\beta}\frac{t}{\sqrt{2h/g}}\right)^2} + 2\beta^2\left\{1 - \frac{1}{4\left(\frac{y}{h}\right)}\left[\frac{d\left(\frac{y}{h}\right)}{d\left(\frac{1}{\beta}\frac{t}{\sqrt{2h/g}}\right)}\right]^2\right\} = 0 \qquad (5)$$

Additional analytical predictions were obtained for the general case of discharge through a tube of any length which accounted for local fluid acceleration as well as for all of the other physical effects listed in Table 1. Typical results from these more extensive analyses are illustrated in Fig. 5.

Experimental data and analytical evidence of the type given in

Figs. 4 and 5 indicate that errors in prediction of discharge rates resulting from omission of the fluid local acceleration are very small for system geometries typically used in practice (large values of D/d, which lead to correspondingly large values of β). If local acceleration is omitted from consideration, the resulting physical model is called "quasi-steady" (see the lowest curves in Figs. 4 and 5). Hence, an analysis based on such a quasi-steady model, and incorporating all of the remaining physical effects listed in Table 1, was carried out. In this analysis a discharge coefficient C_D, was utilized which allows for the possibility of fluid contraction at the exit in addition to accounting for the influence of viscosity. The discharge coefficient is the ratio of the actual discharge rate to the idealized rate predicted for the same situation, but with viscous and contraction effects omitted. The calculation of the idealized rate accounts for both gravitational and pressure driving effects. Thus, the following relations are obtained:

$$\dot{m} = C_D \frac{\rho A}{\beta} \sqrt{2g(y + \Delta P/\rho g)} \tag{6}$$

$$\dot{m} = C_c \frac{\rho A}{\beta} \sqrt{2g(y + \Delta P/\rho g - h_L)} \tag{7}$$

where C_c is the contraction coefficient and h_L is the head loss due to viscosity, $(K + fL/d)\ V^2/2g$. K is the loss coefficient for the discharge tube entrance and f is the Darcy-Weisbach friction factor for the tube.

$$C_D = \frac{C_c}{\sqrt{1 + \left[\frac{K + fL/d}{1 - (d/D)^4}\right] C_c^2}} \tag{8}$$

For orifice type discharge (L/d very small), Vennard [3] has

presented an empirical curve giving C_D in terms of a Reynolds number which was modified to $(d\sqrt{2gh}/\nu)\sqrt{y/h + \Delta P/\rho gh}$ for application to the present problem. In addition, Vennard suggests nominal C_D values of 0.61 when contraction occurs and 0.80 for very short tubes when contraction is absent. Sabersky and Acosta [4] give the corresponding nominal values of 0.60 and 0.82 respectively. For discharge through a tube ($L/d>>1$), the fluid normally fills the tube at its outlet, and $C_c=1$ in Equation (8). Streeter [5] gives a nominal value of 0.5 for K, and f can be obtained from the Moody Chart [5]. For very short tubes, fL/d is negligible compared with K in Equation (8) which yields $C_D=0.82$ for $C_c=1$, $K=0.5$, and $d/D<<1$. Thus, the value of C_D obtained from Equation (8) for very short tubes is in good agreement with the corresponding nominal values recommended by Vennard [3] and by Sabersky and Acosta[4].

Since the friction factor, f, is a function of the instantaneous tube flow Reynolds number, which is dependent on the discharge rate given by Equation (1), it follows that f should in reality depend on all of the similarity parameters appearing on the right hand side of Equation (1). It can be shown by dimensional analysis (and it follows partially from some of the preceding discussions) that K, C_c, and C_D are all tentative functions of these same similarity parameters. Thus, any analysis which incorporates the use of the discharge coefficient is implicitly in agreement with the similarity relationships given by Equations (1) and (2).

Although information for f is available from the Moody Chart [5], further details concerning the influence of the various similarity parameters on the remaining quantities were not found in the literature. For example, as the liquid surface approaches the container exit there is an

alteration of the streamline pattern in this region. It is expected that this would have an influence on C_c and C_D for orifice type discharge as well as on K for tube type discharge. Thus, h/d should be important in the range where (h-L)/d is small. A similar argument suggests that D/d should have an effect on these quantities when D/d is a small number. Similarity information on all of the desired effects such as these apparently is not available.

In many actual situations where h/d and D/d are quite sizeable, effects such as those described above are very small. Thus, the use of the nominal values previously discussed does not produce a severe practical limitation. This was a procedure followed in the present research for prediction purposes. C_D was taken to be close to 0.8 for orifice type discharge and K was taken as 0.5 for discharge through a tube. C_c was normally assumed to be unity while f was obtained for smooth tubes from the Moody Chart [5]. With these values, C_D was calculated from Equation (8) for discharge through a tube. This required estimating the order of magnitude of the discharge rate in advance for the purpose of calculating Reynolds numbers to be applied to the abscissa of the Moody Chart. Since the instantaneous tube flow Reynolds number varies with time during the discharge process, it follows that f, and hence C_D, vary also. In most of the situations for which prediction was attempted, the variations of f and C_D were found to be quite small over the major protion of the discharge period. This made it possible to estimate the maximum discharge rate expected, to obtain from this rate a Reynolds number, and then use the Moody Chart to obtain an average f value for the entire process. This value, in turn, was used to obtain a corresponding average value for

C_D from Equation (8). Equation (6) was then employed to obtain results similar to those given by Equations (3) and (4). These relations, derived with C_D assumed constant over the discharge period, are

$$\sqrt{1 - \left(\frac{d}{D}\right)^4}\left[\frac{\dot{m}}{\rho\left(\frac{\pi d^2}{4}\right)\sqrt{2gh}}\right] = C_D\left[\sqrt{1 + \frac{\Delta P}{\rho gh}} - \left(\frac{C_D}{\beta}\frac{t}{\sqrt{2h/g}}\right)\right] \tag{9}$$

$$\frac{Y}{h} = 1 - 2\sqrt{1 + \frac{\Delta P}{\rho gh}}\left(\frac{C_D}{\beta}\frac{t}{\sqrt{2h/g}}\right) + \left(\frac{C_D}{\beta}\frac{t}{\sqrt{2h/g}}\right)^2 \tag{10}$$

These expressions, when utilized with C_D values obtained as described above, provided good predictions of experimentally obtained discharge results. Typical comparisons of experimental data with these analytical predictions are given in Figs. 6 and 7. Notice that Equations (9) and (10) explicitly contain all of the similarity parameters appearing in Equations (1) and (2) except for L/d and h/d. However, C_D is related to L/d by Equation (8), and is usually a weak function of h/d unless (h-L)/d is very small. Within this approximation, then, Equations (9) and (10) are consistent with Equations (1) and (2).

Resume´

In this paper results obtained from dimensional analysis, from experiments, and from analytical techniques have been correlated for single phase discharge of liquids from containers. It is obvious from these results that good predictions of actual system performance can be obtained using straightforward procedures. These analytical predictions could be

extended over wider ranges of the similarity parameters than were verified experimentally in the present study. However, the accuracy of such predictions would be in doubt unless further experiments covering these extended ranges were carried out. In particular, the variation of the discharge coefficient needs to be investigated over a broader spectrum of system geometries and transient flow conditions. Efforts along these lines are currently in progress and will be reported at a later date. Attempts will be made to develop convenient engineering correlations, in terms of the similarity parameters, which will predict discharge behavior over extremely large ranges of these dimensionless groups for single phase flow.

Since cavitation, causing two phase flow, and some degree of vortex action were both observed during a few experiments, investigations were initiated in order to study these phenomena. The onset of cavitation was predicted analytically in terms of the appropriate similarity parameters. This prediction was verified experimentally for a particular system geometry. The investigations of cavitation and vortex flow are being continued.

References

1. Winter, E. R. F. and Schoenhals, R. J., "Improved Fluid Dynamics Similarity, Analysis and Verification." First Annual Report, Contract NAS 8-20222, George C. Marshall Space Flight Center, Applied Mechanical Research Branch, Propulsion Division, Propulsion and Vehicle Engineering Laboratory, Huntsville, Alabama, August 25, 1966.

2. Nein, M. E. and Thompson, J. F., Jr., "Experimental and Analytical Studies of Cryogenic Propellant Tank Pressurization," Proceedings of the Conference on Propellant Tank Pressurization and Stratification, Volume 1, NASA, George C. Marshall Space Flight Center, Huntsville, Alabama, January 20 and 21, 1965, pages 29-54.

3. Vennard, J. K., "Elementary Fluid Mechanics," Fourth Edition, John Wiley & Sons, Inc., New York, 1961, pages 426 and 427.

4. Sabersky, R. H. and Acosta, A. J., "Fluid Flow, A First Course in Fluid Mechanics," McMillan Co., New York, 1964, page 86.

5. Streeter, V. L., "Fluid Mechanics," Second Edition, McGraw-Hill Book Co., 1958, pages 183 and 188.

List of Figures

Figure No.

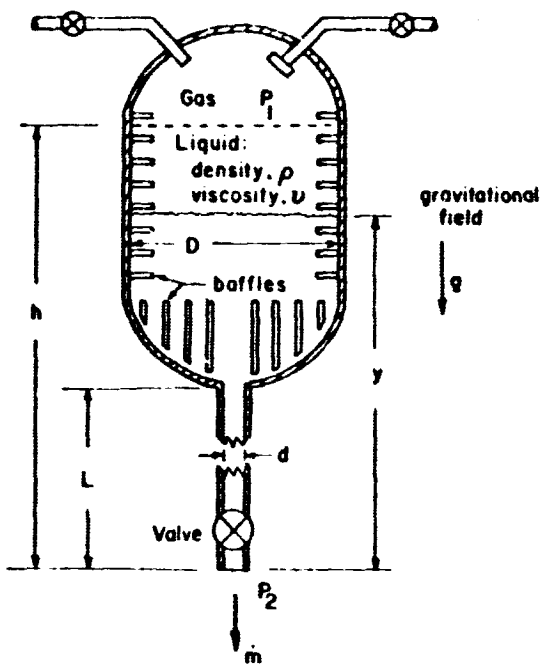

FIG. 1 ILLUSTRATION OF A LIQUID DISCHARGE SYSTEM

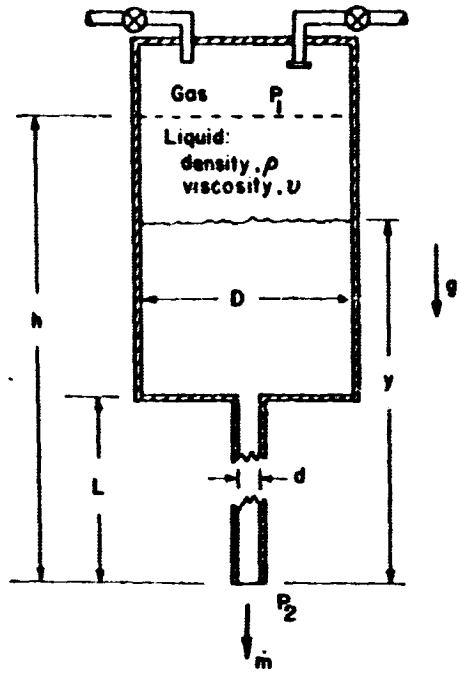

FIG. 2 SIMPLIFIED GEOMETRY FOR ANALYTICAL AND EXPERIMENTAL STUDIES

TABLE I. PHYSICAL EFFECTS

Forces		Fluid Acceleration
Boundary Forces		Convective Acceleration
Gravity Forces	—Produce→	
Forces due to External Pressure Drop		Local Acceleration
Viscous Forces		

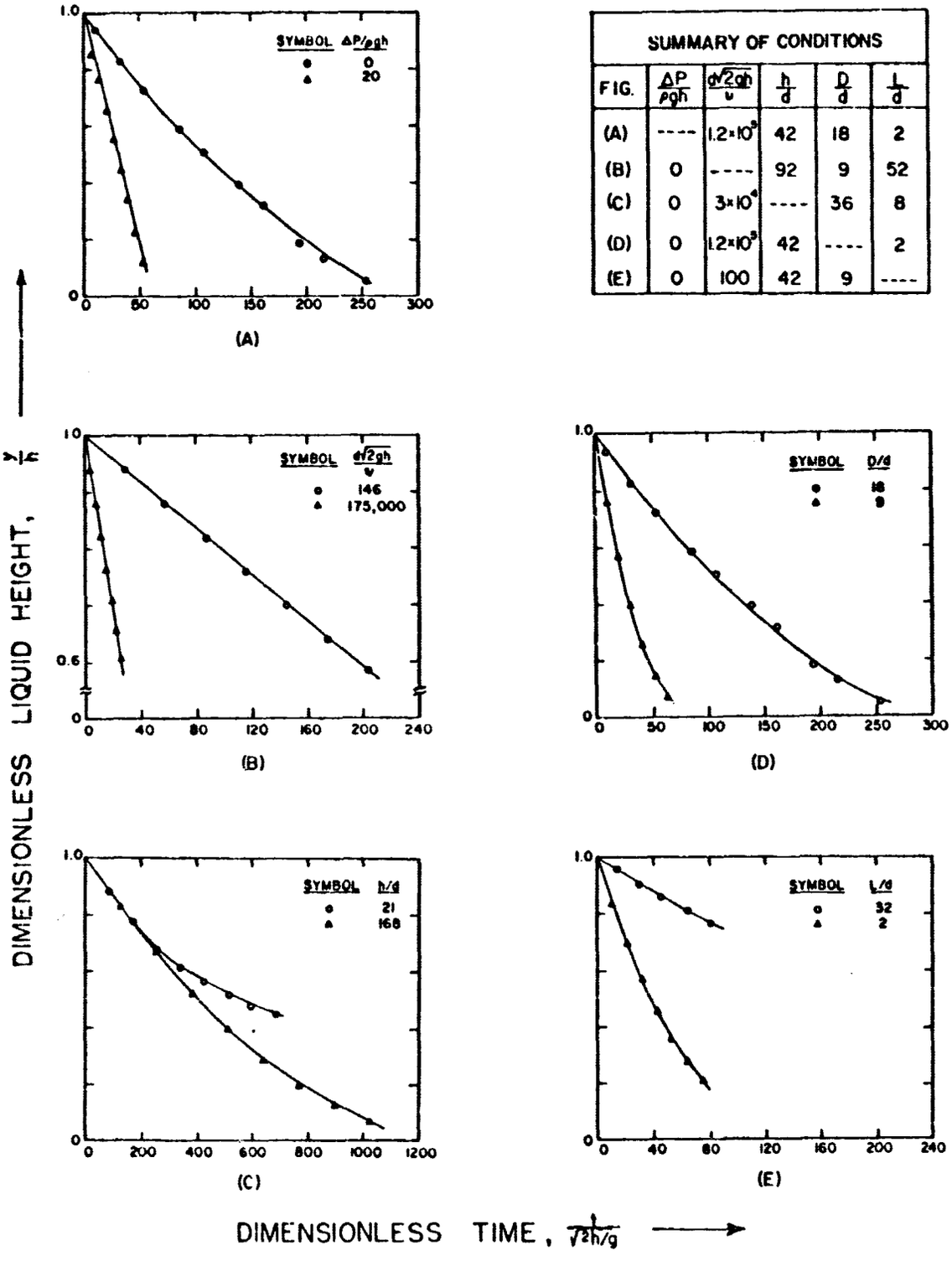

SUMMARY OF CONDITIONS

FIG.	$\frac{\Delta P}{\rho g h}$	$\frac{d\sqrt{2gh}}{\nu}$	$\frac{h}{d}$	$\frac{D}{d}$	$\frac{L}{d}$
(A)	----	1.2×10^5	42	18	2
(B)	0	----	92	9	52
(C)	0	3×10^4	----	36	8
(D)	0	1.2×10^5	42	----	2
(E)	0	100	42	9	----

FIG. 3 TYPICAL EXPERIMENTAL RESULTS IN TERMS OF SIMILARITY PARAMETERS

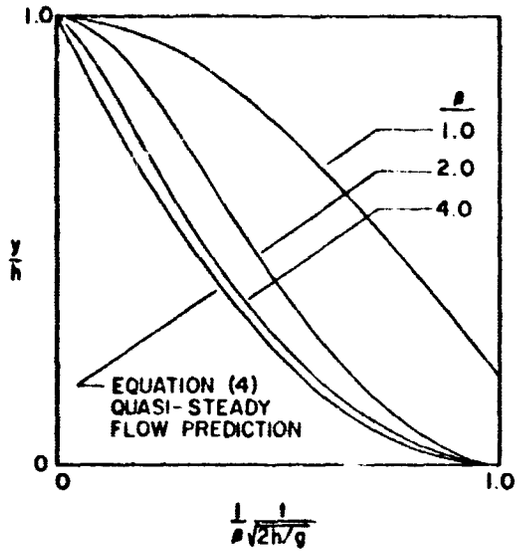

FIG. 4 PREDICTIONS OF LIQUID HEIGHT FOR L/D = 0 WHICH ACCOUNT FOR FLUID LOCAL ACCELERATION, BUT OMIT EFFECTS OF EXTERNAL PRESSURE DROP AND FLUID VISCOSITY.

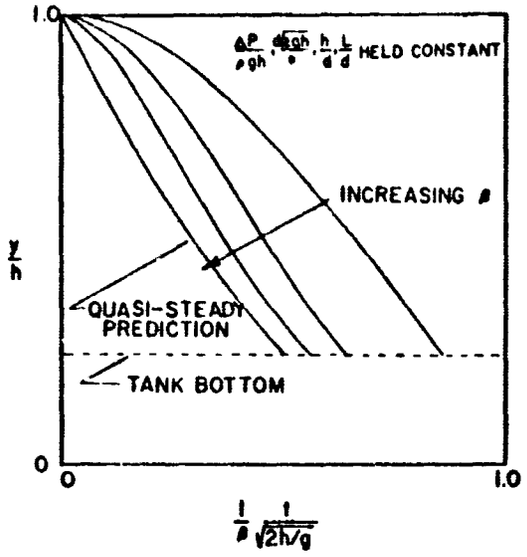

FIG. 5 TYPICAL PREDICTIONS OF LIQUID HEIGHT WHICH INCLUDE ALL PHYSICAL EFFECTS LISTED IN TABLE I.

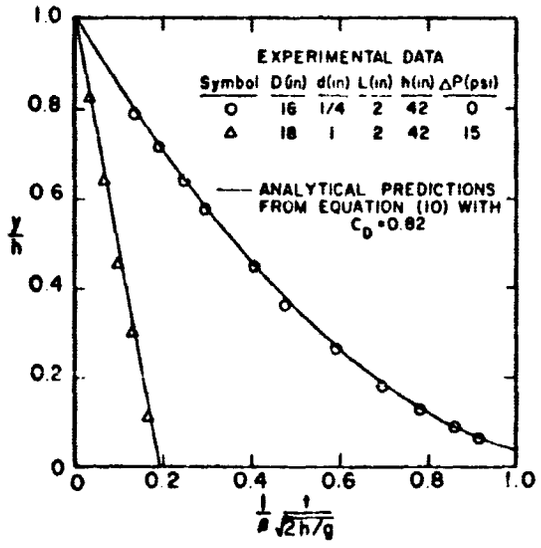

FIG. 6 COMPARISON OF EXPERIMENTAL MEASUREMENTS WITH ANALYTICAL PREDICTIONS FOR SHORT DISCHARGE TUBES.

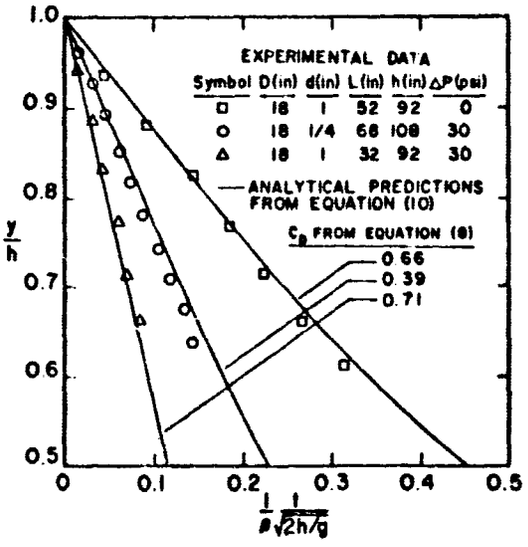

FIG. 7 COMPARISON OF EXPERIMENTAL MEASUREMENTS WITH ANALYTICAL PREDICTIONS FOR LONG DISCHARGE TUBES.

INTRODUCTION

Part II of this Final Report on "Improved Fluid Dynamics Similarity, Analysis and Verification" is entitled EFFECTS OF LONGITUDINAL VIBRATION ON DISCHARGE OF LIQUIDS FROM PROPELLANT TANKS. It consists of two publications and a Master's thesis. Because of this there is a separate page numbering system for each section of the report. Each section is self-contained and has its own Table of Contents and all of the other necessary information.

In the first section a study of gravity and pressure driven discharge of liquids from propellant tanks is described. In particular, the similarity parameters describing such discharge processes were obtained by means of dimensional analysis. Some analytical results, incorporating the various physical effects of importance, are presented graphically in terms of these similarity parameters. Experimental data are also plotted graphically in order to verify the similarity parameters, to indicate the operating ranges for which these parameters are important, and to evaluate the accuracy of the analytical results. This investigation was the starting point for study of the influence of vibration on discharge of liquids from propellant tanks.

The influence of vibration was specifically studied in a

subsequent investigation which resulted in a publication in the Proceedings of the 1967 Heat Transfer and Fluid Mechanics Institute, and that publication forms the second section of this report. It treats discharge of a liquid from a cylindrical container which is exposed to longitudinal vibration. The experimental results presented reveal the existence of a flow retardation effect due to vibration. The magnitude of this retardation increases with vibrational acceleration level and decreases with both the vibration frequency and with the outlet tube length. Photographs showing some of the more interesting visual observations are given. Possible causes of the flow retardation effects are discussed.

Some of the questions raised in the second section and left unanswered were subsequently studied in a research project leading to an MSME thesis, which forms the third section of this report. Of primary interest was the retardation of flow from discharge tanks subjected to vibratory motion. Comparisons of analytical and experimental data exhibit fair agreement in the low frequency range. An explanation is given for the flow retardation based on the decreased average pressure measured at the inlet to the discharge tube.

A Similarity Study of Gravity and Pressure Driven Discharge of Liquids from Propellant Tanks[1]

ABSTRACT

A study of gravity and pressure driven discharge of liquids from propellant tanks is described. Similarity parameters obtained by means of dimensional analysis are given. Analytical results, incorporating the various physical effects of importance, are presented graphically in terms of these similarity parameters. Experimental data are also plotted graphically in order to verify the similarity parameters, to indicate the operating ranges for which these parameters are important, and to evaluate the accuracy of the analytical results. The results presented can be used for making engineering determinations of propellant supply system performance.

---

[1] This section of part II of the final report was presented as a paper by E. R. F. Winter and R. J. Schoenhals at a meeting of the American Astronautical Society in Huntsville, Alabama, and published in the Proceedings of the Southeastern Symposium on Missiles and Aerospace Vehicles Sciences, vol. I, December 1966, Huntsville, Alabama, pages 48-1 to 48-13.

TABLE OF CONTENTS

NOMENCLATURE

C	wave velocity
C_D	discharge coefficient
D	container diameter
d	outlet diameter
F_1, F_2, F_3	functions
f	vibration frequency
G	acceleration level, g_v/g
g	effective gravitational field
g_v	vibrational acceleration amplitude
h	initial liquid height
L	discharge tube length
$\dot{m}$	mass flow rate
P_o	oscillating component of pressure
P_1	ullage pressure
P_2	outlet pressure
ΔP	pressure drop, $(P_1 - P_2)$
t	time
y	liquid height
β	$\sqrt{(D/d)^4 - 1}$
ν	kinematic viscosity
ρ	liquid density
ω	angular frequency, $2\pi f$

INTRODUCTION

The influence of structural vibration on fluid flow behavior is of considerable interest in liquid propellant rocket technology since some of the existing high thrust systems are known to undergo severe vibration during flight (1). Such vibration can cause considerable surface sloshing in the fuel tanks of liquid propellant rockets, and these phenomena have been extensively investigated (2, 3). In certain cases self excited longitudinal oscillations have been attributed to strong periodic variations in engine thrust which are caused by the combined dynamic interaction of the engine, structure, and propellant supply system (1, 4). In view of the importance of these problems it appears desirable to obtain information concerning the possible effects that vibration may have on liquid propellant and oxidizer supply rates.

This paper describes results obtained from a study of liquid discharge from a cylindrical container subjected to longitudinal vibration. Figure 1 shows the system under discussion. The liquid surface is initially at height, h, and transient discharge of the liquid through the outlet occurs. At any given instant of time during the transient period the amount of liquid remaining in

the tank is given by the liquid surface height, y. The effective gravitational field, g, includes a contribution due to the steady component of vehicle acceleration for any situation where the simplified model (Figure 1) is used to simulate an actual propellant supply system during flight. In this study the effective gravitational field (earth's gravity only), the ullage pressure (P_1), and the outlet pressure (P_2) were each maintained constant throughout the transient discharge process.

An experimental and analytical investigation has previously been carried out for the system shown in Figure 1 without consideration of vibratory effects (5). For an incompressible liquid and a rigid confining structure in the absence of vibration, dimensional analysis gives the dimensionless mass flow rate in terms of similarity parameters:

$$\frac{\dot{m}}{\rho\left(\frac{\pi d^2}{4}\right)\sqrt{2gh}} = F_1\left[\frac{t}{\sqrt{2h/g}}, \frac{\Delta P/\rho g}{h}, \frac{d\sqrt{2gh}}{\nu}, \frac{h}{d}, \frac{D}{d}, \frac{L}{d}\right] \qquad (1)$$

This result can also be expressed in terms of the instantaneous liquid height, y, rather than the mass discharge rate, $\dot{m}$, provided that the liquid surface remains planar. This leads to

$$\frac{Y}{h} = F_2\left[\frac{t}{\sqrt{2h/g}}, \frac{\Delta P/\rho g}{h}, \frac{d\sqrt{2gh}}{\nu}, \frac{h}{d}, \frac{D}{d}, \frac{L}{d}\right] \qquad (2)$$

Typical experimental data from Reference (5) are given in Figure 2. These data are plotted following the representation indicated by equation (2). They illustrate the qualitative effects that each of the dimensionless similarity parameters has on the liquid surface height vs time curve. Also, fairly straightforward analytical procedures were developed based on simple physical models, and these were found to predict the measured data reasonably well. Typical comparisons of measured data with the corresponding analytical predictions are reproduced from Reference (5) in Figures 3 and 4.

The present investigation was a logical outgrowth of the similarity study described above. Attention is now directed toward the addition of sinusoidal vibration in the longitudinal direction, as shown in Figure 1, and what influence it might have on the rate of discharge as compared with the non-vibratory situation (Figures 2, 3, and 4).

EXPERIMENTAL APPARATUS AND PROCEDURE

An experimental apparatus was designed and constructed for studying the discharge process under vibratory conditions. Most of the essential features concerning handling of the test liquid and introducing vibration are shown in Figure 5.

The cylindrical fluid container was transparent so that visual observation of the test fluid was possible. It was made from a 4' long section of 9" diameter plexiglass tubing (½" thick

wall) which was attached to a 1½" thick plexiglass plate at the bottom. This plate was fitted with an adaptor so that discharge tubes of different diameters could be attached. Another plexiglass plate at the top contained two fittings for attachment of the test fluid inlet line and a pressurized air line. The latter was used for test runs at elevated ullage pressures. Metal tie rods between the top and bottom plates reinforced the fluid container which was rigidly attached to a supporting structure connected to the vibrator table. The electrodynamic shaker system used had a force capacity of 5000 lbs., and when the vibrator table was oscillated vertically this motion was transmitted through the supporting structure to the fluid container. An accelerometer mounted on the container base was used to monitor the vibrational acceleration amplitude. The signal from the accelerometer was also observed with an oscilloscope for verification of an essentially sinusoidal waveform. The input frequency was accurately measured by means of an electronic counter.

During each experimental run the test fluid drained into a receiving vessel which was supported by a stationary frame attached to the housing of the shaker. A sight glass on the receiving vessel was used to observe the amount of liquid drained from the vibrating fluid container at equal time increments during each transient test run. For each test a strip of paper

with graduated markings was attached with tape to the sight glass so that the instantaneous liquid height in the receiver vessel could be observed and marked on the strip at specified values of elapsed time. Thus, a permanent record of receiving vessel liquid height vs time was obtained for each run in the form of a paper strip with height markings corresponding to known values of time.

Before each test run the receiving vessel liquid height was brought to a predetermined reference level. A paper strip was then attached to the sight glass with the zero marking at this level. Each of the other graduated markings then corresponded to a particular decrease in liquid surface height in the fluid container. The calibration between the graduated markings and the decrease in liquid surface height was carefully determined under non-vibratory conditions before any of the test runs were performed.

During vibratory tests the liquid surface in the fluid container moved up and down due to vibration, and in some situations considerable sloshing occurred. The method used, however, gave measurements of the amount of liquid drained from the vibrating container. This method was accurate since the liquid level in the stationary receiving vessel remained relatively quiescent, although it rose steadily, even in the more severe cases of

violent sloshing in the vibrating fluid container. Use of the predetermined calibration with the markings made on the paper strips yielded idealized y-values corresponding to a smooth horizontal surface (see Figure 1). For those cases in which sloshing was present, each y-value corresponded physically to the liquid surface height that would be obtained for that specific time if both the vibration and the discharge were instantaneously terminated so that the liquid surface could become level. Thus, the y-values obtained have physical significance in that they are proportional to the volume of test liquid remaining in the fluid container even for those situations where sloshing occurred.

A plug at the lower end of the discharge tube was used to prevent the liquid from draining before each test was started. As soon as the chosen vibrational conditions were obtained the plug was removed to begin the transient discharge process. Time was measured with a stop watch, and the corresponding marks were made on the paper strip. At the end of each test the vibration was stopped and the paper strip was removed. The valve in the drain line was then opened so that the liquid could pass to the overflow vessel until the liquid level in the sight glass reached the zero reference. At this point the valve in the drain line was closed, the plug was inserted at the lower end of the discharge tube, and a new paper strip was attached to the sight glass in

preparation for the next test run.

Figures 6 through 10 contain some of the experimental data obtained using water as the test fluid. These data were non-dimensionalized and plotted following the procedure indicated in Figures 3 and 4. Values of the various non-vibratory parameters used are given in the captions. These can easily be converted to a dimensionless form if desired in accordance with the pattern indicated by equation (2) and by Figure 2. Figures 11 through 19 contain photographs of some of the more interesting visual observations obtained using water as the test fluid. All of the results are discussed in the following section.

DISCUSSION OF RESULTS

Figures 6A through 6D clearly show that the flow was retarded by vibration, and the amount of retardation increased with the vibrational acceleration amplitude (given as a dimensionless ratio, $G = g_v/g$). In addition, the retardation for a given G-level decreased with rising frequency. This is also illustrated in Figures 6E and 6F which contain crossplots of the data appearing in Figures 6A through 6D for G=1 and for G=5 respectively, with frequency as a parameter. Since the data shown in Figure 6 were obtained with an L/d ratio of only 4, this case is referred to as a short discharge tube situation.

Figure 7 shows the effect produced when the discharge tube

was lengthened from 2" to 12", giving an L/d ratio of 24. In obtaining these data the initial liquid surface was at the same height above the container bottom (44") as in the case associated with Figure 6. However, with L=12" instead of 2" the outlet was 10" lower so that the h-value was increased from 46" to 56". The other parameters were maintained identical to those indicated in Figure 6. The curves of Figure 7 exhibit trends which are qualitatively like those of Figure 6, but the retardation magnitudes are very much reduced. Thus, according to Figures 6 and 7 the length of the discharge tube, or more appropriately the L/d ratio, is a very important parameter in determining how strongly the discharge rate is affected by the imposed vibration.

Experiments equivalent to those associated with Figures 6 and 7 were also performed using a smaller diameter discharge tube (d=¼") and with all other conditions being the same. The retardation trends and the orders of magnitude were about the same as those indicated in Figures 6 and 7. For the sake of conciseness these data are not included in this presentation.

One difficulty was encountered in conducting the experiments associated with Figures 6 and 7. At low frequencies and high G-levels rather sizeable surface motions were observed (Figure 11). The transverse inertia of the fluid produced a low amplitude, slowly varying, periodic side motion of the upper portion of the

fluid container during the early part of the discharge time period when the liquid column was relatively high. This resulted from a coupling between the longitudinal motion imposed on the system and a nonlinear subharmonic response of the liquid, an effect which is well known and has been studied previously (2, 3). At higher frequencies the liquid surface remained relatively level so that large scale surface motions and severe sloshing did not occur. However, in some cases small droplets were continuously ejected from the surface forming a fairly continuous upward spray (Figure 12). Each droplet would merely fall back to the liquid surface, perhaps after striking the container wall or top. Any influence of this kind of surface behavior certainly had no appreciable effect on the discharge rate. At the higher G-levels bubbles often formed in the liquid, producing two phase conditions, either at the top of the liquid column or further down in regions far removed from the liquid surface (Figures 13 and 14). In some cases a single cavity formed at the bottom where the cylinder wall was attached to the base (Figure 15). These phenomena have all been observed previously and are described elsewhere (6-12).

In order to avoid the small amplitude side motion of the upper portion of the fluid container (described in the previous paragraph) additional experiments were carried out using a smaller

initial liquid height. This virtually eliminated the problem associated with container side motion, even in the presence of severe surface motions which occurred at low frequencies and high G-levels. Except for this favorable difference, the visual observations obtained were qualitatively the same as those described in the previous paragraph. Experimental date for a 26" initial liquid height are shown in Figure 8. Corresponding measurements (not shown) were obtained with L=12" instead of 2" (h=36" instead of 26"). All of these data exhibited the same trends and about the same percentage effects as those shown in Figures 6 and 7. Thus, the subharmonic side motion observed in connection with figures 6 and 7 was not a major factor contributing to the retardation effects shown.

One of the more pertinent questions at this point is associated with whether or not a sloshing surface can have an appreciable influence in producing flow retardation. The data shown in Figure 6 through 8 did not answer this question since the operating range of appreciable retardation effect coincided with the range in which sloshing was observed (low frequencies and high G-levels). In order to provide further information a styrofoam float was placed on the liquid surface (Figure 16) in order to prevent sloshing, and a set of experimental measurements was obtained. Some of these data are shown in Figure 9B. Comparison of these

curves with those shown in Figure 9A reveals that there were no major differences. Hence, the sloshing effects at the liquid surface had essentially no influence in producing discharge flow retardation.

Experiments carried out at elevated ullage pressures ($P_1 > P_2$ in Figure 1) revealed a lesser retarding influence of vibration as compared with corresponding experiments conducted with zero pressure drop. The data shown in Figure 10 are typical of those obtained during pressure driven discharge. It appeared from the measurements that the generally faster rates of discharge resulting from sizeable pressure drops caused any retarding influence of the vibration to be almost negligible by comparison.

Figure 17 shows a uniform discharge stream in the absence of vibration, and Figure 18 shows how the stream was typically altered to form a pulsating type flow in the presence of vibration having a sufficiently high G-level. Such a pulsating pattern undoubtedly occurred due to the presence of a sizeable pressure amplitude at the bottom of the vibrating fluid container near the entrance to the discharge tube. It should be noted, however, that the time averaged flow for a pulsating stream did not necessarily exhibit a strong retardation effect compared with the corresponding no vibration situation. This was particularly evident when a long discharge tube was used (Figure 7).

When a short discharge tube was used a spreading discharge stream composed of liquid droplets was often observed (Figure 19). With this kind of flow pattern the discharge tube was probably not full of liquid. This would amount to a reduction in the corss-sectional area of the discharge stream, and a corresponding decrease in the effective contraction coefficient to a value considerably below unity. Flow patterns of the type shown in Figure 19 were often present in those situations in which sizeable vibratory effects were measured (Figures 6 and 8), and a reduction in the discharge stream area appears to be a most plausible explanation for the retardation obtained.

It is appropriate at this point to consider the system from an analytical viewpoint to see what further explanations of fluid behavior can be established. Consider an incompressible liquid being discharged under the influence of a gravitational field, g, only ($P_1 = P_2$ in Figure 1). In the absence of vibration the quasi-steady flow rate, according to the Bernoulli equation, is proportional to $\sqrt{yg}$. If vibration is now imposed, then the resulting gravitational field acting on the fluid is $(g + g_v \cos \omega t)$. For very low frequencies the fluid responds to the time-varying field in a quasi-steady manner, and the instantaneous flow rate is proportional to $\sqrt{y \cdot |g + g_v \cos \omega t|}$. By integrating this expression over a complete vibration cycle the time averaged flow

rate can be obtained, and this can be compared with the corresponding steady flow rate in the absence of vibration. The results of this procedure show a retarding influence of vibration due to the nonlinear square root relationship between instantaneous flow rate and the combined gravitational-vibrational force field. The amount of retardation increases with G-level as indicated in Figure 20 in agreement with the experimental data. However, the predicted retardation values given in Figure 20 are somewhat larger than the corresponding experimentally observed values (Figures 6 through 9). This is understandable since the analytical prediction shown is valid only for very low frequencies, and is restricted to a liquid with a horizontal free surface inside a rigid container. As frequency increases the fluid can no longer respond to the vibration in a quasi-steady manner due to its inertia. Accurate analytical predictions accounting for a frequency dependency due to fluid inertia would most probably show lesser retardation effects than those given in Figure 20. It should be pointed out here that a general relationship accounting for these inertia effects, as well as all of the other parameters, would be of the form

$$\frac{Y}{h} = F_3\left[\frac{t}{\sqrt{2h/g}}, \frac{\Delta P/\rho g}{h}, \frac{d\sqrt{2gh}}{\nu}, \frac{h}{d}, \frac{D}{d}, \frac{L}{d}, G, f\sqrt{2h/g}\right] \qquad (3)$$

where G and $f\sqrt{2h/g}$ are the dimensionless vibrational acceleration

amplitude and frequency respectively. This expression follows the form given in equation (2). It should be valid for an incompressible single phase fluid in a rigid container exposed to vibration even if the free surface does not remain horizontal, provided that y/h is interpreted as the fractional portion of the initial liquid remaining in the container (as discussed in the previous section dealing with experimental procedure).

Within the frequency range investigated experimentally the system did not behave as an incompressible fluid - rigid container combination for most of the cases studied. Therefore analytical attempts based on the kind of model just described were not pursued further. However, it is revealing to consider the longitudinal one-dimensional wave behavior of a compressible fluid in a cylindrical container with elastic walls which is closed at the bottom (10, 11, 12). For this situation the oscillating component of pressure at the container bottom, if dissipation effects are neglected, is given by

$$P_o = \frac{\rho g_v C}{\omega} \tan\left[\frac{\omega(y-L)}{C}\right] \cos \omega t. \qquad (4)$$

C is the longitudinal wave velocity of the system which was found to be about 1000 fps for the experimental system used provided that no bubbles were present as shown, for example, in Figures 13 and 14. When bubbles are present in a liquid the compressibility of the fluid column is increased, and this causes a

reduction in the wave velocity. The variation of pressure amplitude with vibrational frequency, as given by equation (4), is shown in Figure 21.

The first resonant frequency is obtained from equation (4) as $\omega(y-L)/C = \pi/2$ where large pressure amplitudes can result even if g_v is not large. The pressure amplitude for a given g_v value decreases as the vibrational frequency deviates from resonance. Above this resonance there is a phase shift of 180 degrees. The lowest resonance encountered during the experimental runs (in the absence of bubbles) was in the neighborhood of 60 to 70 cps, and corresponded to the largest liquid height. As the liquid height decreases the first resonant frequency increases according to the expression given above. The higher resonant frequencies (second, third, and so on) were always well above the vibration excitation frequency used.

At near resonant conditions actual pressure amplitudes are lower than predicted by equation (4) due to energy dissipation (10, 12). In the present study further reduction probably occurred since the fluid container was not closed at the bottom. Thus, the discharge opening in the center of the bottom plate provided a direct path to the atmosphere for pressure release, and this probably caused considerable attenuation of the actual pressure amplitudes at the container bottom in the experimental

apparatus. In addition, bubbles were often present in the liquid and were unevenly distributed during many of the experimental test runs. This creates another complicating factor which would cause further inaccuracy in predicting actual system behavior with any simplified analytical model. Nevertheless, equation (4) provides a starting point for constructing qualitative explanations of the observed pulsating flow patterns shown in Figures 18 and 19, as well as establishing a basis for a more complete and detailed study of these phenomena.

CONCLUSIONS

A study of the discharge of liquid from a cylindrical container subjected to longitudinal vibration has been performed. Flow retardation effects as high as 30% were measured using a length-to-diameter ratio of 4. The magnitude of the retardation was found to increase with G-level and decrease with frequency. The retarding influence of the vibration was greatly reduced when the L/d ratio was increased. The effect of vibration was also strongly reduced when the ullage pressure was increased. Sizeable surface motions and sloshing were found to produce no appreciable contribution in causing the retardation observed. At the higher G-levels used bubbles were present in the liquid in accordance with observations reported by previous investigators, but they were not usually located in the immediate vicinity of the container outlet.

An analytical prediction for very low frequencies exhibits a retarding influence in qualitative agreement with the trends observed from the measurements, but the measured retardation effects are smaller than predicted. This prediction, if extended, should be attenuated with rising frequency. A more refined analytical approach requires consideration of the compressibility of the liquid column and how it is affected by the elastic deformation of the container walls. An analytical prediction accounting for these effects is available from previous studies of containers closed at the bottom. The actual pressure amplitudes at the bottom were probably somewhat lower than the values given by the idealized expression due to the influence of dissipation, the effect of the discharge opening, and the presence of bubbles in the liquid. These items are presently under study and will be reported upon at a later date. However, use of this simplified expression suggests that strong pressure variations can exist near the entrance to the discharge tube, which explains the probable cause of the strongly pulsating flow patterns observed photographically.

The largest retardation effects were measured in the presence of strongly pulsating flows which tended to break up into streams of droplets diverging from the outlet. One of the most plausible explanations of the retardation in these cases appears to be a reduction in the cross-sectional area of the liquid stream.

REFERENCES

1. Fashbaugh, R. H., and V. L. Streeter, Resonance in Liquid Rocket Engine Systems, Journal of Basic Engineering, Trans. ASME, Series D, 1965, 87 (4), 1011-1017.

2. Abramson, H. N., Dynamic Behavior of Liquid in Moving Container, Applied Mechanics Reviews, 1963, 16 (7), 501-506.

3. Dodge, F. T., D. D. Kana, and H. N. Abramson, Liquid Surface Oscillations in Longitudinally Excited Rigid Containers, AIAA Journal, 1965, 3 (4), 685-695.

4. Lehner, J. W., "Analog Simulation of Uprated Saturn I First Stage Propulsion System Dynamic Characteristics", American Astronautical Society, Proceedings of the Southeastern Symposium on Missiles and Aerospace Vehicles Sciences, vol. II, December 1966, Huntsville, Alabama, pages 88-1 to 88-12.

5. Winter, E. R. F. and R. J. Schoenhals, "A Similarity Study of Gravity and Pressure Driven Discharge of Liquids from Propellant Tanks", American Astronautical Society, Proceedings of the Southeastern Symposium on Missiles and Aerospace Vehicles Sciences, vol. I, December 1966, Huntsville, Alabama, pages 48-1 to 48-13.

6. Bleich, H. H., Effect of Vibrations on the Motion of Small Gas Bubbles in a Liquid, Jet Propulsion, 1956, 26 (11) 958-964.

7. Buchanan, R. H., G. Jameson, and D. Oedjoe, Industrial and Engineering Chemistry Fundamentals, 1962, 1 (2), 82-86.

8. Baird, M. H., Resonant Bubbles in a Vertically Vibrating Liquid Column, Canadian Journal of Chemical Engineering, 1963, 41 (2) 52-55.

9. Ponder, C. A., D. H. Blount, and C. G. Fritz, "Bubble Coalescence in a Longitudinally Vibrated Liquid Column (Part I)", NASA TM X-53180, George C. Marshall Space Flight Center, Huntsville, Alabama, December 1964.

10. Schoenhals, R. J., and T. J. Overcamp, "Pressure Distribution and Bubble Formation Induced by Longitudinal Vibration of a Flexible Liquid-Filled Cylinder", NASA TM X-53353, George C. Marshall Space Flight Center, Huntsville, Alabama, September 1965.

11. Kana, D. D., and F. T. Dodge, "Bubble Behavior in Liquids Contained in Vertically Vibrated Tanks", AIAA Paper No. 66-86, presented at AIAA 3rd Aerospace Sciences Meeting, New York, N. Y., January 1966.

12. Schoenhals, R. J., and T. J. Overcamp, Pressure Distribution and Bubble Formation Induced by Longitudinal Vibration of a Flexible Liquid-Filled Cylinder, to be published in Journal of Basic Engineering, Trans. ASME, Series D.

LIST OF FIGURES

Figure No.	Caption
15	Single Cavity Formed At The Container Bottom Adjacent To The Cylindrical Wall
16	Styrofoam Float Used To Prevent Sloshing At The Liquid Surface
17	Discharge Stream In The Absence Of Vibration
18	Pulsating Discharge Stream Induced By Vibration
19	Diverging Discharge Stream From A Short Tube Induced By Vibration
20	Analytical Prediction Of Flow Retardation At Very Low Frequencies for $\Delta P=0$
21	Variation Of Pressure Amplitude With Vibrational Frequency

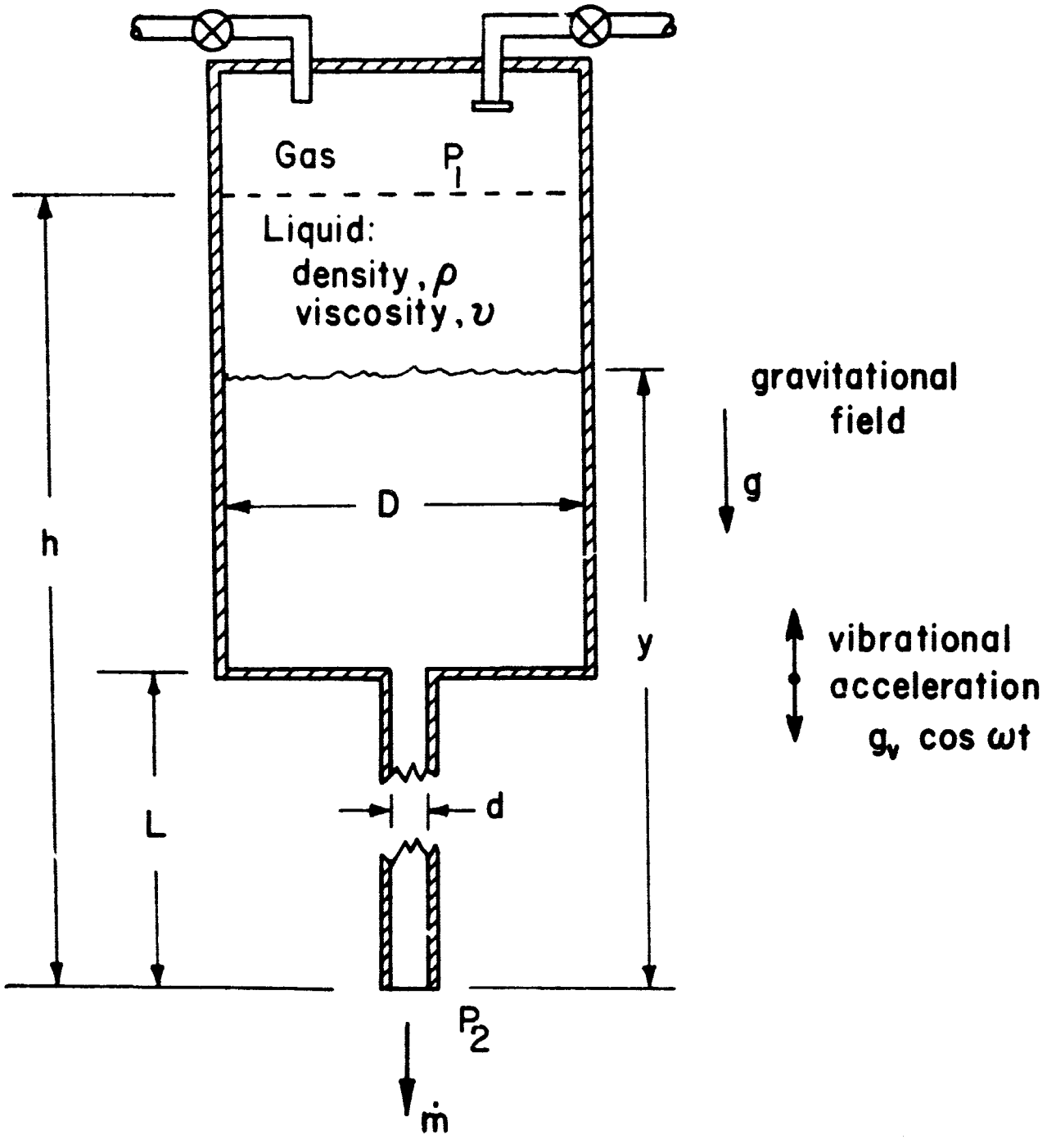

Figure 1. Discharge of Liquid From A Container Subjected to Longitudinal Vibration

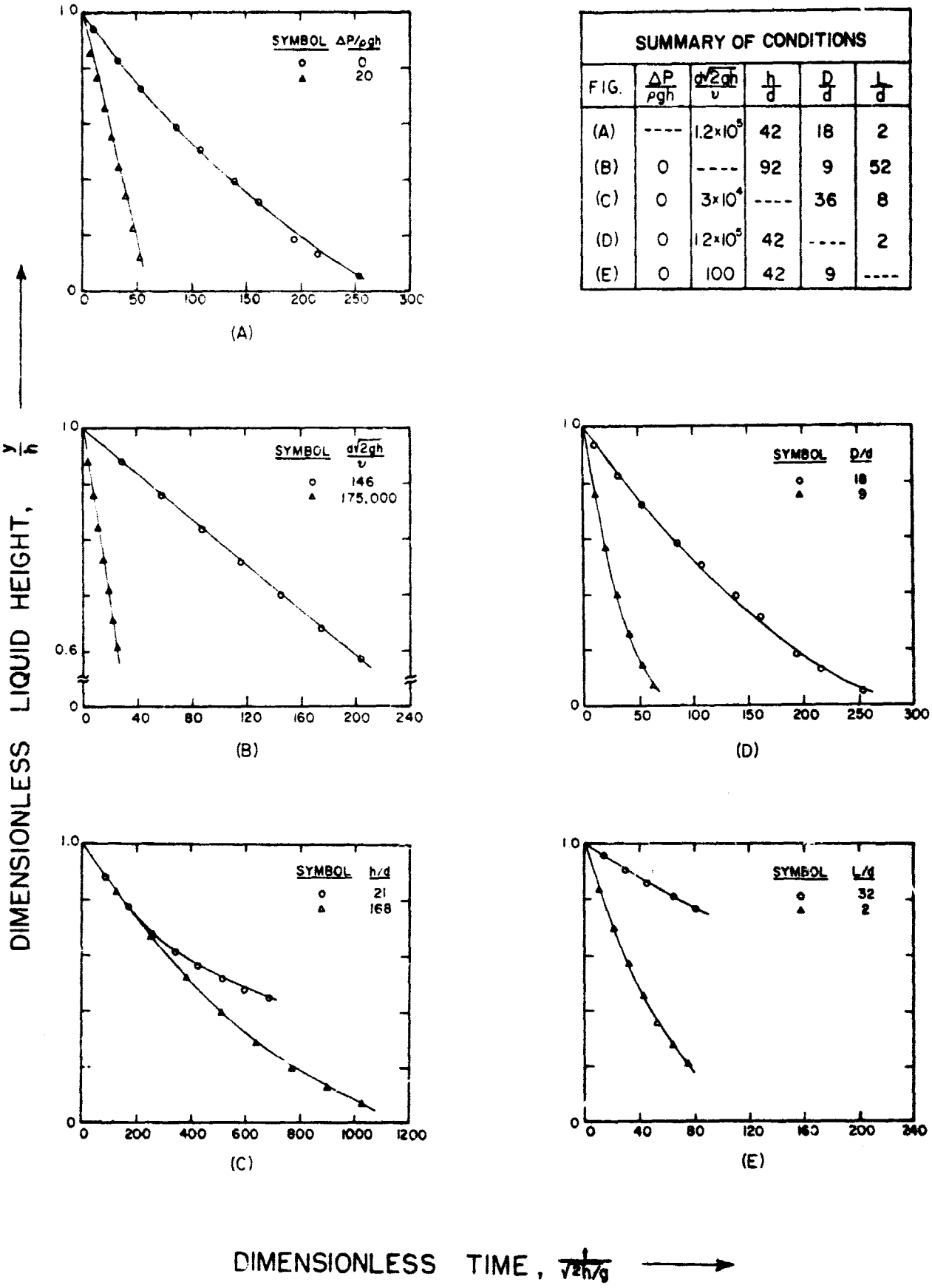

SUMMARY OF CONDITIONS

FIG.	$\frac{\Delta P}{\rho g h}$	$\frac{d\sqrt{2gh}}{\nu}$	$\frac{h}{d}$	$\frac{D}{d}$	$\frac{L}{d}$
(A)	----	1.2×10^5	42	18	2
(B)	0	----	92	9	52
(C)	0	3×10^4	----	36	8
(D)	0	1.2×10^5	42	----	2
(E)	0	100	42	9	----

Figure 2. Typical Experimental Results in Terms of Similarity Parameters From Reference (5) - No Vibration

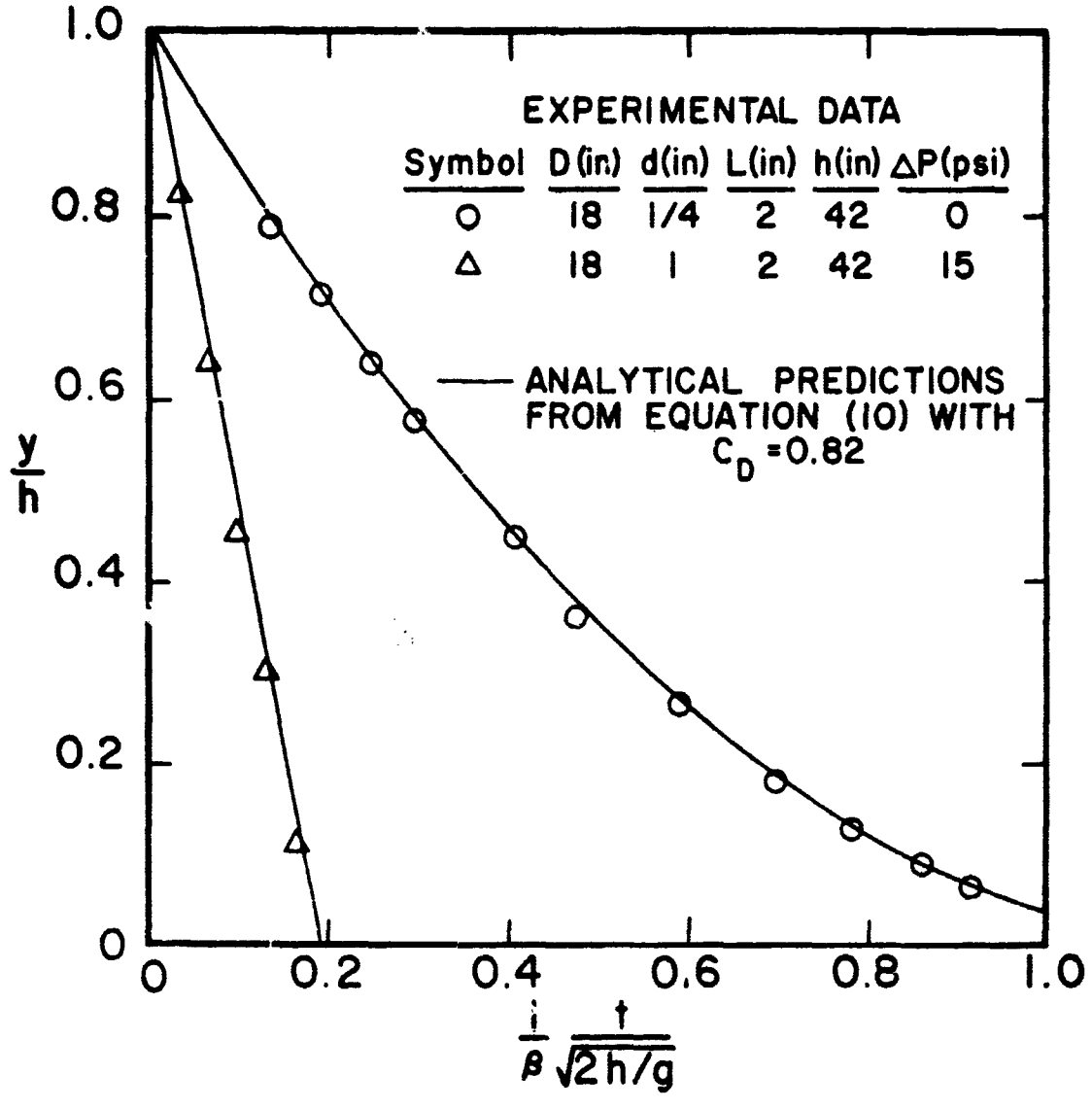

Figure 3. Comparison of Experimental Measurements With Analytical Predictions For Short Discharge Tubes From Reference (5) - No Vibration

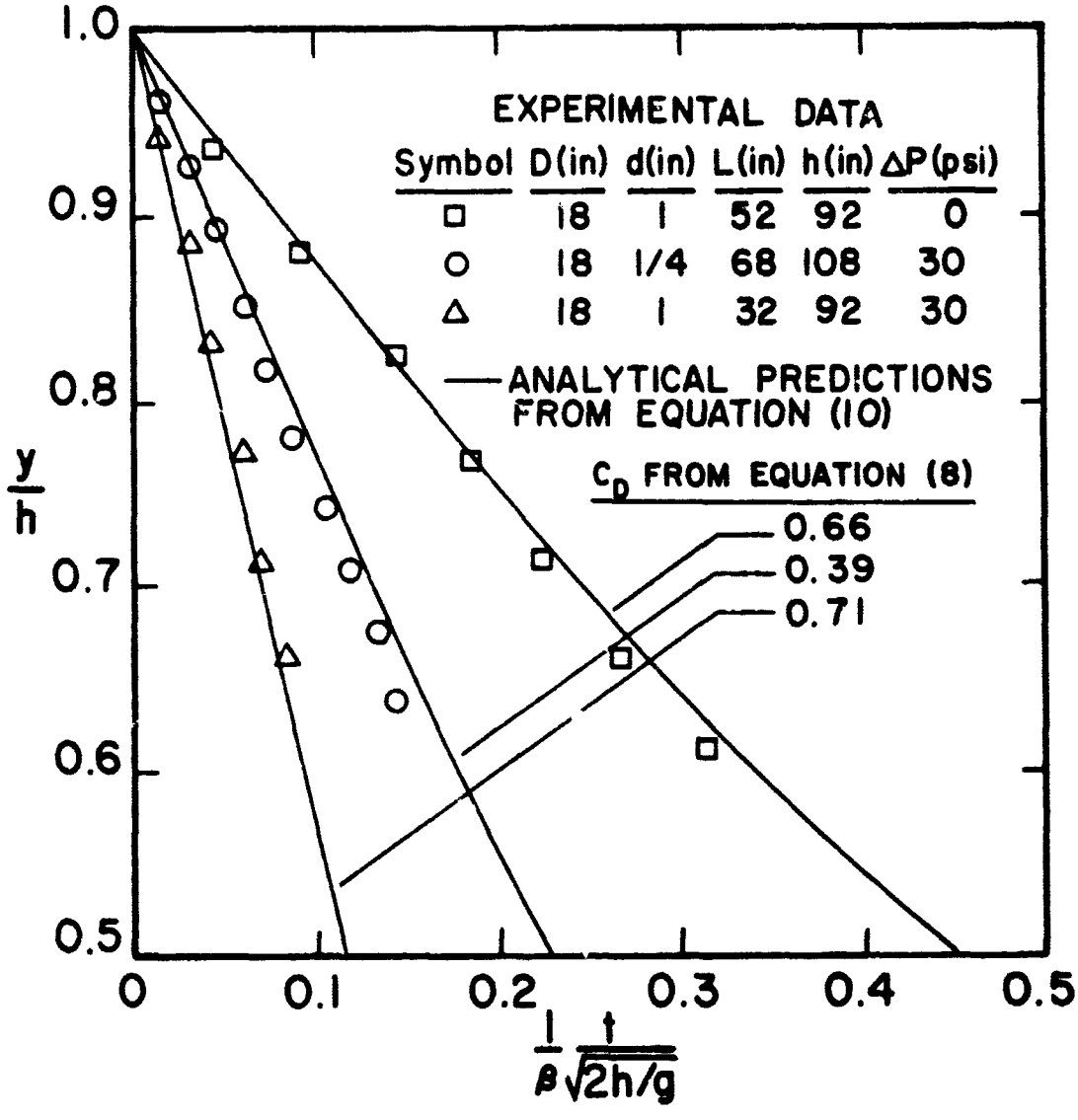

Figure 4. Comparison Of Experimental Measurements With Analytical Predictions For Long Discharge Tubes From Reference (5) - No Vibration

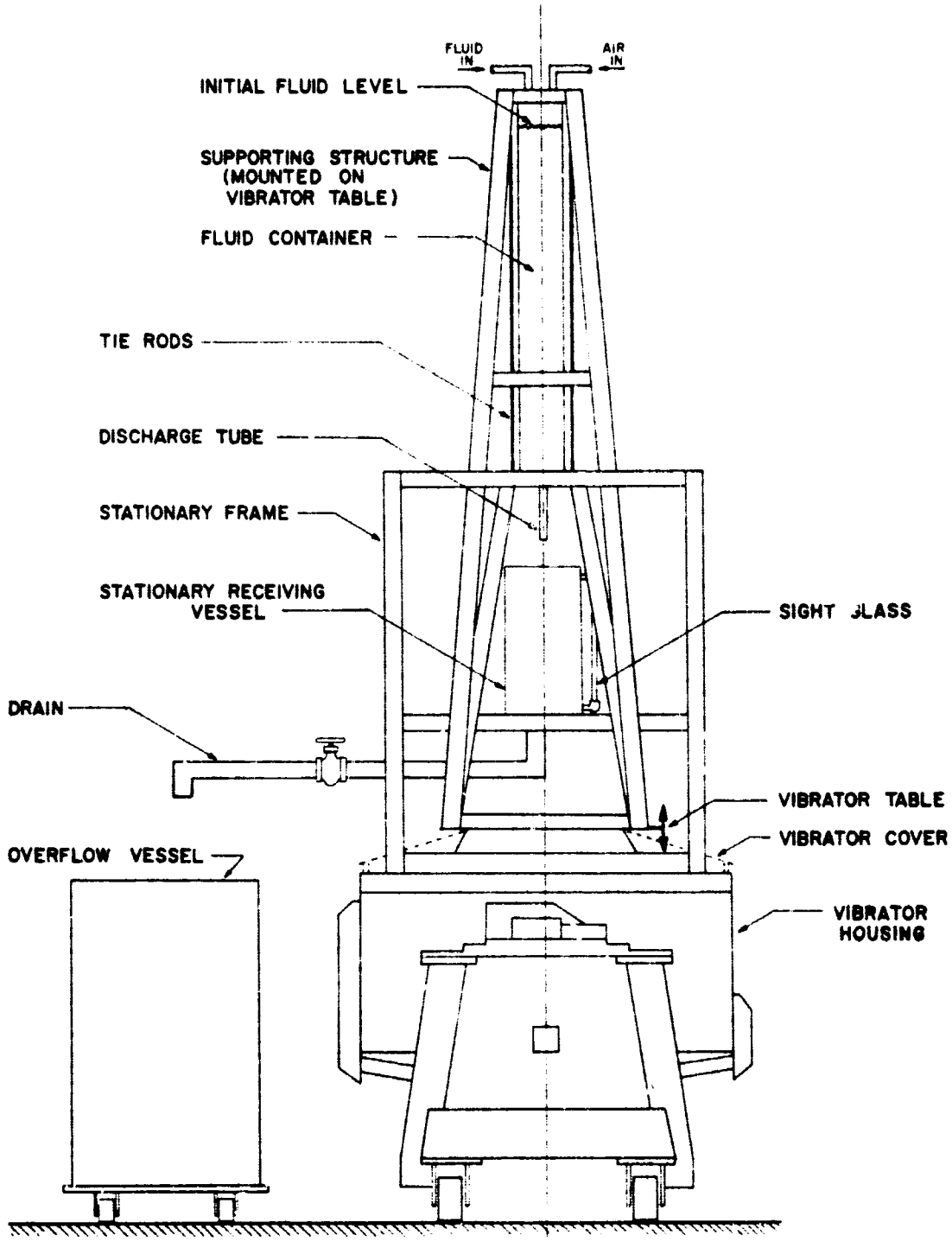

Figure 5. Discharge Test Apparatus For Study of Vibratory Effects

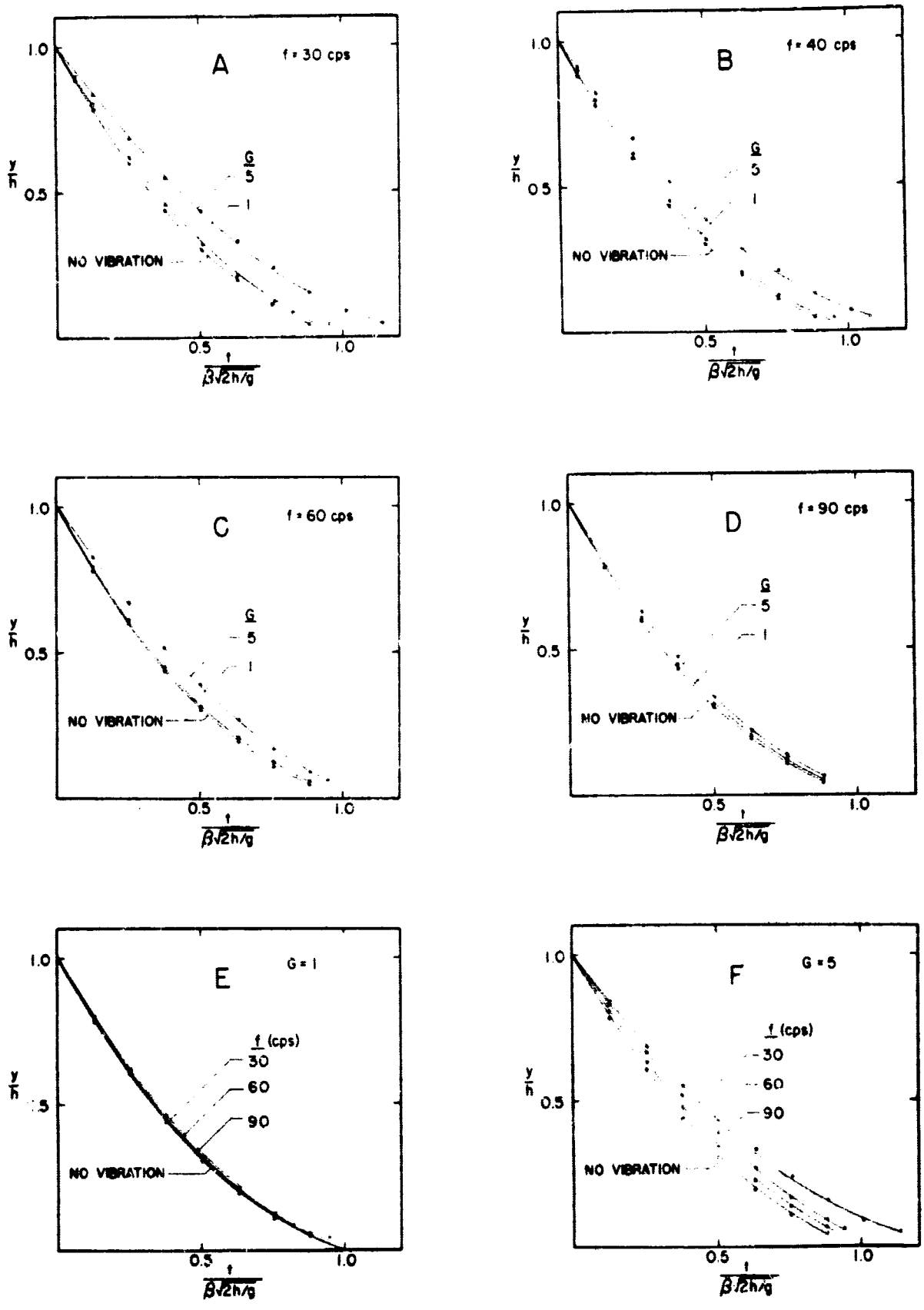

Figure 6. Experimental Results Obtained Using A Short Discharge Tube (D=9", d=½", h=46", L=2", ΔP=0)

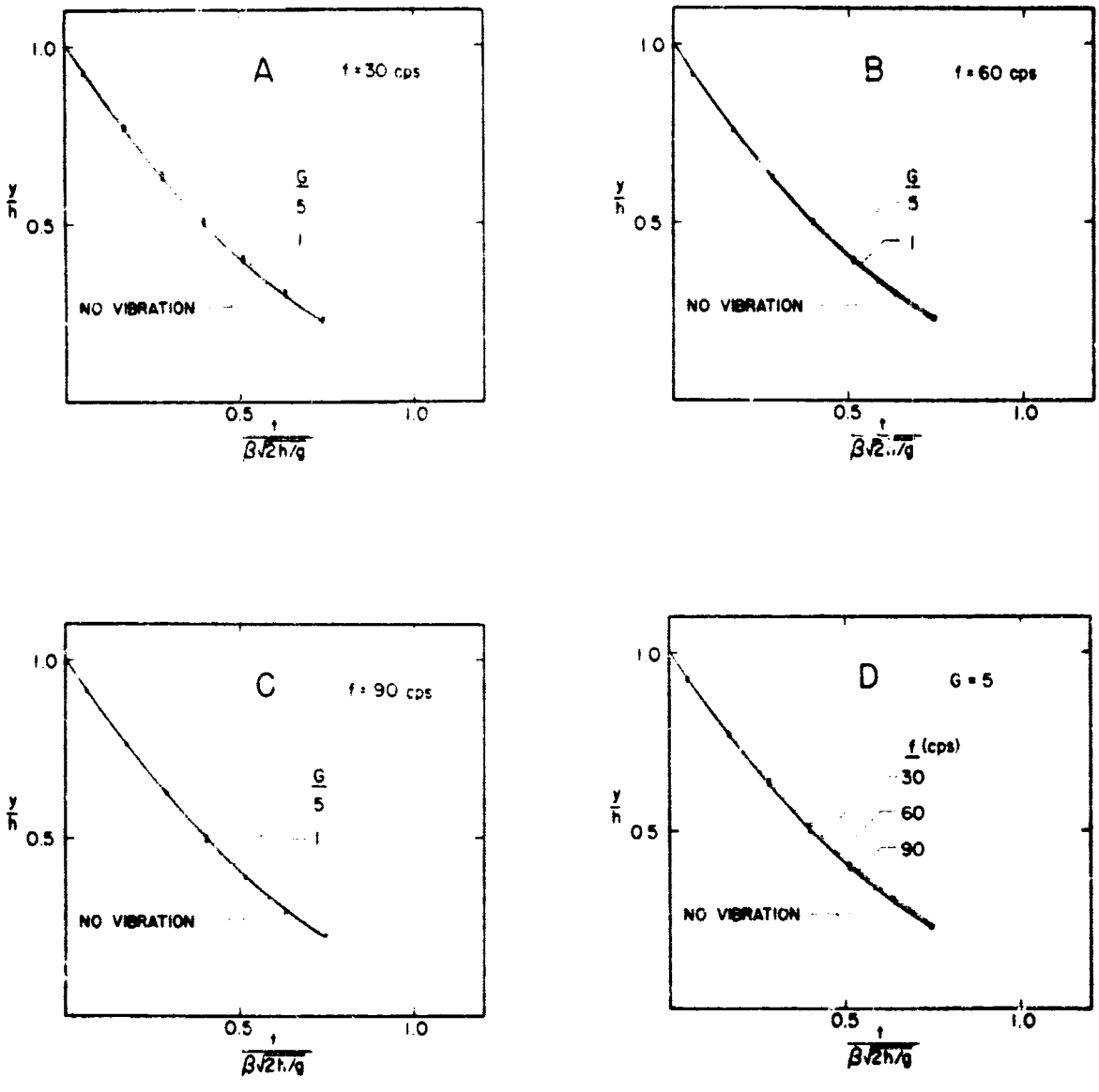

Figure 7. Experimental Results Obtained Using A Long Discharge Tube (D=9", d=½", h=56", L=12", ΔP=0)

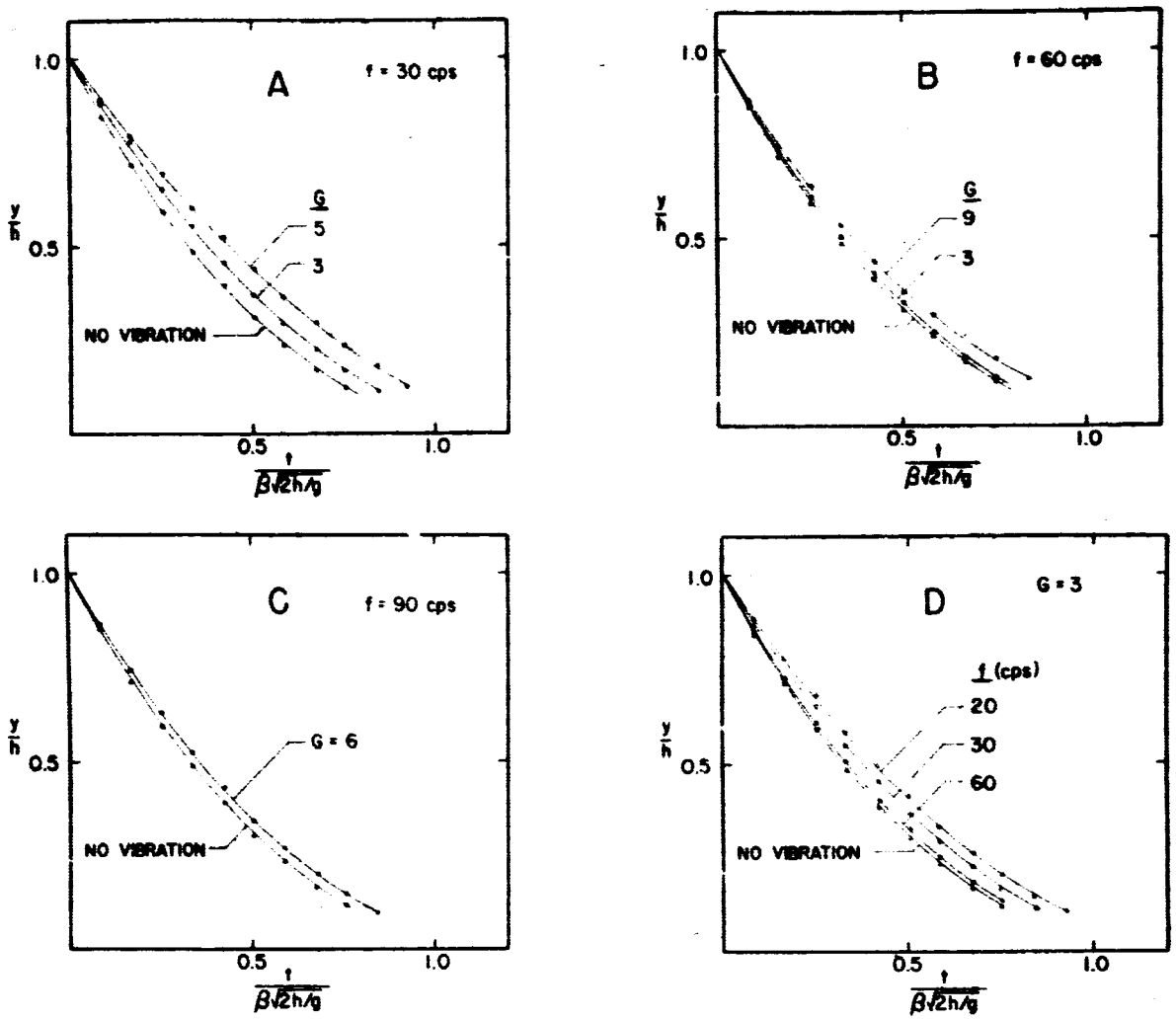

Figure 8. Experimental Results Obtained Using A Short Discharge Tube (D=9", d=½", h=26", L=2", ΔP=0)

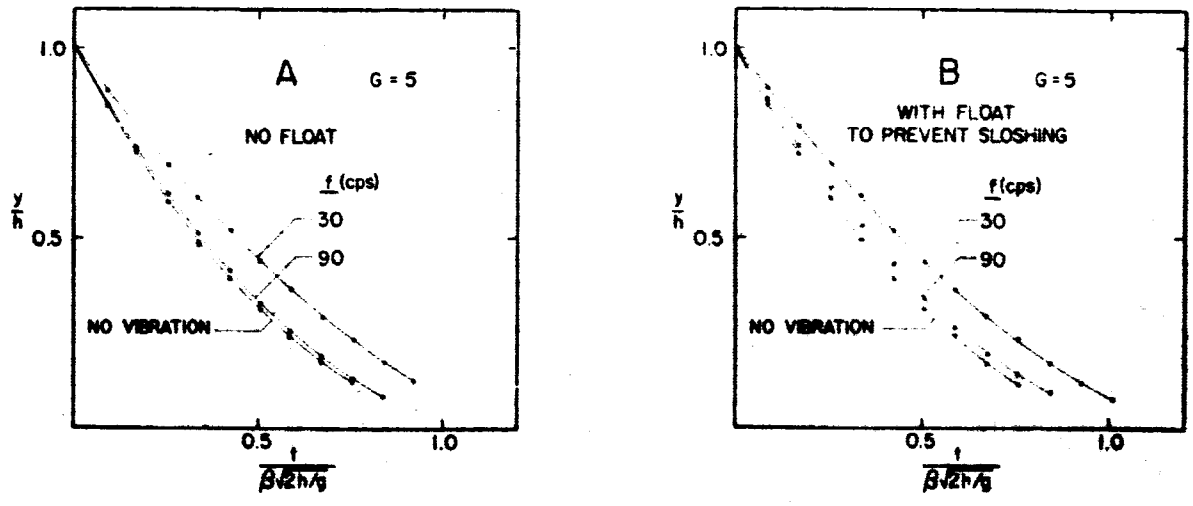

Figure 9. Comparison Of Experimental Results For G=5 (A) With Sloshing, And (B) With Sloshing Prevented By Use Of A Styrofoam Float

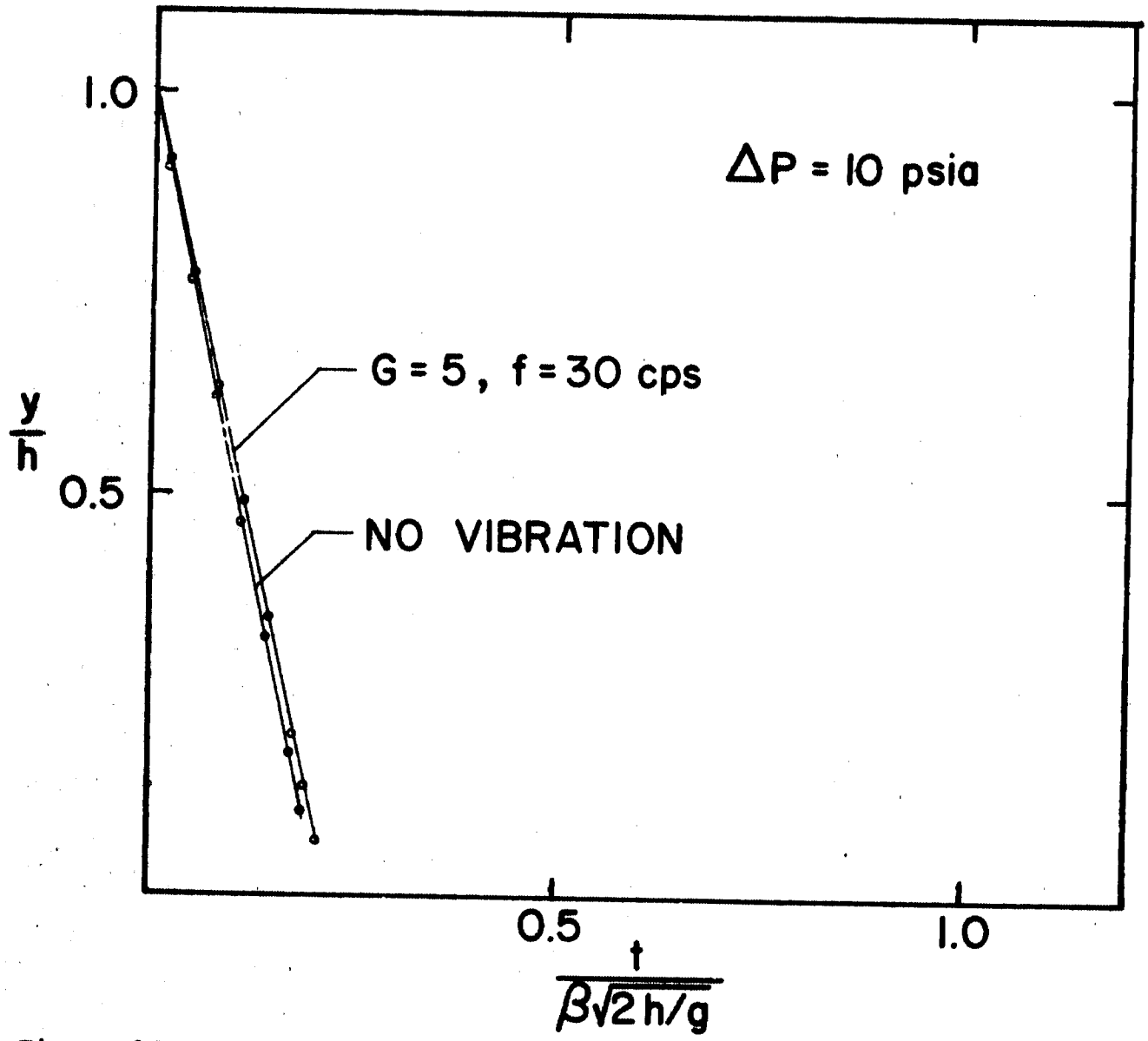

Figure 10. Experimental Results Obtained With A Pressure Difference (D=9", d=¼", h=46", L=2")

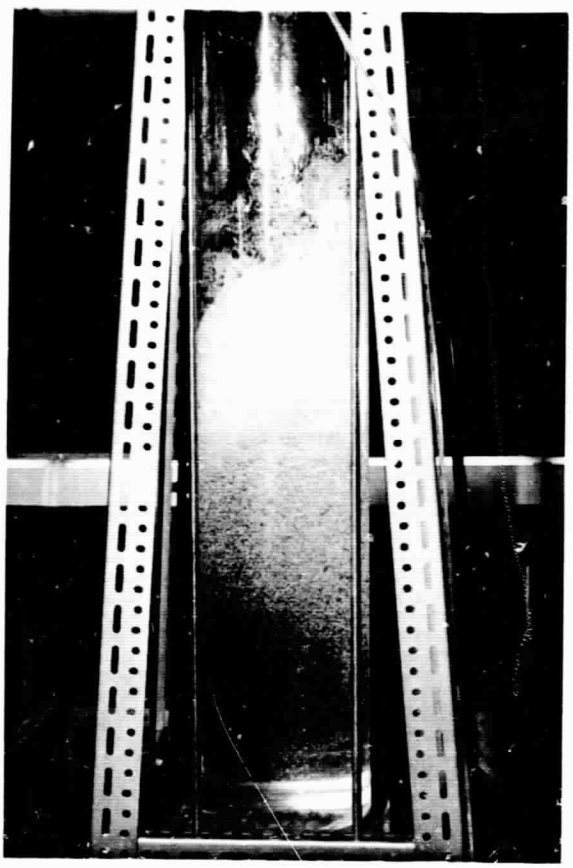

Figure 11. Large Surface Disturbances Produced By Vibration

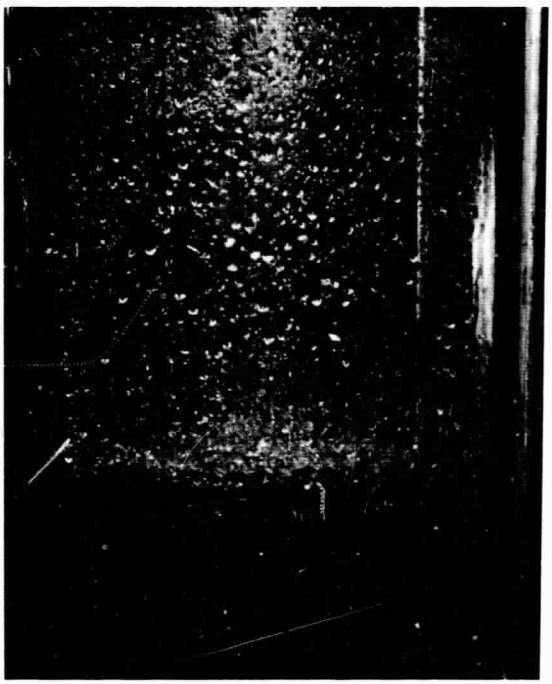

Figure 12. Ejection Of Liquid Droplets From The Surface At Higher Frequencies

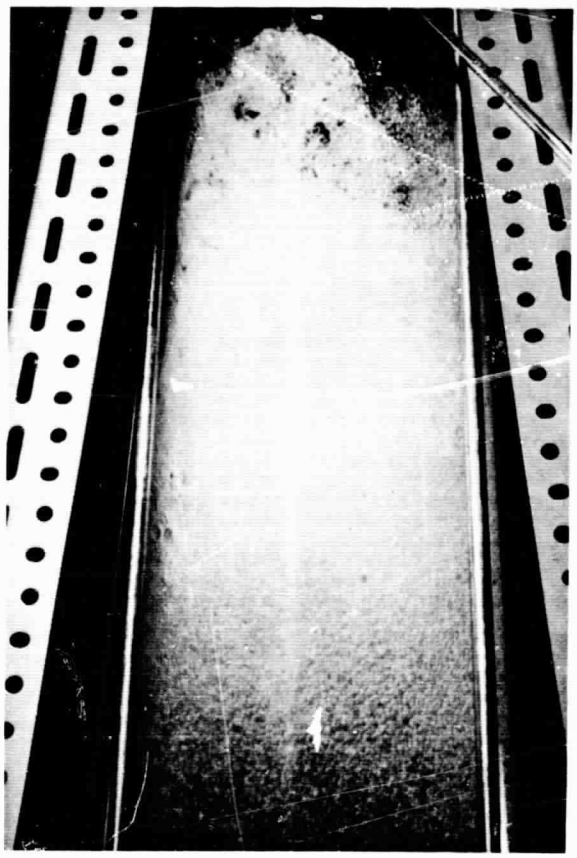

Figure 13. Bubble Formations Near The Liquid Surface

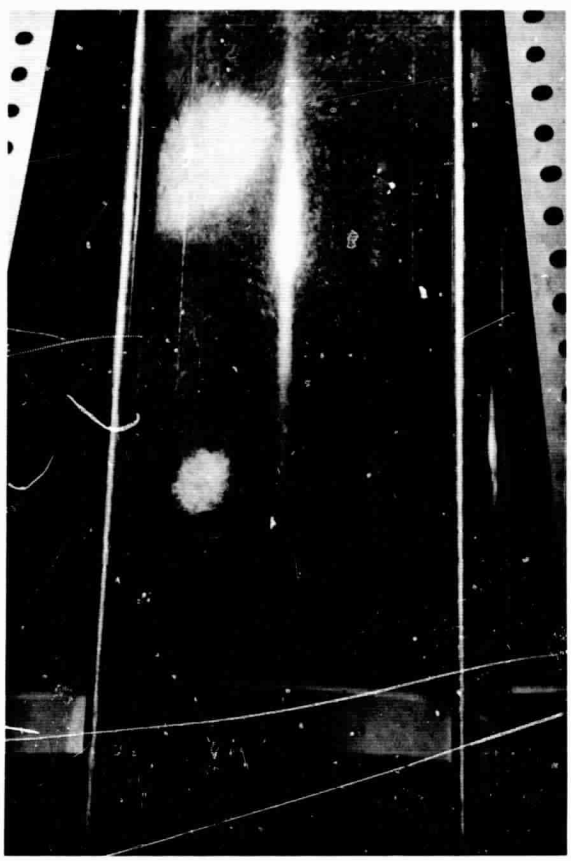

Figure 14. Bubble Formations Far Removed From The Liquid Surface

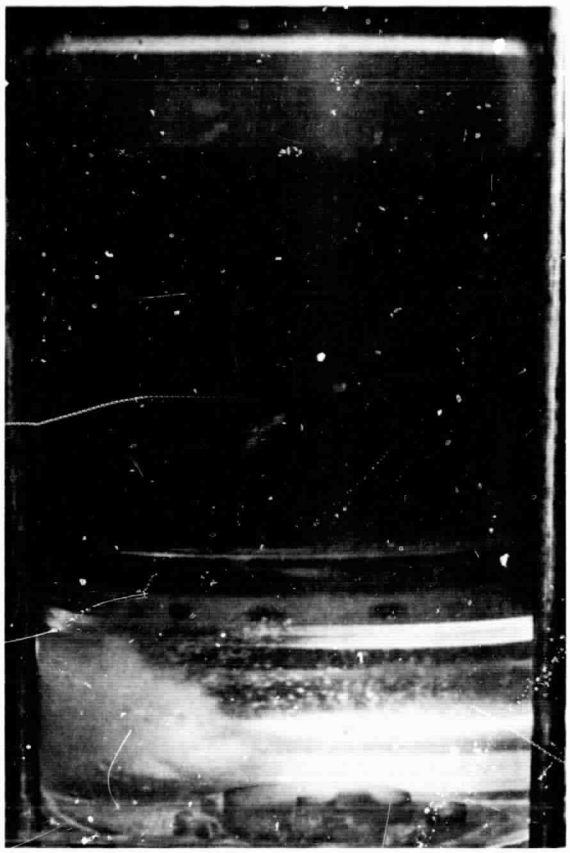

Figure 15. Single Cavity Formed At The Container Bottom Adjacent To The Cylindrical Wall

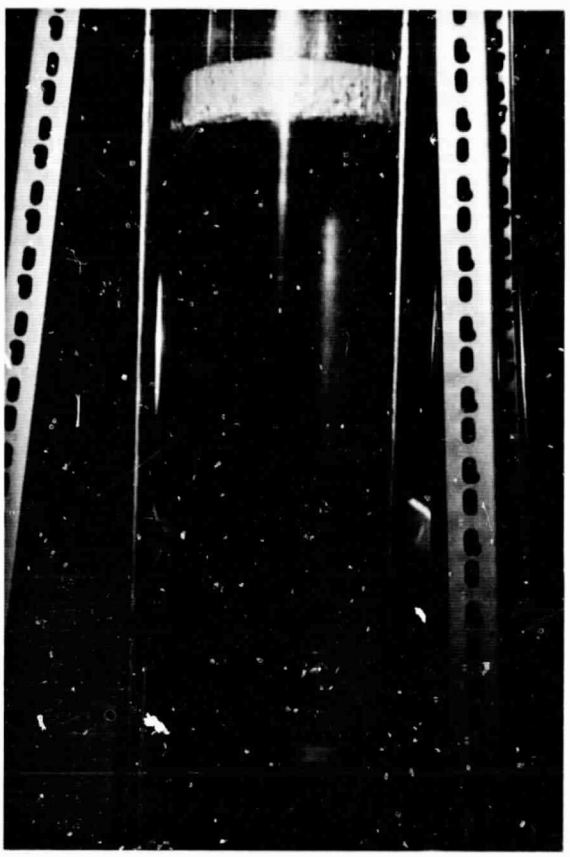

Figure 16. Styrofoam Float Used To Prevent Sloshing At The Liquid Surface

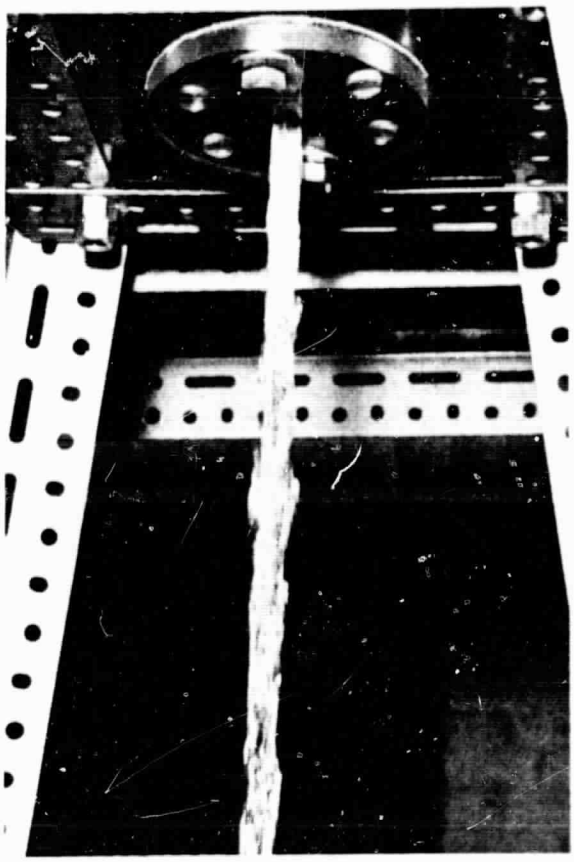

Figure 17. Discharge Stream In The Absence Of Vibration

Figure 18. Pulsating Discharge Stream Induced By Vibration

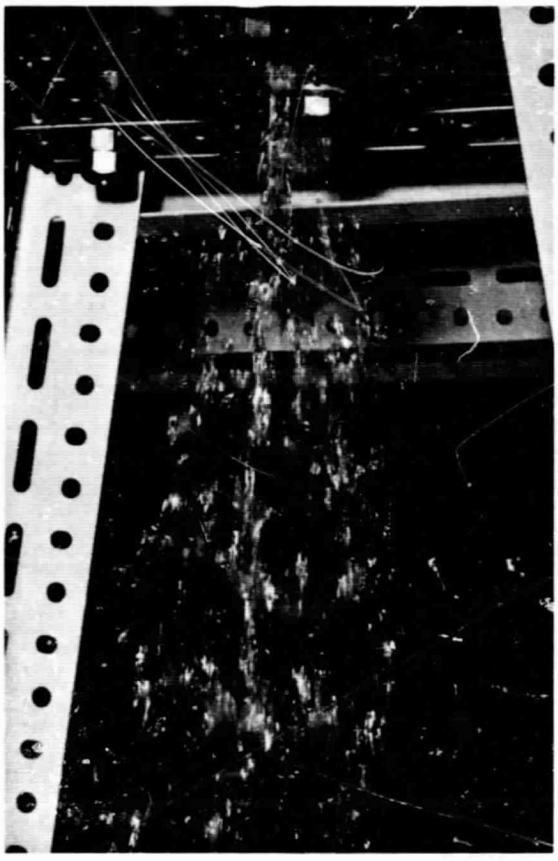

Figure 19. Diverging Discharge Stream From A Short Tube Induced By Vibration

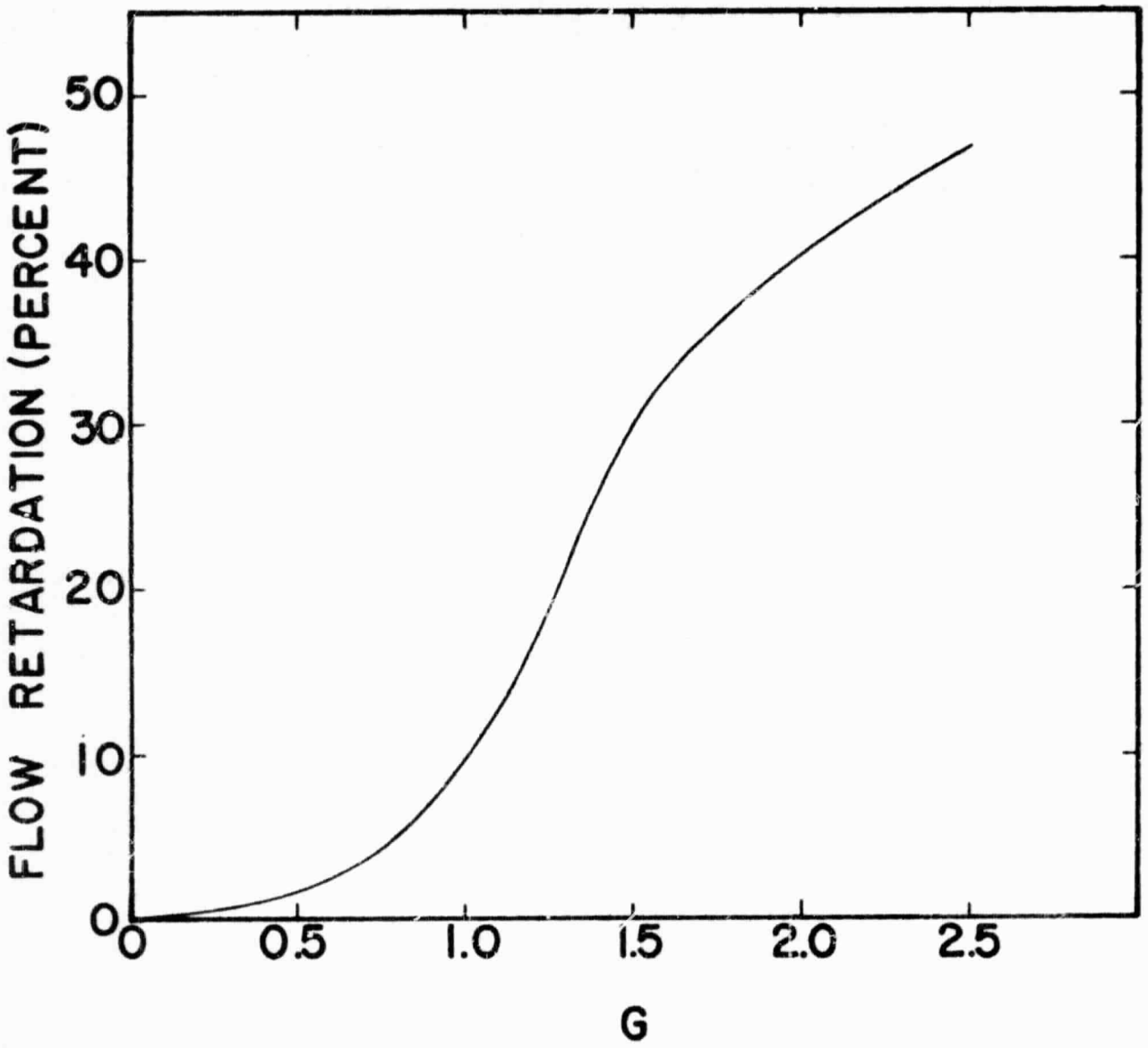

Figure 20. Analytical Prediction Of Flow Retardation At Very Low Frequencies for $\Delta P=0$

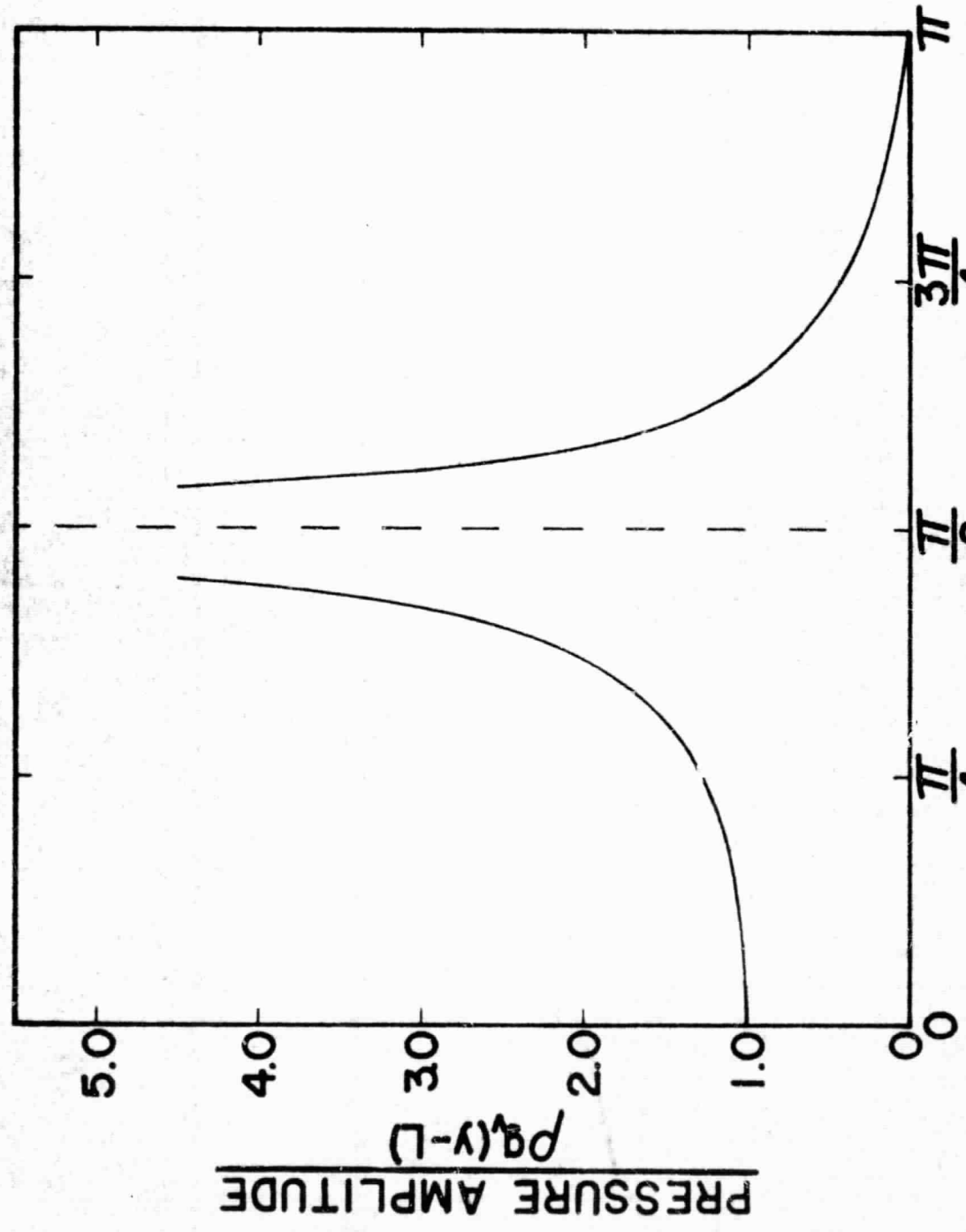

Figure 21. Variation Of Pressure Amplitude With Vibrational Frequency

Liquid Discharge from Tanks Subjected to Forced Longitudinal Vibration[1]

ABSTRACT

Results of an investigation of discharge from vibrating discharge tanks are presented in this study. A primary objective of this research was to explain the retardation of flow from discharge tanks subjected to vibratory motion previously found. Measurements are presented describing the effect of various vibratory conditions on discharge. An investigation was made of the pressure amplitudes at the bottom of a container with a closed discharge tube. Measurements were also made at the same position during discharge. Both the discharge and the no discharge pressure amplitudes are compared with previously obtained analytical results. The functional dependency of flow retardation on vibrational acceleration level was experimentally determined. Experimental results were obtained for very low frequencies (5 cps) and higher values (30 cps). The measurements are compared to a previous prediction which is valid for low frequencies. The variation of the time

[1] This section of part II of the final report was published as a Master's thesis on "Liquid Discharge from Tanks Subjected to Forced Longitudinal Vibration" by James Allen Pesar, School of Mechanical Engineering, Purdue University, Lafayette, Indiana, June 1968.

averaged pressure at the discharge tube entrance was measured for both vibratory and nonvibratory discharge. The measurements indicated a decreased average pressure at the discharge tube inlet during vibration. An explanation is given for the flow retardation based on the decreased average pressure measured at the discharge tube inlet.

TABLE OF CONTENTS

LIST OF FIGURES

Figure Page

Figure | Page

NOMENCLATURE

a	Acoustic velocity
B	Fluid bulk modulus
c	Longitudinal wave velocity
D	Diameter of discharge tank
d	Diameter of discharge tube
E	Young's modulus for the container
F_b	Body force
F_p	Pressure force
F_s	Shear force
f	Vibration frequency
G	Vibration acceleration level, g_v/g
g	Effective gravitational field
g_v	Vibration acceleration amplitude
h	Initial liquid height
L	Discharge tube length
m	Mass
$\dot{m}$	Instantaneous mass flow rate
$\bar{\dot{m}}$	Time averaged mass flow rate
p_o	Oscillating component of pressure
p_1	Pressure measured at position 1
p_2	Pressure measured at position 2

$\bar{p}$	Time averaged pressure
t	Time
Y	Longitudinal displacement of fluid cross section
Y_o	Steady component of Y
Y_1	Oscillating component of Y
Y_L	Amplitude of Y_1 at cylinder base
y	Instantaneous liquid height
v	Instantaneous velocity
v_t	Absolute velocity of tank
v_f	Absolute velocity of fluid particle
v_{ft}	Relative velocity of fluid particle with respect to the tank
β	$\sqrt{(D/d)^4 - 1}$
ρ	Density
ω	Angular frequency, $2\pi f$

Dimensionless Groups

$\frac{y}{h}$	Dimensionless liquid height
$\frac{t}{\beta\sqrt{2h/g}}$	Dimensionless time
$\frac{p_o}{\rho g_v (y-L)}$	Dimensionless pressure amplitude
$\frac{\omega(y-L)}{c}$	Dimensionless frequency

1. INTRODUCTION

The influence of a vibratory environment upon liquid propellants is becoming increasingly important in rocket technology. Large rockets are known to undergo severe structural vibration during flight. This vibration is known to cause considerable surface sloshing as well as large moments which effect vehicle stability (1, 2)*. It has been found that when cylindrical discharge tanks are exposed to longitudinal vibration, there is actually a retardation of flow which can be attributed to the vibration (3). Experimental results indicate that the magnitude of this flow retardation increases with increased vibrational acceleration level and decreases with increasing frequency when the vibrational acceleration level is maintained constant.

In the investigation reported here, an attempt was made to explain the flow retardation described in Reference 3. It was found that the average pressure occurring in the discharge tube inlet is lower when vibration is present (see Figure 1). This appears to be the most feasible cause of the retardation effects observed previously.

---

*Numbers in parentheses refer to Bibliography.

In the discharge experiments performed, the test fluid used was water. Experiments were conducted for vibratory discharge conditions and for vibratory situations in the absence of flow. The experimental results are presented in the form of plots of dimensionless liquid height as a function of dimensionless time, dimensionless pressure amplitude as a function of frequency, and time-averaged pressure at the discharge tube entrance as a function of time. Where possible, these results are compared with previous predictions and with results of further analysis carried out as part of this research.

A brief discussion of a previous attempt to explain the retardation of Reference 3 is given first. This is followed by a review of some of the pertinent literature, a description of the experimental apparatus and procedure, an analysis of discharge under vibratory conditions, and finally a presentation of experimental results and comparison with theory.

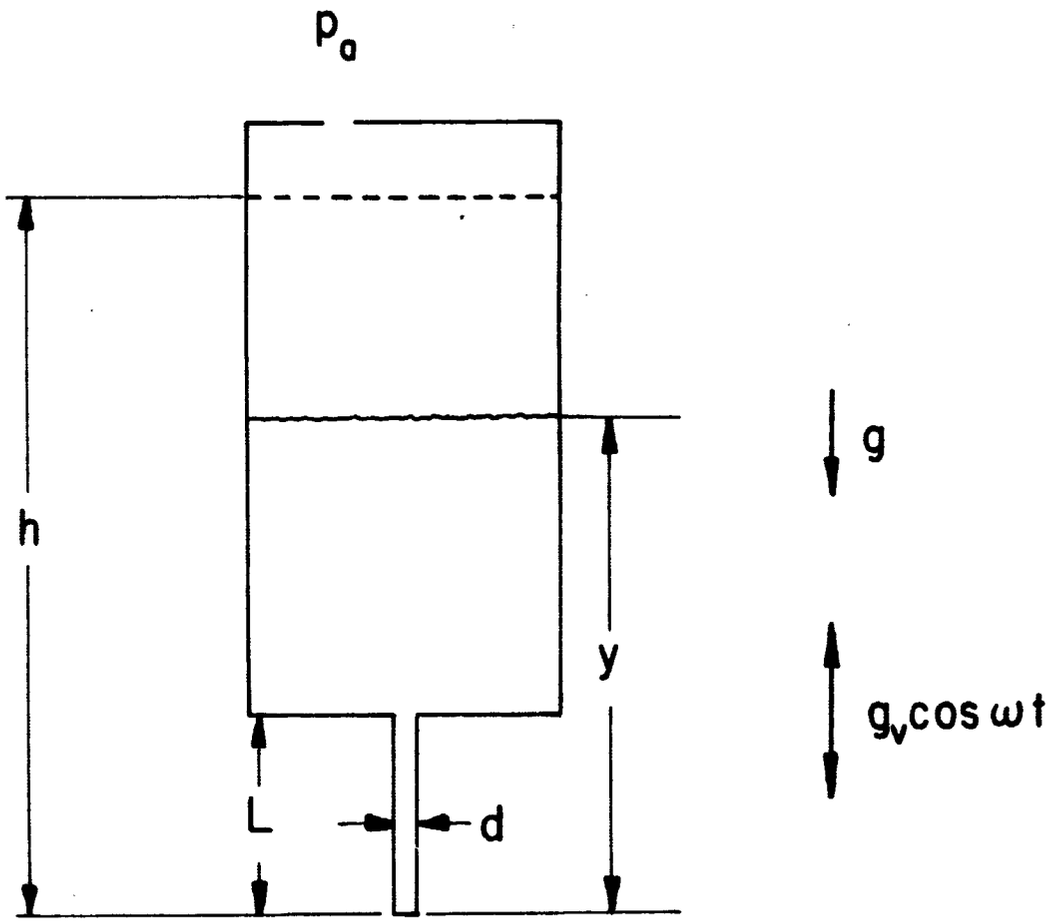

Figure 1. Simplified Geometry of Discharge Container

2. BACKGROUND OF THE PROBLEM

Originally the test apparatus employed by Schoenhals, Winter and Griggs was used (Figure 2). The inlet to the discharge tube was modified in such a way that pressure measurements could be made there. The measurements were to be made using variable-capacitance diaphragm type pressure transducers. They were mounted in such a way that there was no relative motion between the transducers and the vibrating discharge tank. They were also mounted so that the diaphragms were subjected to only pressure forces and not to forces caused by the vibrational acceleration level maintained on the discharge apparatus. The resulting pressure fluctuations recorded were in many cases not repeatable, and no correlation could be made using the data obtained.

It was felt that the inconsistencies found in the resulting data could be attributed to one or both of the following conditions:

(A) In mounting the pressure transducers, it was often necessary to use copper tubing which was 10 to 12 inches in length. The effect of this extra length on the pressure measured by the transducers was not known (see Appendix A).

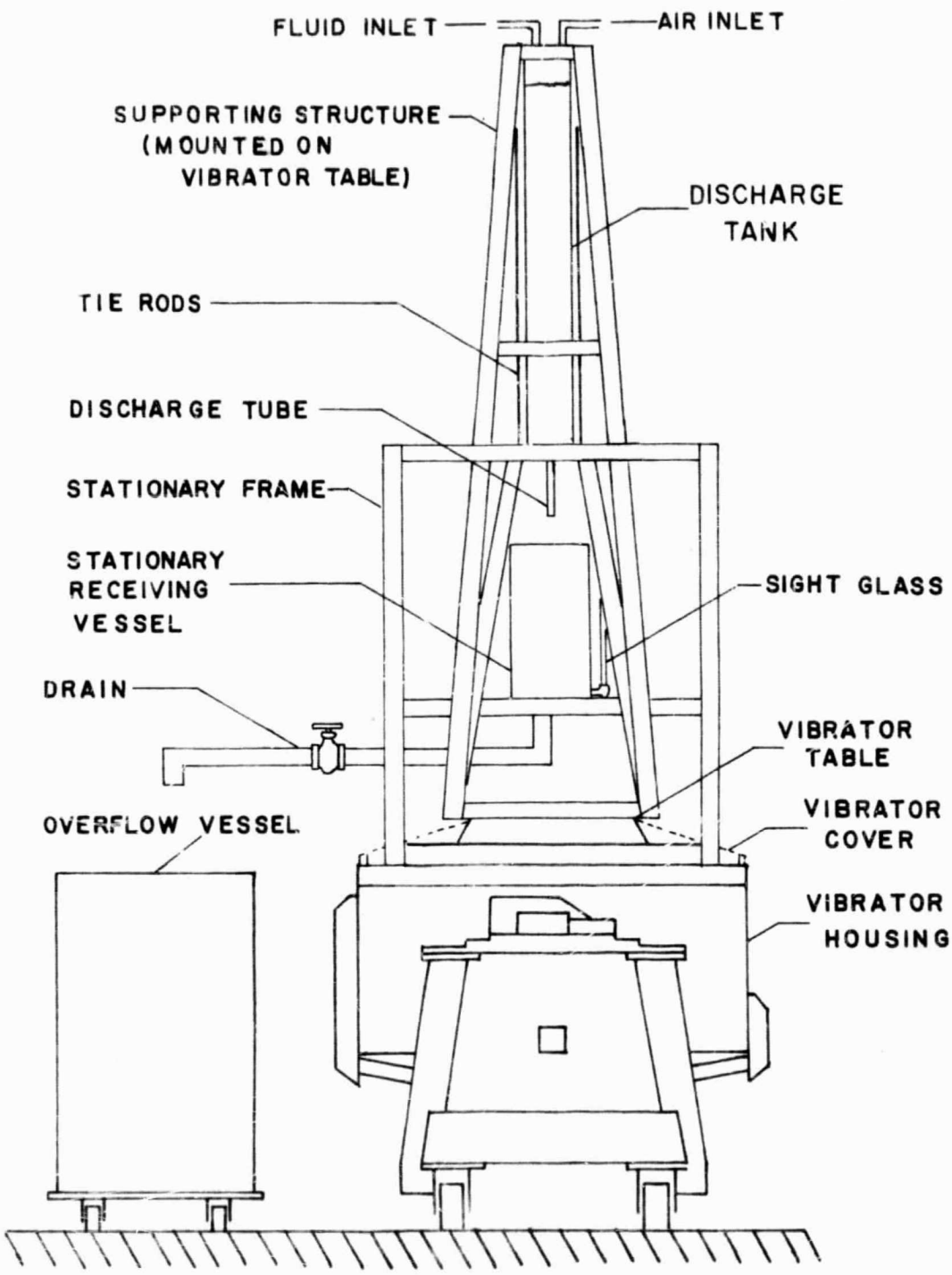

Figure 2. Original Test Apparatus

(B) The test section supporting structure was constructed of long, slender members which were subjected to considerable flexure (Figure 2). Because the supporting structure was not rigid, there was often considerable lateral motion in addition to the longitudinal motion imposed. It was found that the discharge tank was subjected to both rotation about its axis and translation perpendicular to its axis. An accelerometer was mounted perpendicular to the direction of vibratory excitation, and in the worst case it was found that the magnitude of acceleration perpendicular to the longitudinal motion was even greater than the input acceleration.

With these two conditions under consideration, a new test section was designed and built (Figure 3). This new test apparatus had all of the capabilities of the earlier one. Also, it was possible to measure the pressure fluctuations using piezoelectric type pressure transducers. Using this improved apparatus, the experiments of Schoenhals, et al., were repeated and pressure measurements were simultaneously made during the liquid discharge.

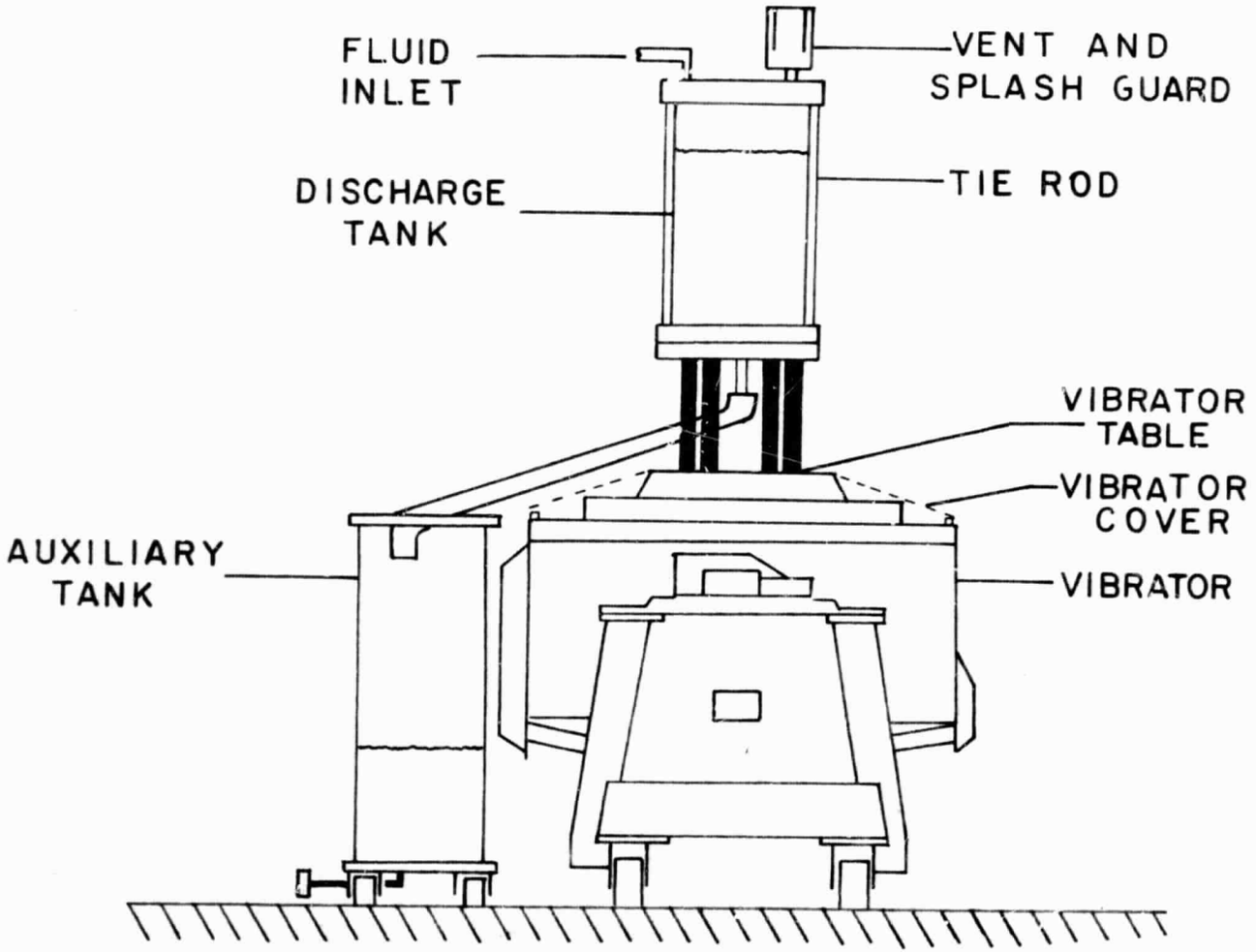

Figure 3. Improved Test Apparatus

3. LITERATURE SURVEY

With the advent of large multistage liquid fueled rockets, a great deal of interest has arisen with regard to the behavior of liquid fuel systems during flight. Fuel and oxidizer tanks are of particular importance because of their effects on vehicle stability. In certain cases self excited longitudinal vibration has been attributed to strong periodic variations in engine thrust which are caused by the combined dynamic interaction of engine, structure and propellant supply system (1, 4).

Abramson (2) has reviewed much of the work done on the behavior of liquids exposed to vibratory environments.

Ponder, Blount and Fritz (5) have studied bubble coalescence in a longitudinally vibrated liquid container. An analytical method was developed to predict the inception and growth rates of gas and vapor bubbles. Bleich (6) has investigated the basic equations governing the motion of small gas bubbles in a liquid in the presence of vibration. The mechanism which causes bubbles to move contrary to gravity is also explained. The cyclic migration of bubble clusters in a vibrating liquid column has been investigated by Buchanan, Jameson, and Odjoe (7). Kana and Dodge (8) and Schoenhals and Overcamp (9, 10) have also investigated bubble

behavior under the same conditions. Buchanan, et al., have developed an equation which accurately predicts the minimum frequency required for bubble migration. Baird (11) has investigated the dynamics of large bubbles formed in a high viscosity liquid.

In addition to the study of bubble motion, Schoenhals and Overcamp (9, 10) have measured and analytically predicted the pressure distribution in vertically vibrated liquid containers.

Dodge, Kana, and Abramson (12) have analyzed liquid surface oscillations in rigid cylindrical containers exposed to low frequency vibration. They have presented an experimental and analytical study of the nonlinear liquid surface sloshing and jump-phenomenon which occur when a confined liquid is subjected to forced longitudinal acceleration.

Fashbaugh and Streeter (1) and Lehner (4) have developed analog methods to solve the partial differential equations of continuity and momentum describing the unsteady flow occurring in the propulsion system of a rocket during flight.

Winter and Schoehnals (13) have performed a similarity study of gravity and pressure driven liquid discharge from propellant tanks. The study was done using discharge tanks with simplified geometries. The instantaneous liquid height was found as a function of various similarity parameters, namely dimensionless time, pressure drop, and various geometric parameters. Experimental results were presented in

the form of plots of instantaneous dimensionless liquid height versus dimensionless time, and these were compared with analytically predicted results. Test fluids associated with high Reynolds number (water) and with low Reynolds number (glycerin) were used in the experiments.

Schoenhals, Winter and Griggs (3) have investigated the effect of a vibratory environment on the discharge of fluids from discharge tanks of simplified geometries. It was found that there is a flow retardation caused by the vibratory conditions. The magnitude of this flow retardation increases with increasing vibrational acceleration level at constant frequency, and decreases with increasing frequency at constant acceleration level. An investigation of the physical phenomena accompanying discharge under vibratory conditions was also conducted. Photographs depicting the violent surface sloshing, and the formation and migration of bubble clusters were presented. Results of discharge experiments were given by means of plots of the instantaneous dimensionless liquid height versus dimensionless time. Using a visco-elastic model, a prediction of the dimensionless pressure amplitude (independent of vibrational acceleration level) was given as a function of dimensionless frequency.

4. EXPERIMENTAL APPARATUS AND PROCEDURE

4.1 Introduction

In order to experimentally investigate discharge from tanks subjected to longitudinal vibration, it was necessary to design and construct a specialized apparatus. As explained previously, it was desirable to use an apparatus as rigid as possible. A method of measuring the pressure in the discharge tube inlet with both piezoelectric and diaphragm type pressure transducers was incorporated into the inlet design. An auxiliary tank for making flow rate measurements during vibratory experiments was designed and installed (Figure 4).

4.2 Overall Vibratory System and Control Equipment

Vibratory excitation of the test apparatus was supplied by means of a 5000-pound-force electrodynamic shaker system (Figure 1). The system consisted of a Ling-Callidyne Shaker (Figure 4), and a Westinghouse Industrial Audio Amplifier, Type FG-11. The shaker was controlled using an MB Electronics Company Automatic Vibration Exciter Control, Type N-572 (Figure 4). With this vibration control, it was possible to set and maintain a given vibrational acceleration level and frequency during each discharge experiment. The

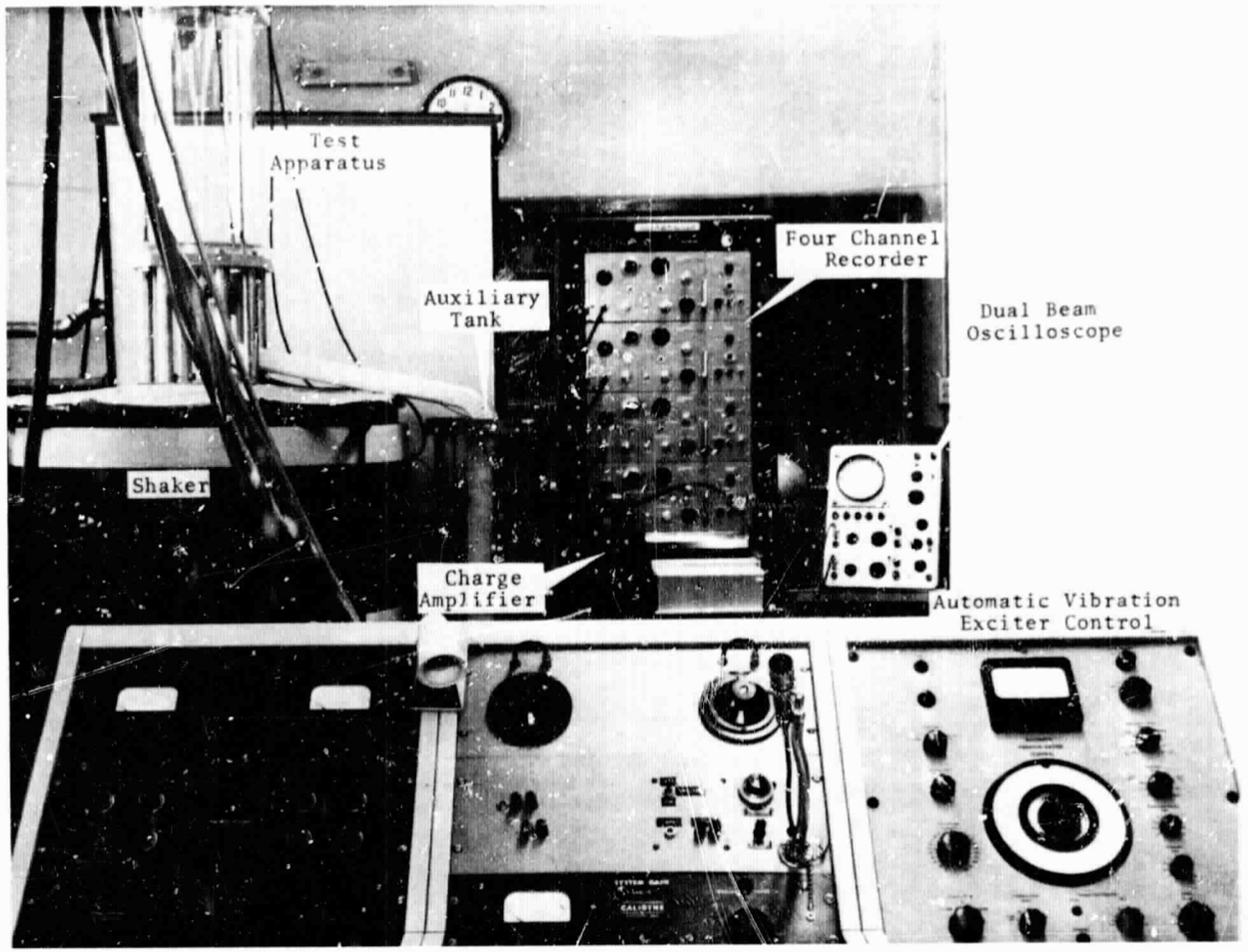

Figure 4. View of Experimental Facility

vibrational acceleration level was monitored with a Brüel and Kjaer Type 4334-150025 accelerometer (Figure 5). The electric charge generated by the accelerometer was converted to voltage and displayed using an Unholtz-Dickie, Model 8PMCVA Charge Amplifier (not shown). The input frequency was accurately measured using a Computer Measurements Corporation Model 226-A Universal Timer-Counter.

4.3 Test Apparatus

4.3.1 Supporting Structure

The test apparatus was rigidly attached to the vibrator table of the shaker by means of eight 1½ inch diameter twelve inch long A-325 aluminum rods (Figure 5). A 1¼ inch thick aluminum plate was bolted to these supporting rods. Using ½ inch diameter brass rods, the bottom plate and top plate were held in position with the discharge tank held between them. These brass rods served the dual purpose of holding the discharge tank in position, and of giving the system added rigidity.

4.3.2 Discharge Tank

The discharge tank was constructed using a twelve inch outside diameter, ½ inch wall thickness plexiglass cylinder twenty four inches in length (Figure 5). The cylinder was held between two 1¼ inch plexiglass plates by the brass rods previously described. The top plate had a specially adapted fixture to enable the tank to be filled with the test fluid.

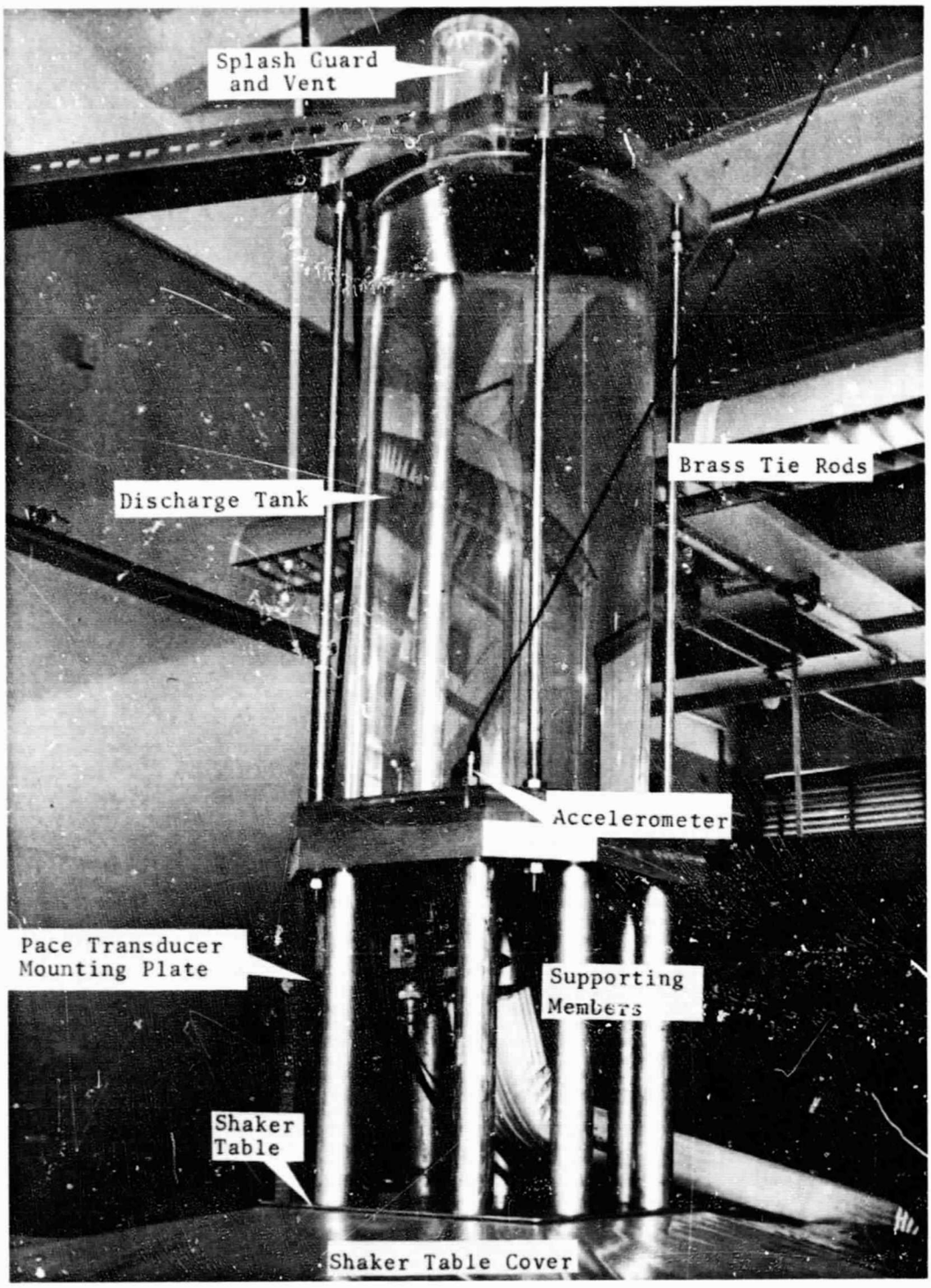

Figure 5. Discharge Tank Mounted on Vibrator Table

A splash guard was also installed to keep the water from splashing out during the early stages of discharge. The bottom plate had a hole in it so that the discharge tube adaptor could be installed and held in position. Both the bottom and top plates contained machined grooves in which the plexiglass cylinder was placed. A rubber gasket was used in each groove. These served as compression gaskets and as seals against leaks.

4.3.3 Discharge Tube

The discharge tube adaptor was made from plexiglass plate and tubing (Figures 6 and 7). The tube was ¼ inches in diameter and 6 inches in length as measured from the top of the bottom plate. Pressures were measured at two locations; in the discharge tube, and at the tank bottom near the entrance to the tube (Figure 7). Pressure measurements were made using two types of pressure transducers. The piezoelectric type (Kistler, Model 701A) was mounted in the adaptor plate itself. The variable capacitance diaphragm type (Pace, Model P7D) had to be mounted on an auxiliary plate which was rigidly bolted to the aluminum rods described previously, (Figure 5). The Pace Transducers were connected to the discharge tube by means of ¼ inch diameter copper tubing (Figure 6).

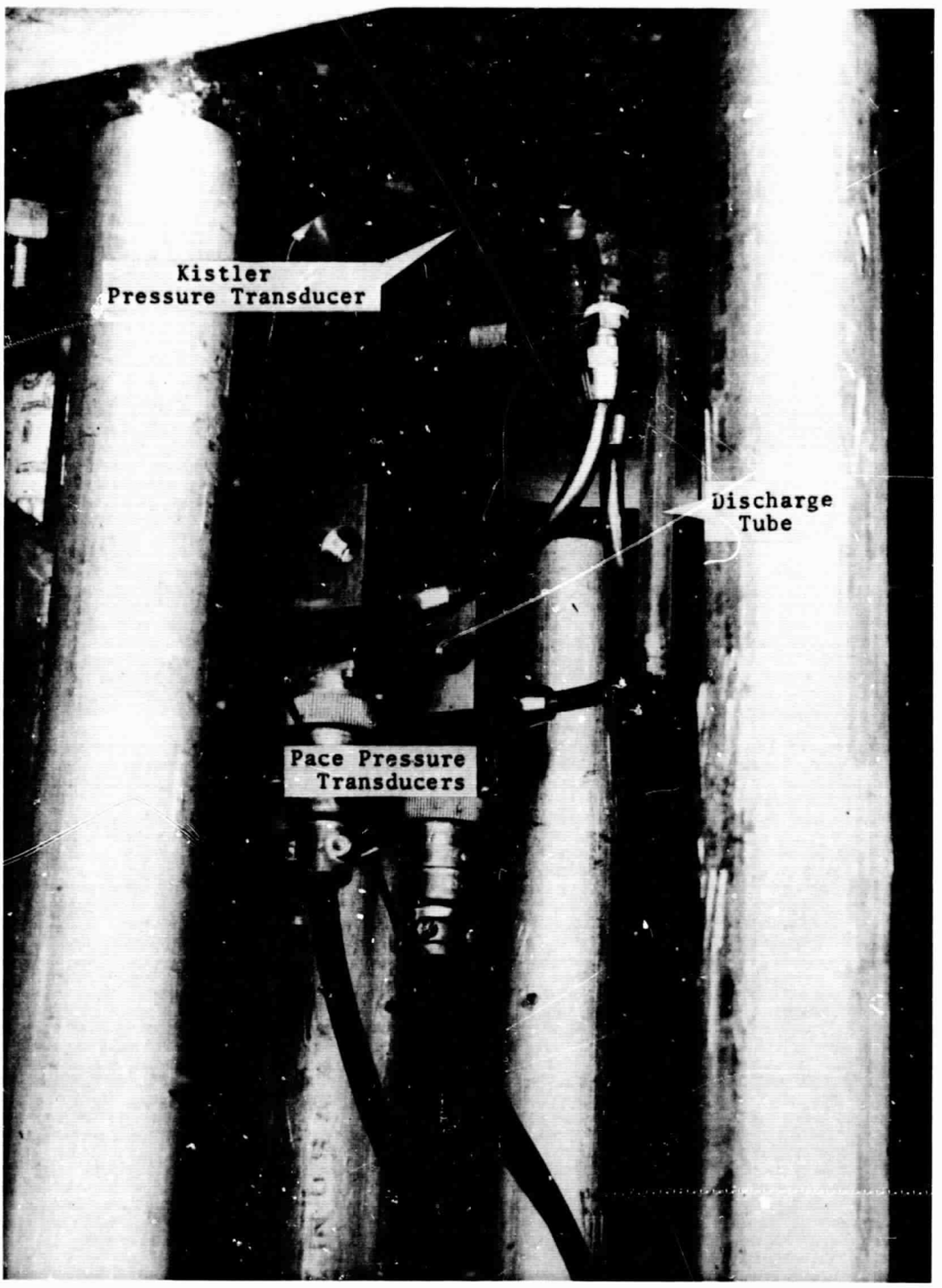

Figure 6. View of Pressure Transducers and Discharge Tube

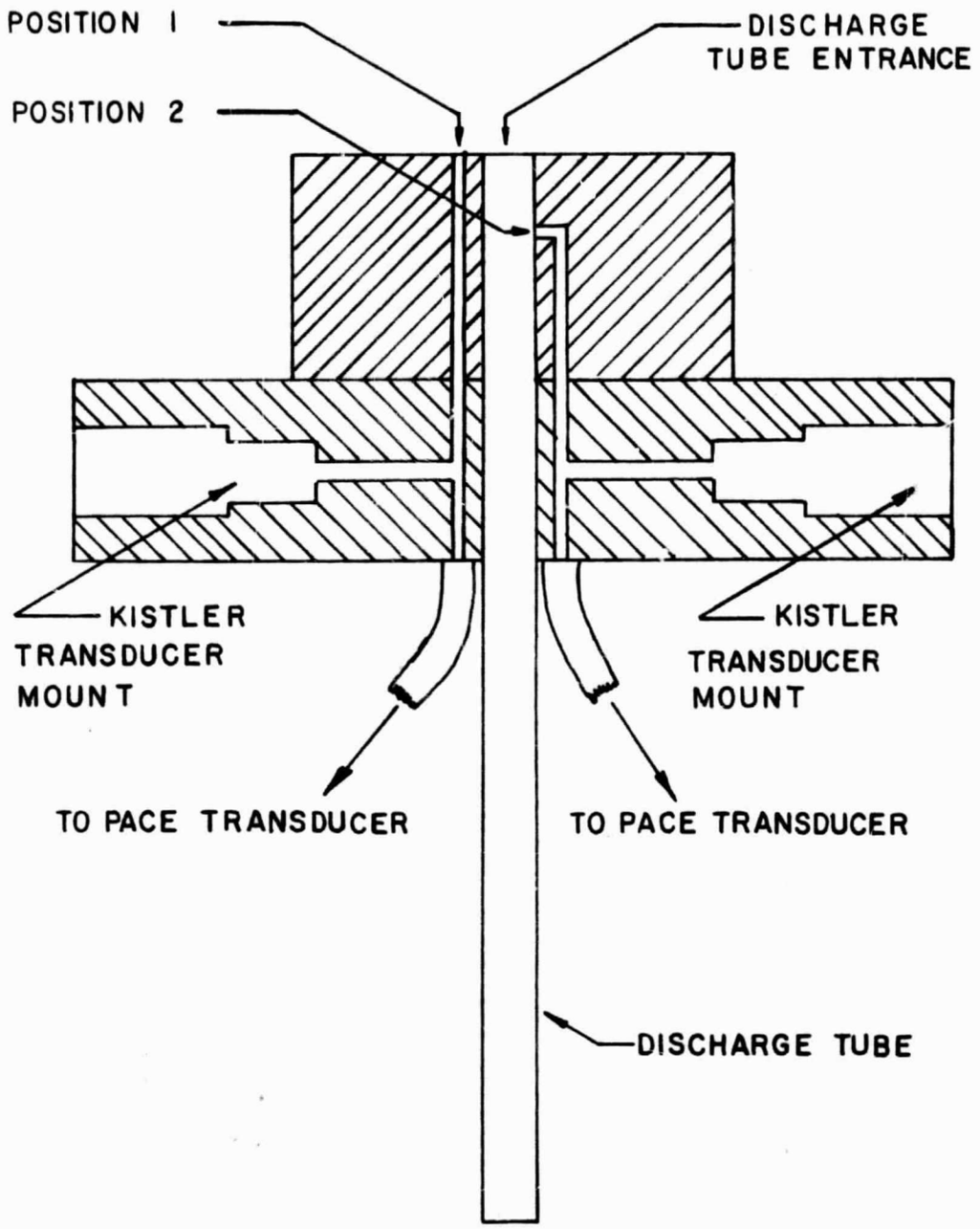

Figure 7. Discharge Tube Adaptor With Pressure Tap Positions

4.3.4 Auxiliary Tank

The auxiliary tank used for measurement of the liquid height as a function of time consisted of a plexiglass cylinder 9 inches in diameter (Figure 4). A Pace pressure transducer was located at the bottom of the tank. With this transducer, it was possible to find the height of water in the auxiliary tank. During discharge experiments, water from the discharge tank flowed from the test cylinder into the auxiliary tank. The pressure at the bottom of the auxiliary tank was recorded as a function of time using the Sanborn Recorder (Figure 4). Since there was a definite relationship between the pressure at the auxiliary tank bottom and the height of liquid in the discharge tank, the liquid height was known as a function of time.

4.4 Procedure

Before each discharge experiment, the liquid height in the auxiliary tank was brought to a predetermined reference level. The pressure at the auxiliary tank bottom was then recorded on a Sanborn Model 154-100B Four Channel Recorder (Figure 4). The pressure signal from the Pace transducer was conditioned using a Pace Engineering Company Carrier Demodulator, Model CD10 before being introduced into the Sanborn Recorder.

The discharge tank was filled to a predetermined initial height of either 28 or 17 inches. The shaker system was

activated. The vibrational acceleration level and input frequency were set using the vibration control (Figure 4). The input frequency was accurately checked with the electronic counter. The acceleration level was monitored with an accelerometer (Figure 5). When both the acceleration and frequency level were adjusted to the desired values, discharge was initiated.

The time-averaged pressure and the pressure amplitude in the discharge tube inlet were measured with two different pressure transducer systems (Figure 6 and 7). The Pace system was similar to that employed in the auxiliary tank. In order to obtain the time-averaged pressure acting in the inlet, an electrical filtering system was employed. This system could be switched on or off during discharge experiments thus giving either time-averaged inlet pressure or the pressure amplitude, whichever was desired. The pressure amplitude was measured using a Kistler Pressure Transducer Model 701A (Figure 6). The charge generated by the pressure transducer was converted to voltage using a Kistler Charge Amplifier, Model 504 (Figure 4). The signal was then displayed on a Tektronix Model 502A Dual Beam Oscilloscope (Figure 4).

5. ANALYSIS

5.1 Introduction

Two separate analyses of the physical phenomena encountered are presented in this section. The first is an analysis of discharge from a liquid discharge tank which is vibrating at low frequencies. D'Alembert's principle is employed in this analysis. The resulting expression is one which predicts the time averaged mass flow rate of fluid from a vibrating discharge tank. This time averaged value is compared to the flow rate from a stationary discharge tank, and a prediction is made as to the functional dependence of the flow retardation on the vibrational acceleration level.

The second analysis yields a prediction of the pressure amplitude at the bottom of a closed container. Studies of this type have been given previously and are cited in References 3, 8, and 9. Only the pertinent features of the analysis are presented here. The dimensionless pressure amplitude is given as a function of the dimensionless angular frequency.

5.2 Quasi Steady Analysis

Consider an incompressible fluid being discharged in a quasi steady manner from a discharge tank oscillating at

very low frequency (Figure 8). The velocity of a fluid particle of mass m, moving with respect to the fixed coordinate system, is v_f. The velocity of this particle with respect to a coordinate system moving with the tank velocity v_t, is v_{ft}. The velocity of the fluid element v_f, is the vector sum of the absolute velocity of the tank v_t, and the relative velocity v_{ft}.

$$\bar{v}_f = \bar{v}_t + \bar{v}_{ft} \tag{1}$$

The equation of motion of the particle for the y direction is

$$\sum F_y = m \frac{dv_f}{dt} = m \frac{d}{dt}(v_t + v_{ft}) \ . \tag{2}$$

Here the vector symbols are deleted since only the y direction is considered. The only forces acting on the particle are the net pressure force, F_p, the net viscous shear force, F_s, and the gravitational force, mg. Thus equation 2 can be written as

$$m \frac{d}{dt}(v_t + v_{ft}) = F_p + F_s - mg \tag{3}$$

or

$$m \frac{dv_{ft}}{dt} = F_p + F_s - mg - m \frac{dv_t}{dt} \ . \tag{4}$$

$\frac{dv_t}{dt}$ is the acceleration of the vibrating tank, and is equal to $g_v \cos \omega t$. Now,

$$m \frac{dv_{ft}}{dt} = F_p + F_s - mg - mg_v \cos \omega t \tag{5}$$

or

$$m \frac{dv_{ft}}{dt} = F_p + F_s - m(g + g_v \cos \omega t) \tag{6}$$

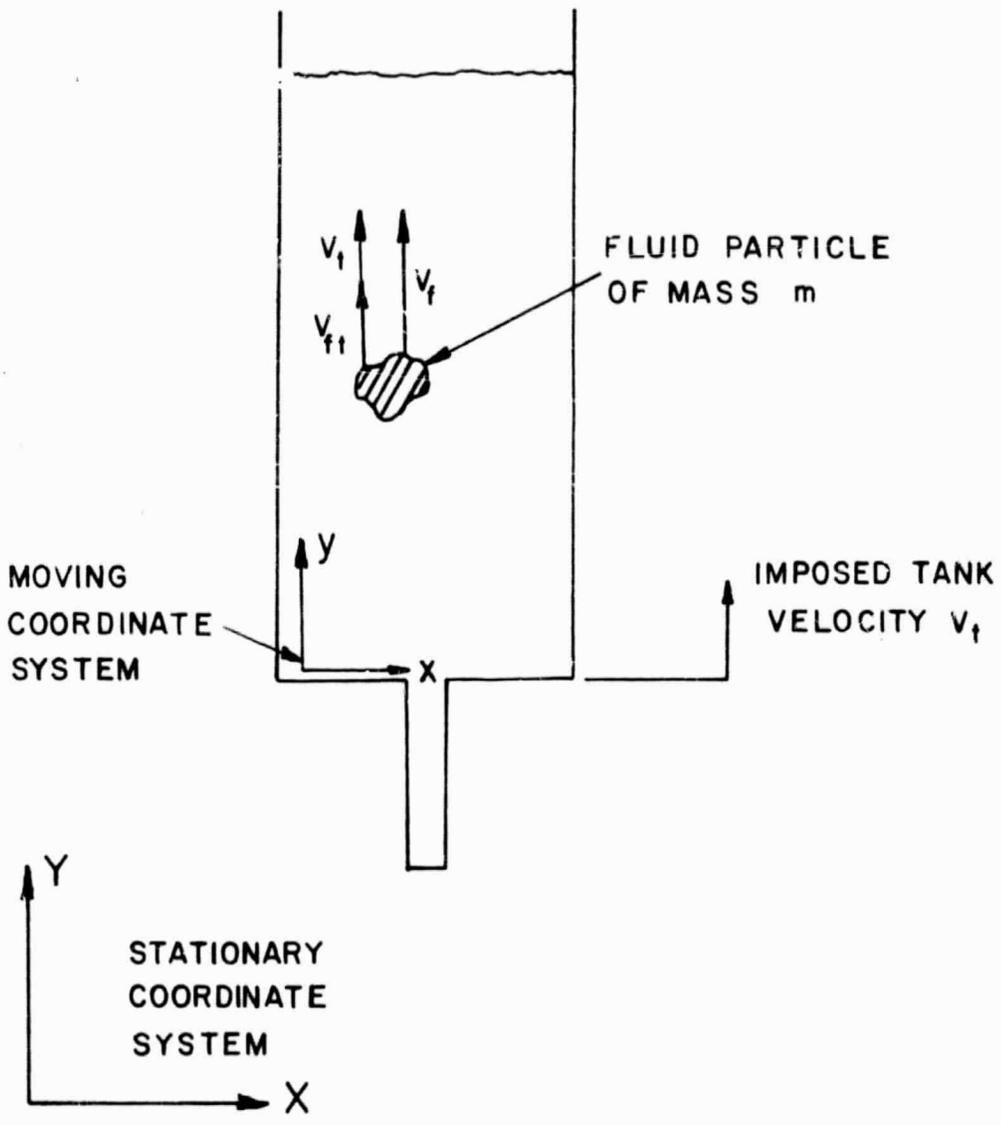

Figure 8. Container Geometry Used in Analysis

The term ($-mg_v \cos \omega t$) is the D'Alembert force, i.e., the effective body force acting on the fluid particle caused by the acceleration imposed on the discharge tank.

Now consider an incompressible fluid being discharged under the influence of a gravitational field g. In the absence of vibration the quasi steady flow rate, according to the Bernoulli equation, is proportional to $\sqrt{gy}$. When the tank is vibrated the effective body force field acting on the fluid in the container is ($g + g_v \cos \omega t$) according to Equation (6). If the oscillations are of very low frequency, the fluid responds to this gravitational field in a quasi-steady time varying manner. Again employing the Bernoulli equation, one obtains the result that the instantaneous velocity is proportional to $\sqrt{y|g + g_v \cos \omega t|}$. Thus the instantaneous mass flow rate is proportional to the instantaneous velocity;

$$\dot{m} \sim v \sim \sqrt{y|g + g_v \cos \omega t|} \quad . \tag{7}$$

If the instantaneous mass flow rate is integrated over the complete vibration cycle, the time averaged value can be obtained as

$$\bar{\dot{m}} \sim \frac{1}{2\pi} \int_0^{2\pi} \sqrt{y|g + g_v \cos \omega t|} \; d(\omega t) \tag{8}$$

If this relation is integrated over the completed vibration and compared with the result for $g_v = 0$, a prediction of the flow retardation is obtained. The percent retardation is

$$\text{Percent Retardation} = \frac{\dot{m}_{\text{no vibration}} - \dot{m}_{\text{vibration}}}{\dot{m}_{\text{no vibration}}} \qquad (9)$$

Equation (9) may be written as

$$\text{Percent Retardation} = 1 - \frac{\frac{1}{2\pi}\int_0^{2\pi} \sqrt{y\,|g + g_v \cos \omega t|}\; d(\omega t)}{\sqrt{gy}} \qquad (10)$$

or

$$\text{Percent Retardation} = 1 - \frac{1}{2\pi}\int_0^{\pi} \sqrt{|1 + G \cos \omega t|}\; d(\omega t) \qquad (11)$$

This procedure has been carried out by Schoenhals, Winter, and Griggs (3). This prediction is presented in Figure 9.

5.3 Pressure Amplitude at the Bottom of a Closed Container

Consider the longitudinal one-dimensional wave behavior of a compressible fluid in a cylindrical container with elastic walls. (For a detailed analysis, see References 3, 8, and 9.) For the container shown in Figure 10, the equation of motion is

$$\frac{\partial^2 Y}{\partial t^2} = c^2 \frac{\partial^2 Y}{\partial x^2} + g \qquad (1)$$

where c is the longitudinal wave velocity given by

$$c = \frac{a}{\sqrt{1 + \frac{B}{\left(\frac{S}{D} E\right)}}} \qquad (2)$$

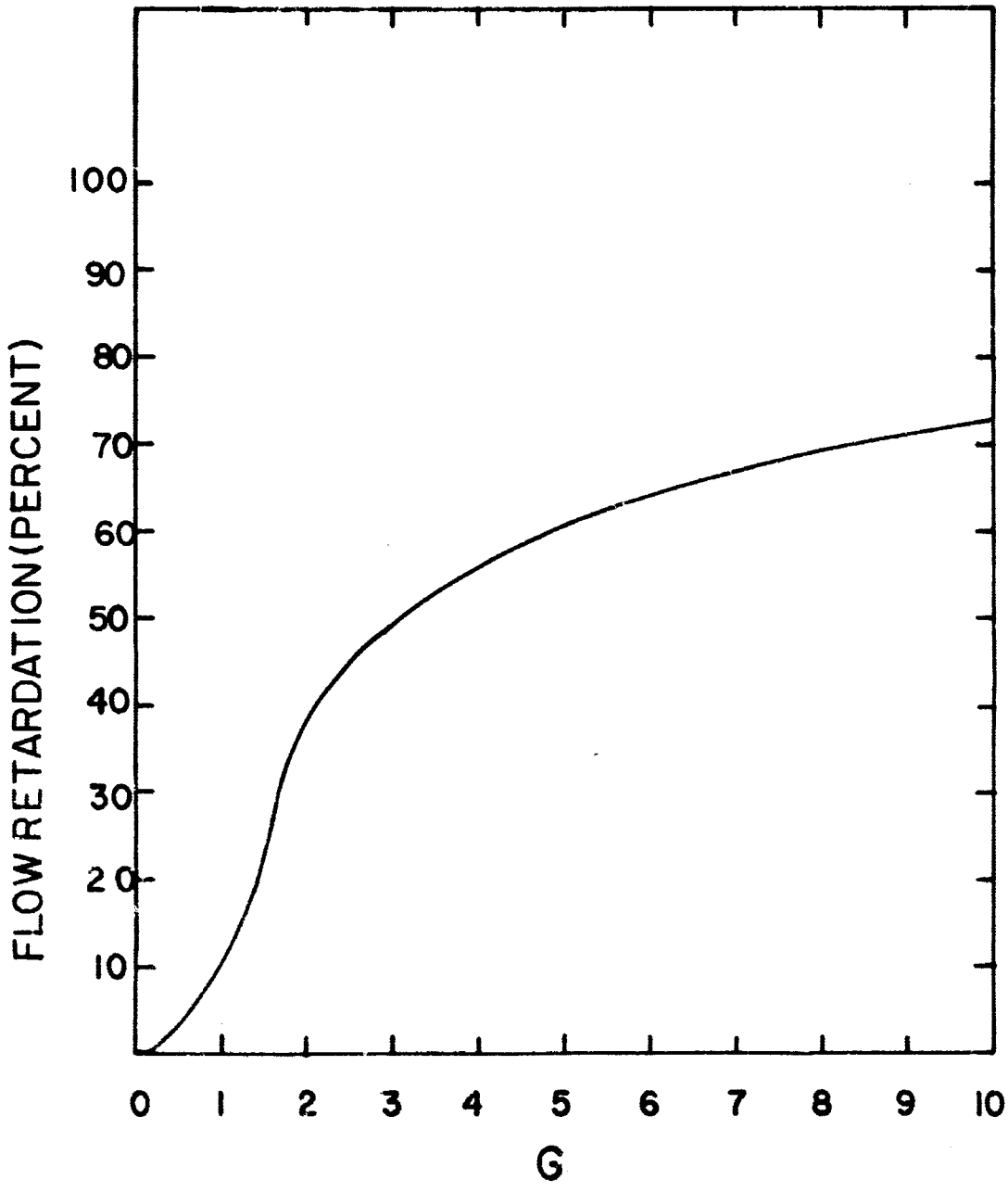

Figure 9. Analytical Prediction of Flow Retardation At Very Low Frequencies

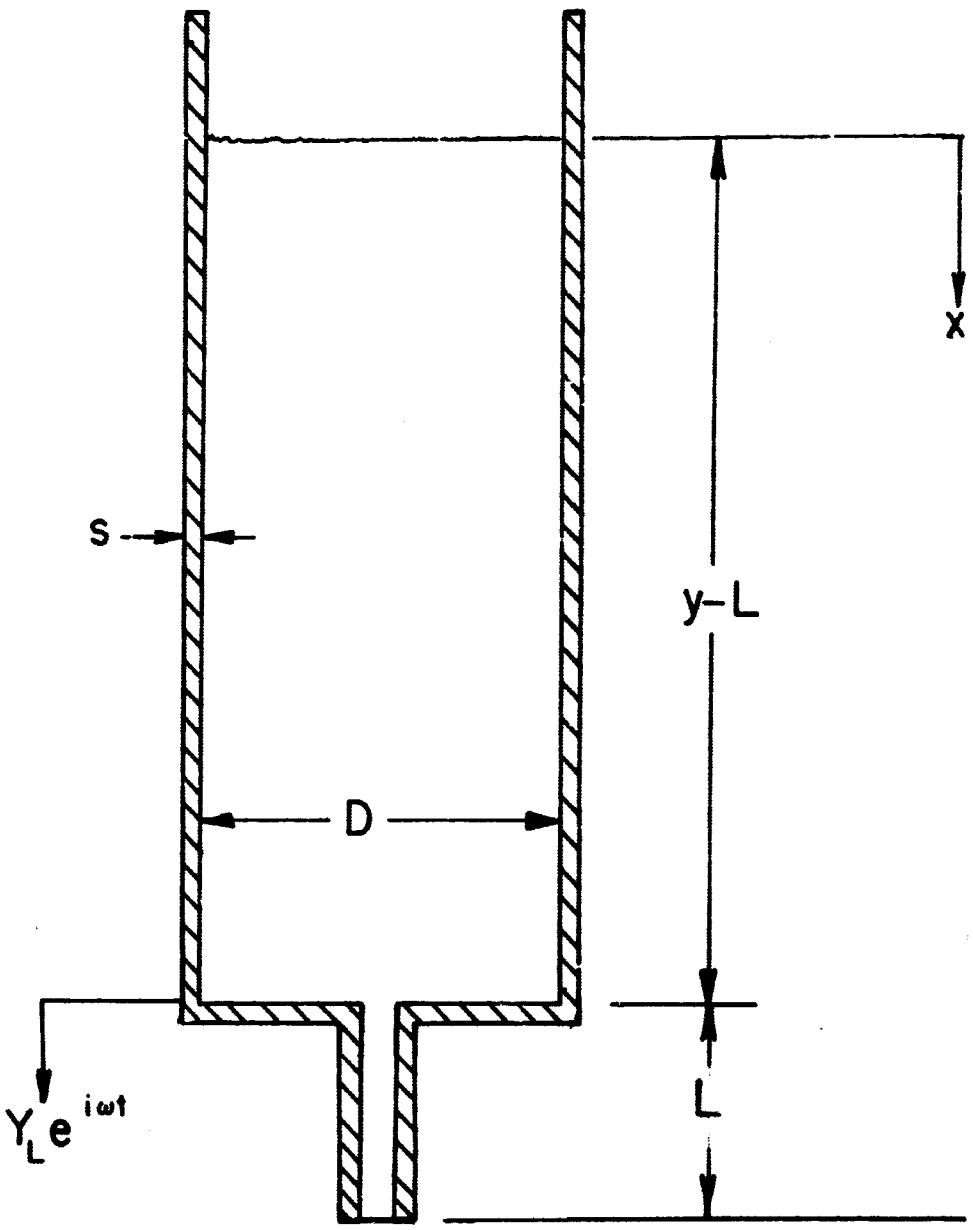

Figure 10. Container Geometry Used in Analysis

In Equation (2) a is the acoustic velocity for the fluid; B is the fluid bulk modulus; D is the cylinder diameter; E is Young's modulus for the container and s is the thickness of the container wall. The boundary conditions are

$$-E_x \frac{\partial Y}{\partial x}(o, t) = P_u \tag{3}$$

and

$$Y(y - L, t) = Y_L e^{i\omega t} \tag{4}$$

The solution to the boundary value problem is of the form

$$Y(x,t) = Y_o(x) + Y_1(x,t) . \tag{5}$$

The pressure distribution is obtained by differentiating the solution Y(x,t). The pressure distribution at any position x is given by

$$p(x,t) = P_u + \rho g x + \rho g_v \left(\frac{c}{\omega}\right) \frac{\sin \frac{\omega x}{c}}{\cos \frac{\omega(y-L)}{c}} e^{i\omega t} \tag{6}$$

The pressure distribution at the container bottom (x = Y-L) is given by

$$p(y-L,t) = P_u + \rho g(y-L) + \rho g_v \left(\frac{c}{\omega}\right) \frac{\sin \frac{\omega(y-L)}{c}}{\cos \frac{\omega(y-L)}{c}} e^{i\omega t} \tag{7}$$

The steady component of pressure consists of two parts, the ullage pressure, P_u, and the hydrostatic pressure, $\rho g(y-L)$. The real part of the oscillating pressure, p_o, is given by

$$P_o = \rho g_v \left(\frac{c}{\omega}\right) \left[\tan \frac{\omega(y-L)}{c}\right] \cos \omega t. \tag{8}$$

This result was obtained by Schoenhals and Overcamp (8, 9). It is valid, provided that no bubbles are contained in the fluid. If bubbles are present, the oscillating component of pressure is altered.

The first resonant frequency is obtained from Equation (8). It occurs when $\frac{\omega(y-L)}{c} = \frac{\pi}{2}$. The pressure amplitude becomes very large at resonance, even if g_v is small. The dimensionless pressure amplitude, $\frac{P_o}{\rho g_v (y-L)}$, as a function of the dimensionless angular frequency, $\frac{\omega(y-L)}{c}$, was presented by Schoenhals, Winter and Griggs (3), and is illustrated in Figure 11. For the system used in the present study the resonant frequency was about 170 cps, and for all but a few discharge experiments the resonant frequency was well above the imposed frequency.

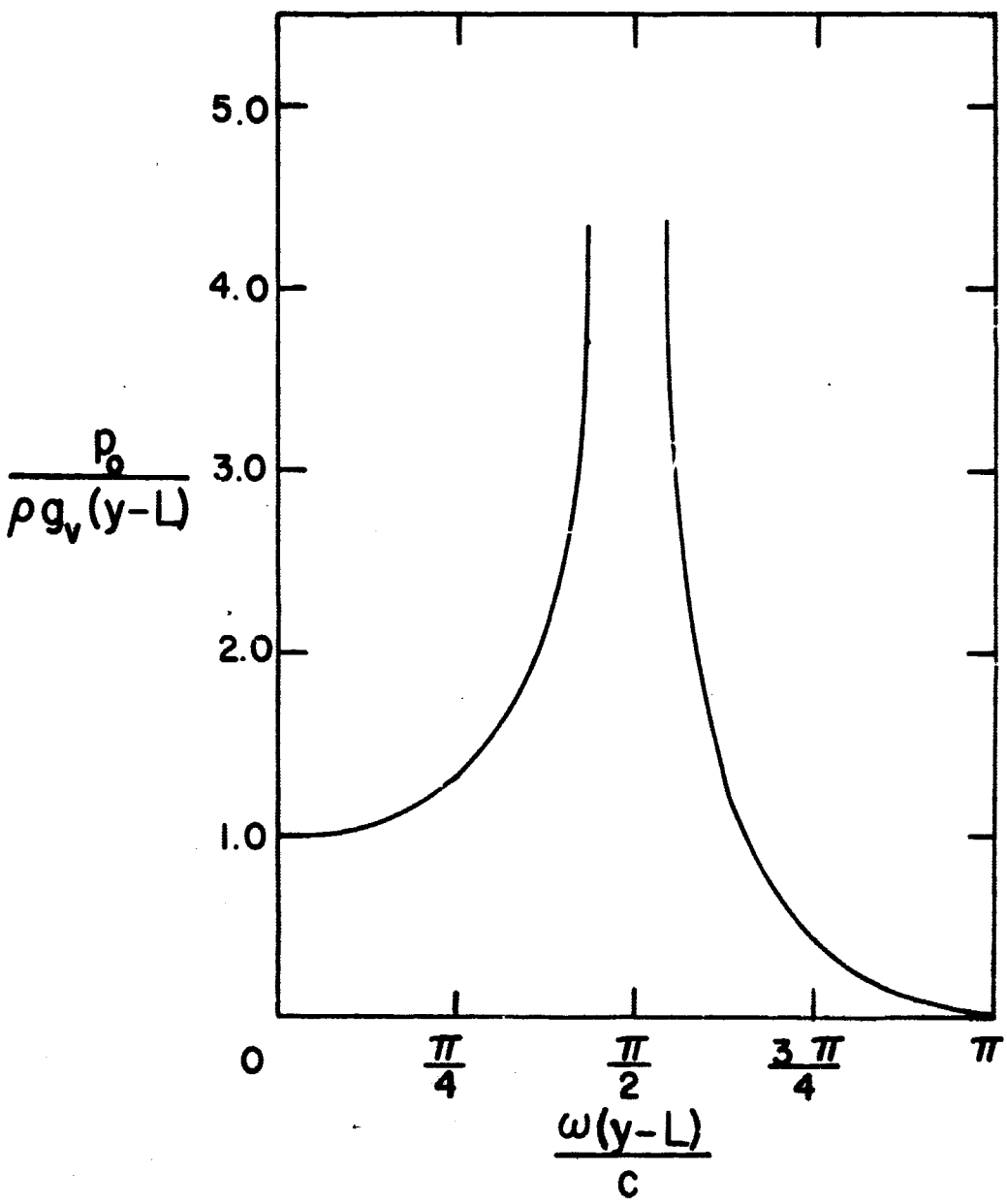

Figure 11. Variation of Pressure Amplitude With Dimensionless Vibrational Frequency

6. RESULTS

6.1 Introduction

The data obtained from measurements performed are presented in this chapter. Results are first given in the form of plots of dimensionless liquid height versus dimensionless time. Then, experimental measurements of the pressure amplitude at the inlet of the discharge tube are plotted for both transient discharge and for a closed bottom container in the absence of flow. Predictions of the total discharge time, as determined from the analysis of Reference 3 are compared with the corresponding total discharge times observed experimentally. Finally, measurements of the time averaged pressure at the discharge tube inlet during discharge are presented.

6.2 Measurements of Liquid Height As a Function of Time

The measurements described in this section qualitatively agree with those obtained by Schoenhals, Winter, and Griggs (3). In Figures 12 and 13, the retardation effect of increasing G-level on the discharge process is illustrated for various frequencies of vibration. In Figures 14 through 21 the data has been plotted to show the attenuating effect of frequency.

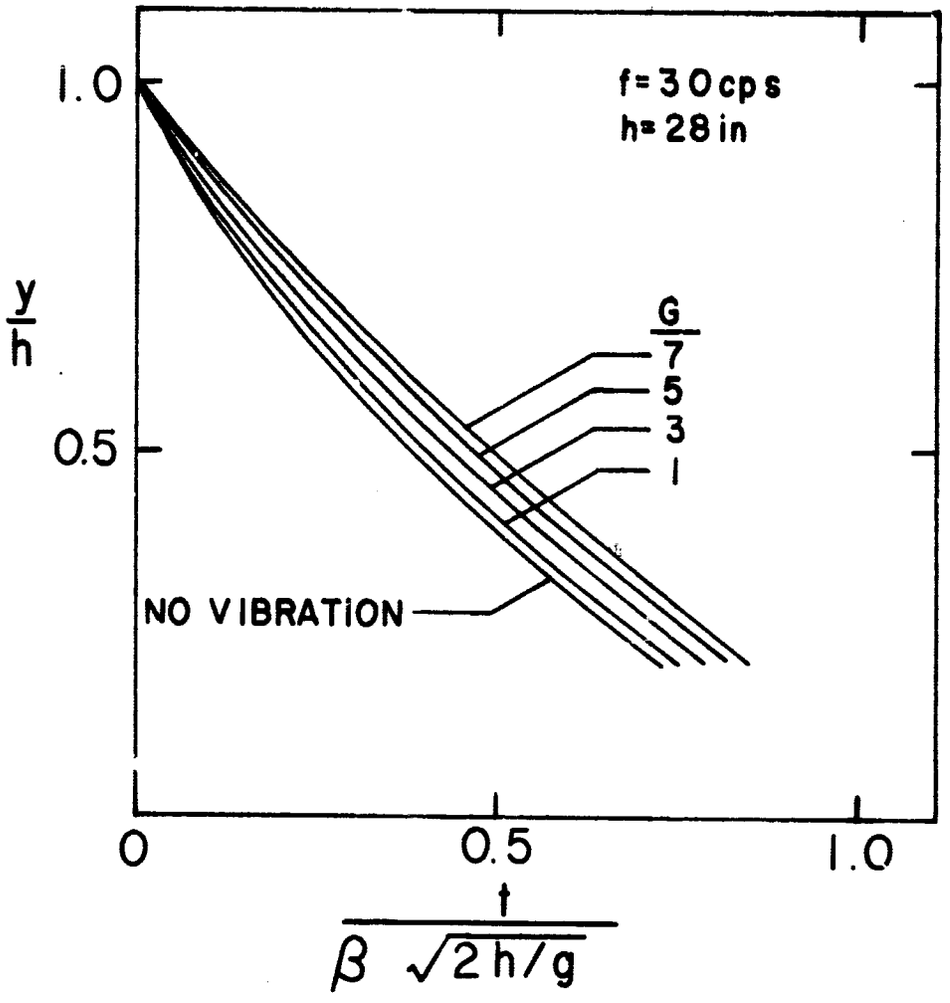

Figure 12. Variation of Dimensionless Liquid Height With Dimensionless Time for Various Acceleration Levels

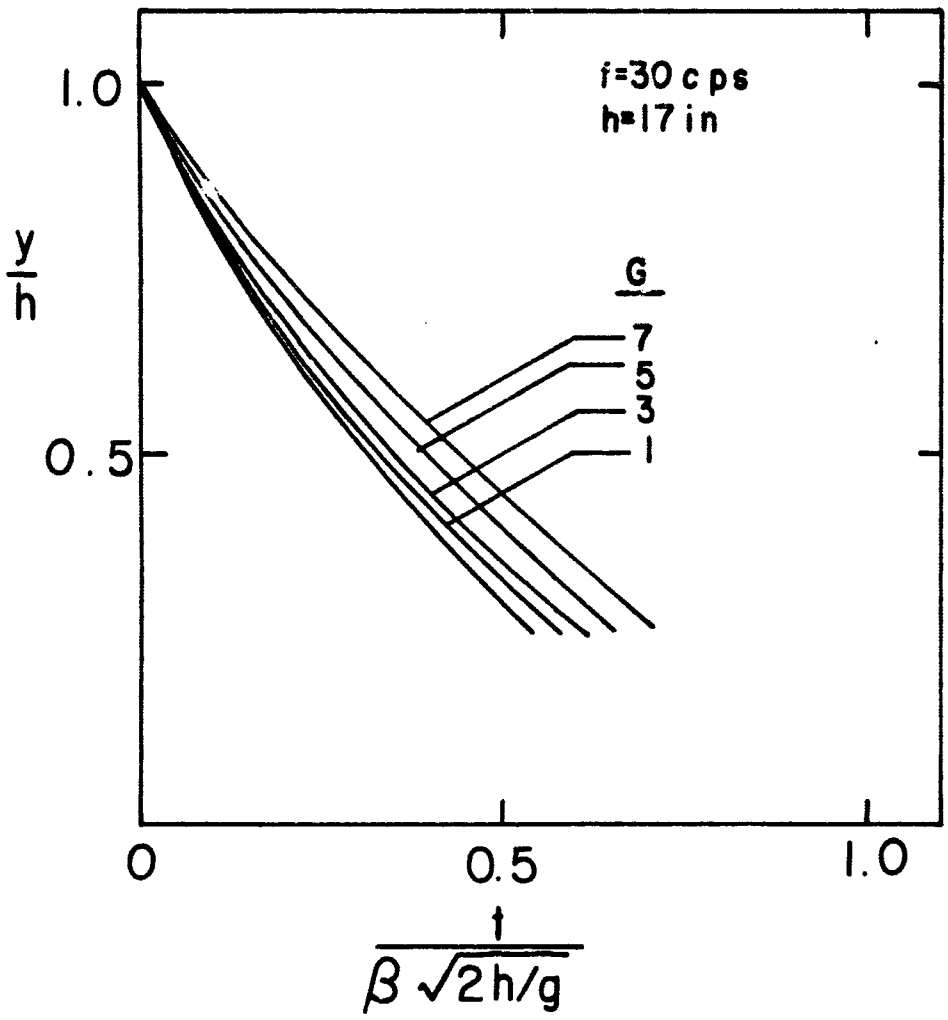

Figure 13. Variation of Dimensionless Liquid Height With Dimensionless Time for Various Acceleration Levels

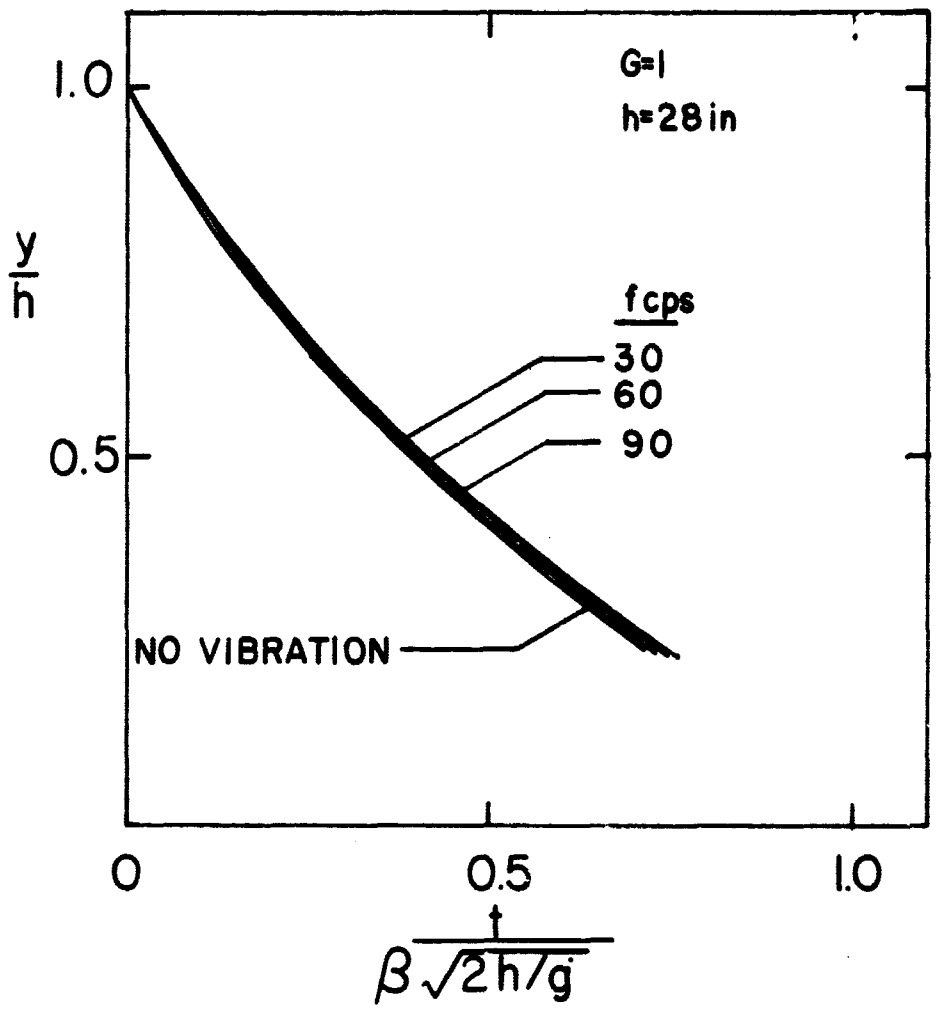

Figure 14. Variation of Dimensionless Liquid Height With Dimensionless Time For Various Frequencies

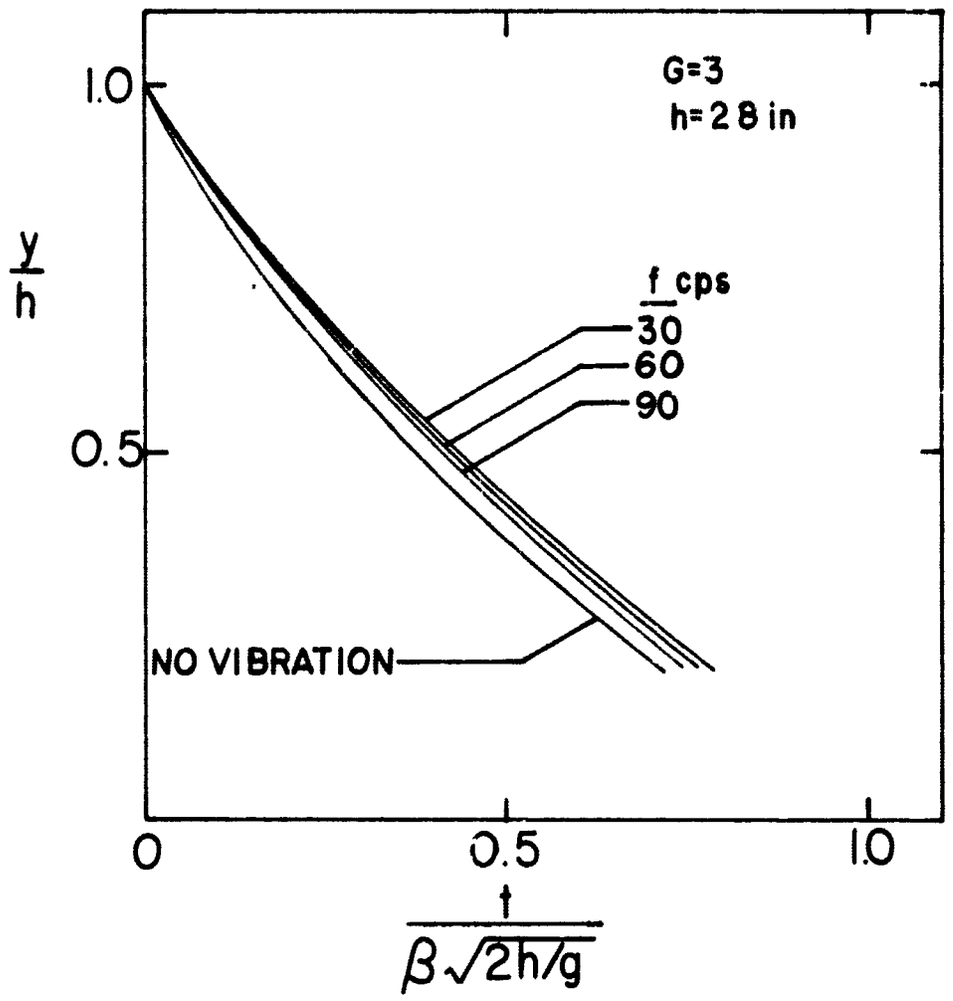

Figure 15. Variation of Dimensionless Liquid Height With Dimensionless Time for Various Frequencies

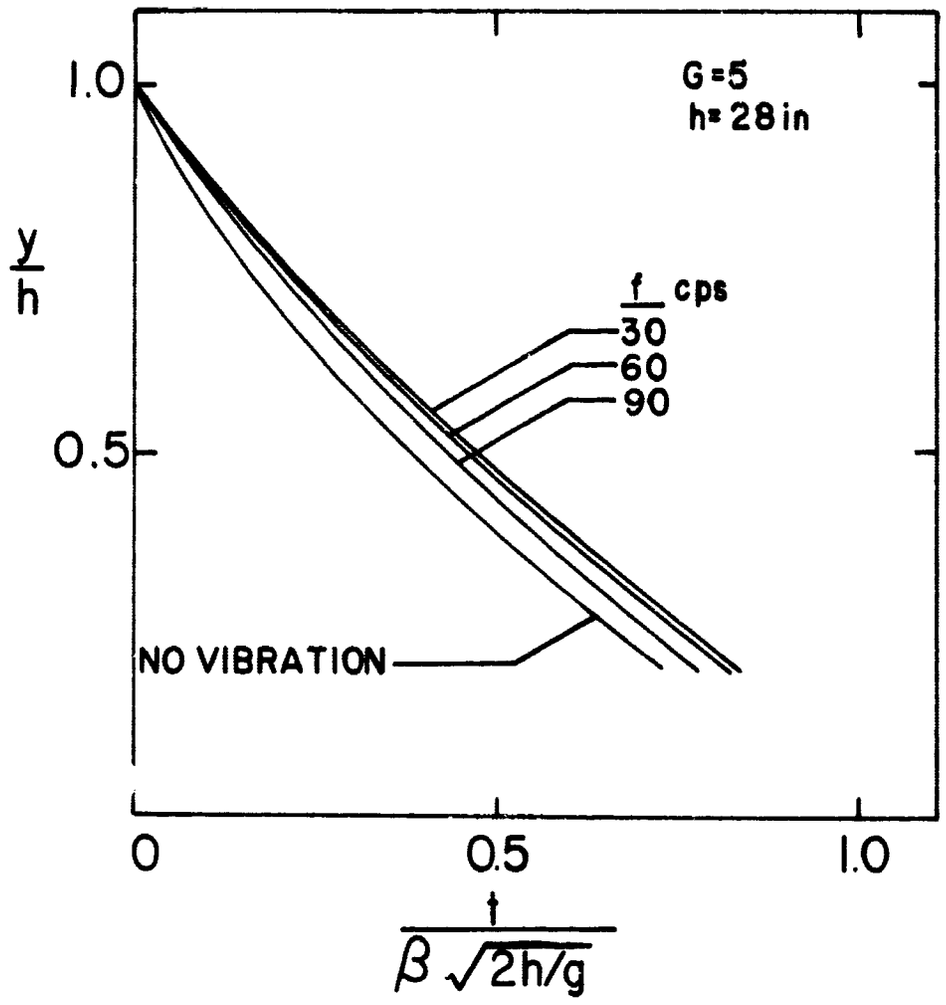

Figure 16. Variation of Dimensionless Liquid Height With Dimensionless Time for Various Frequencies

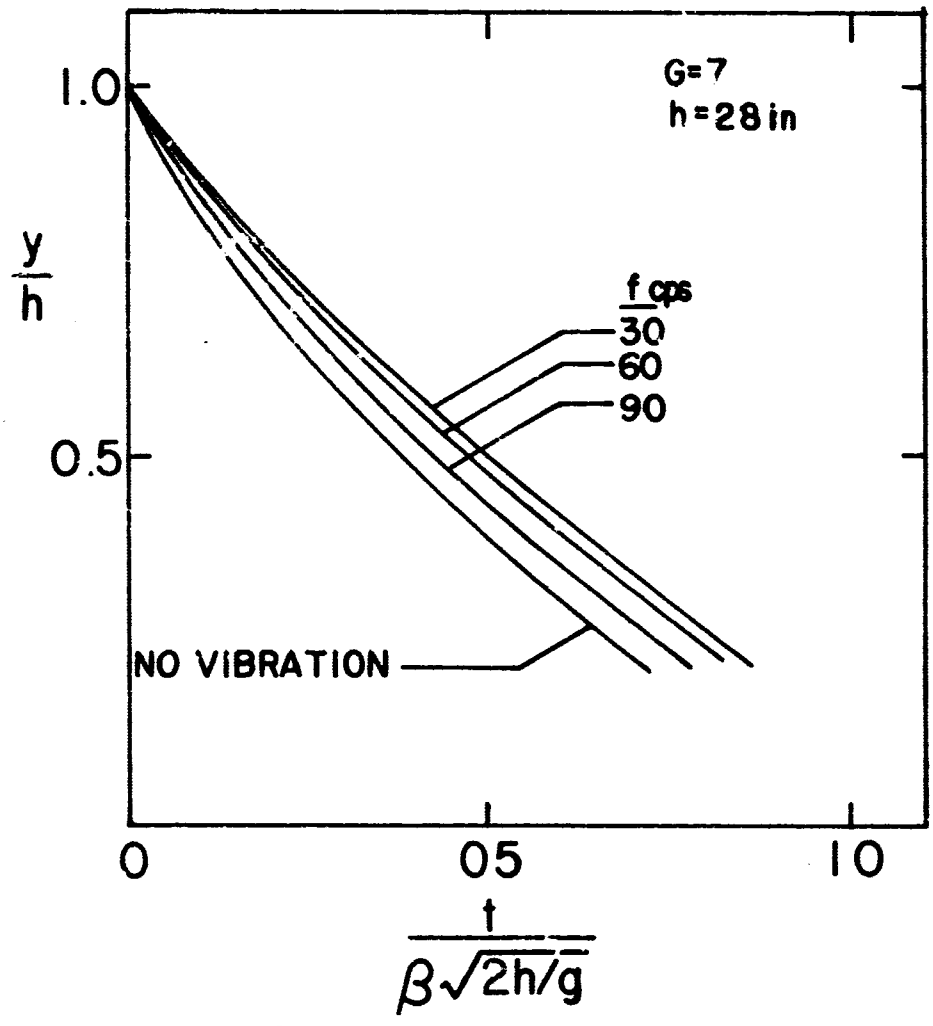

Figure 17. Variation of Dimensionless Liquid Height With Dimensionless Time for Various Frequencies

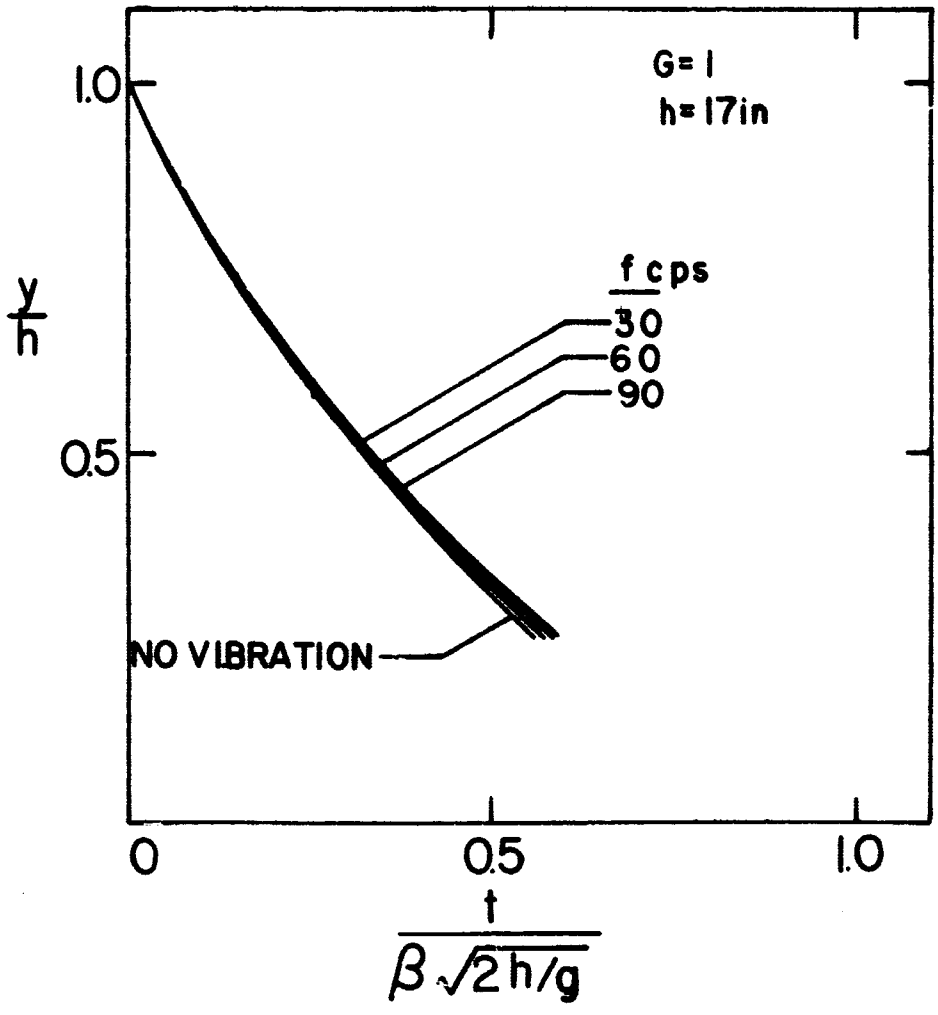

Figure 18. Variation of Dimensionless Liquid Height With Dimensionless Time for Various Frequencies

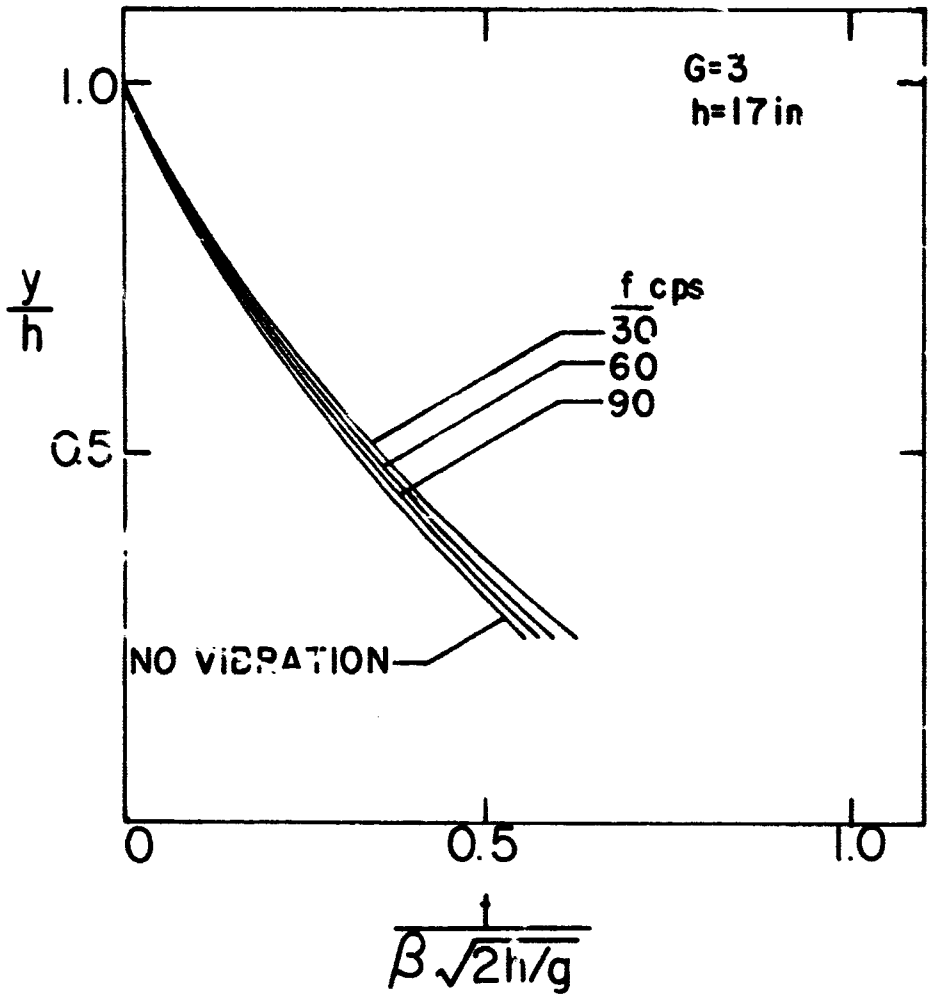

Figure 19. Variation of Dimensionless Liquid Height With Dimensionless Time for Various Frequencies

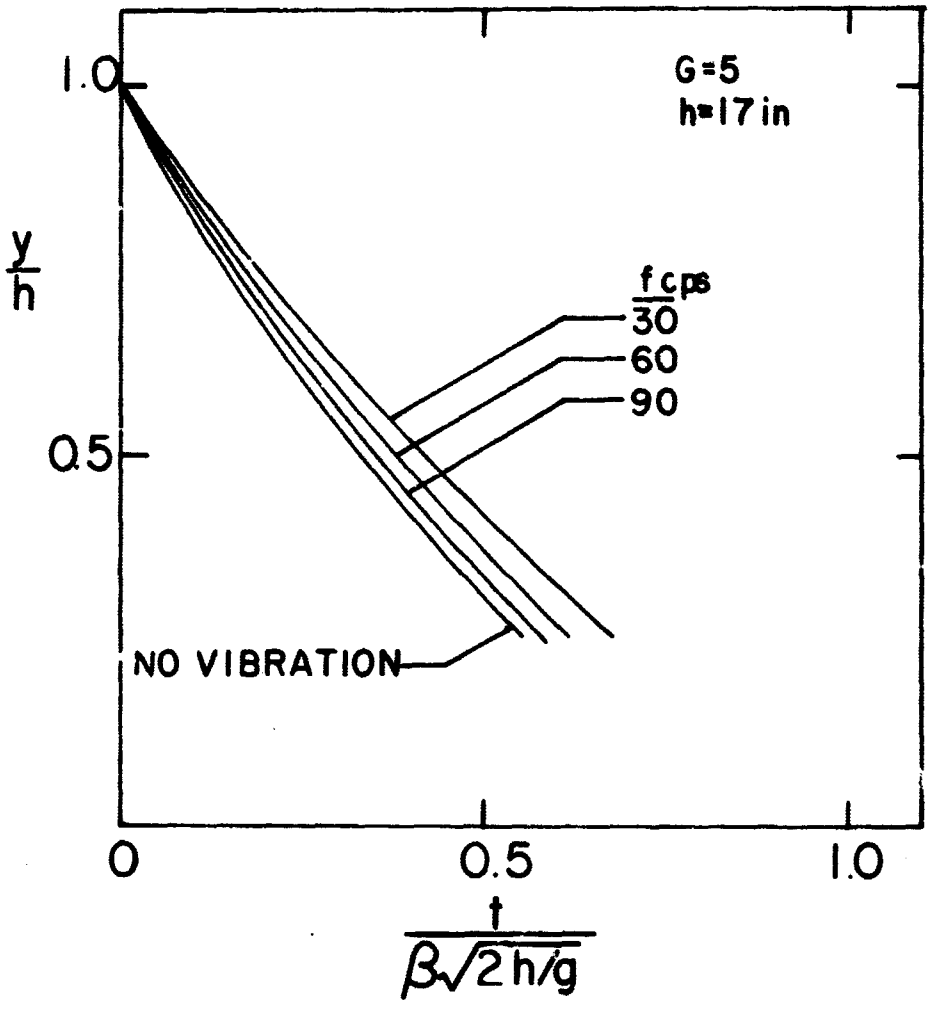

Figure 20. Variation of Dimensionless Liquid Height With Dimensionless Time for Various Frequencies

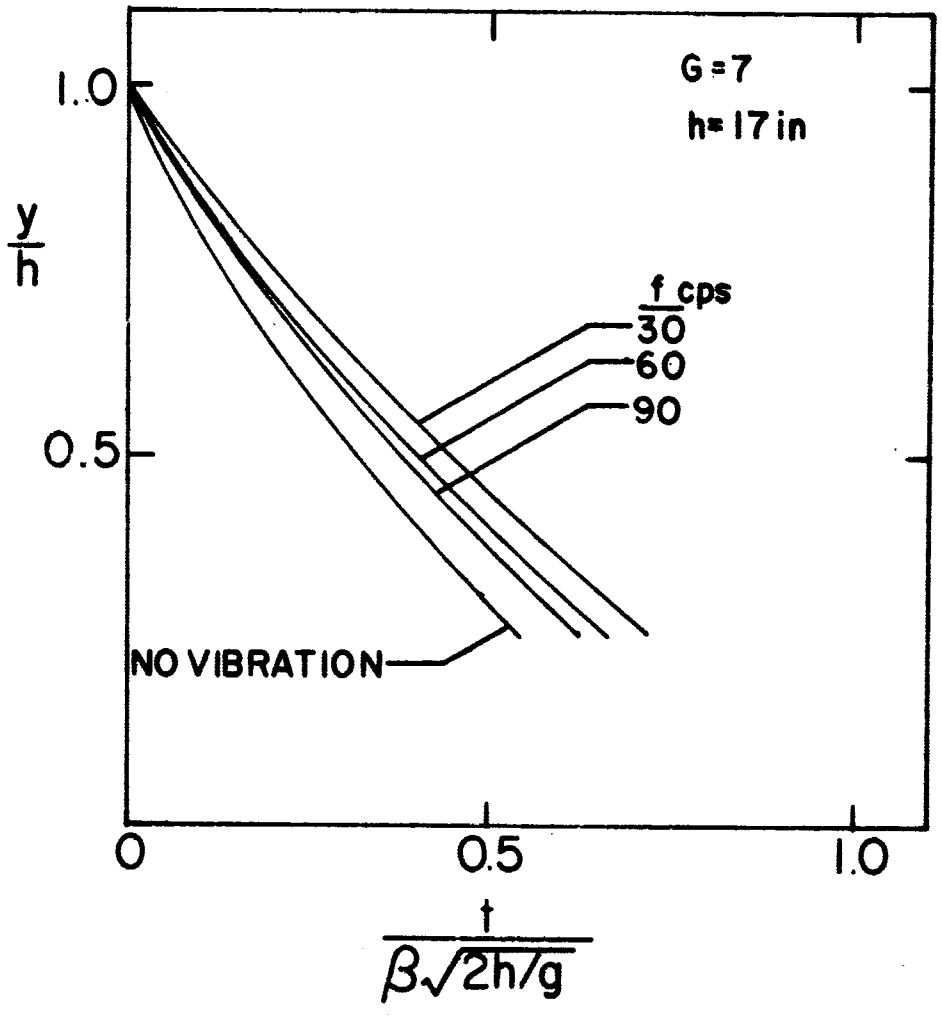

Figure 21. Variation of Dimensionless Liquid Height With Dimensionless Time for Various Frequencies

6.3 Measurements of Pressure Amplitudes

Experiments were first performed with the discharge tube closed so that no flow from the tank occurred. The measurements were repeated for the discharge situation by simply opening the discharge tube. Measurements were made at two positions, namely in the entrance region of the discharge tube, and at the tank bottom very close to the discharge tube entrance.

In Figures 22 and 23, the pressure amplitudes measured at position 1 and 2 respectively, are compared with the predictions for a closed bottom container (Figure 11). These measurements were obtained by first filling the discharge tank to a specified level and then beginning at low frequency (5 cps), increasing the frequency up to 200 cps. The first natural frequency was encountered at about 175 cps. The natural frequency is indicated by the large pressure amplitudes which have been discussed in Section 5.3. Figures 22 and 23 contain the comparison of the experimental data with the closed bottom prediction.

Experimental verification of the one dimensional wave theory (3, 8, 9, 10) by varying the liquid height, y, is presented in Figure 24. In these experiments the dimensionless frequency was varied by varying (y-L). The pressure amplitudes measured at position 1 follow only the trend of the analytical prediction and only for values of $\frac{\omega(y-L)}{c} > 0.50$. When $\frac{\omega(y-L)}{c} < 0.50$, the dimensionless pressure amplitudes

at position 1 increased with decreasing dimensionless frequency. For transducer position 2, the trend is the same as predicted over the entire range of dimensionless frequency, although the measured values are slightly lower than predicted.

In Figures 25 and 26 the pressure amplitudes at the discharge tube inlet are presented. These experiments were performed at a high frequency (250 cps) and a low G-level. The experimental results of Figure 24 are replotted for the purpose of comparison. In both Figures 25 and 26 pressure amplitudes for the discharge experiments are greater than those obtained in the closed bottom experiments. It can be seen in Figure 25 that the resonance peak during discharge is shifted to a higher dimensionless frequency compared with that for the no discharge situation. Correspondingly, in Figure 26 the resonance peak for the discharge case is located to the right of that for no discharge.

6.4 Total Discharge Time

In Figures 27 and 28, the experimentally measured total discharge time is compared with the low frequency prediction illustrated in Figure 9. The frequencies used were 5 and 10 cps for the measurements given in Figure 27, while in Figure 28 a much higher frequency (30 cps) was used.

There is good agreement between the prediction and the measurements only for the lower frequency cases.

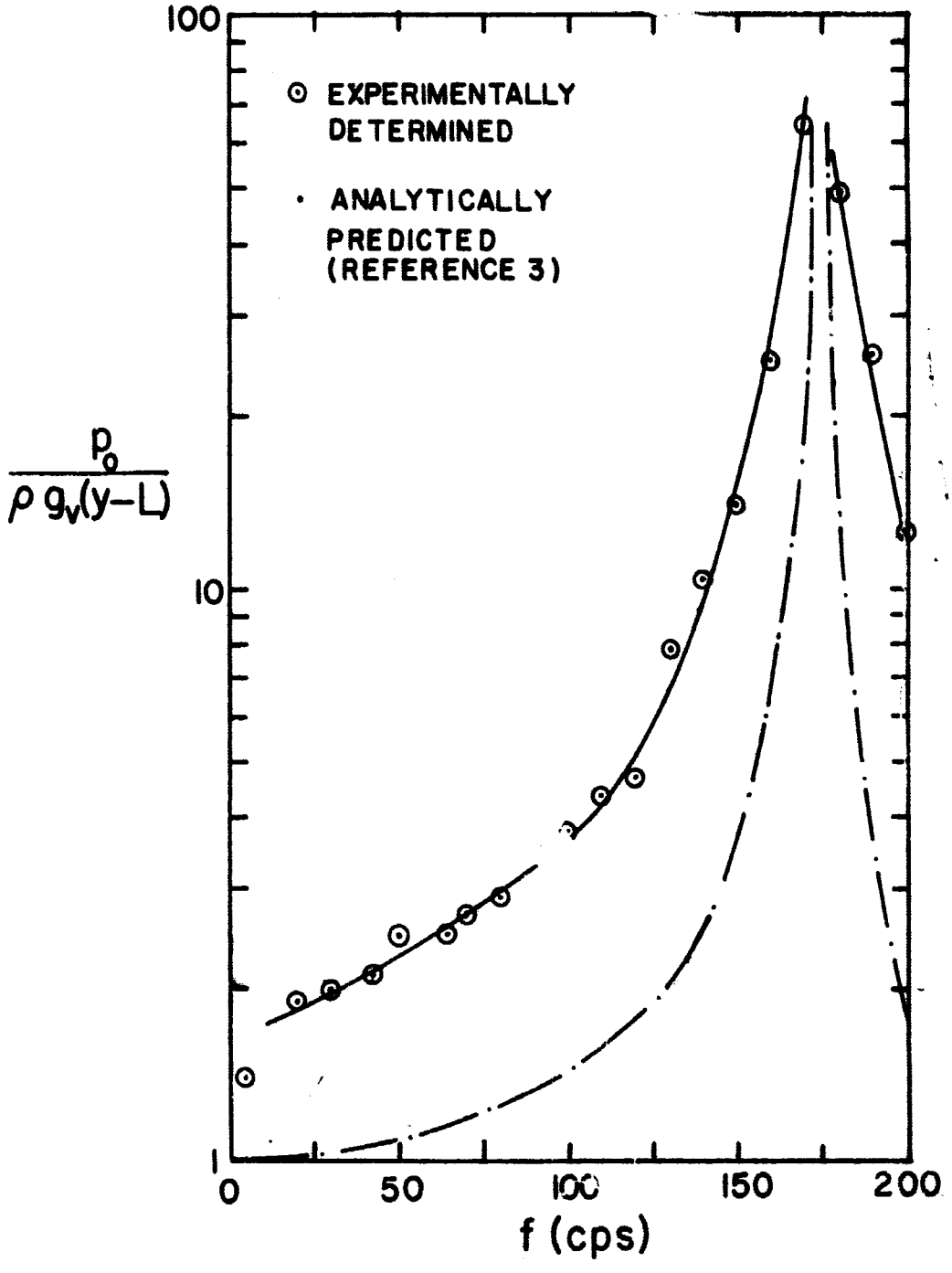

Figure 22. Comparison of Pressure Amplitude Measurements (Position 1) With Analytical Prediction

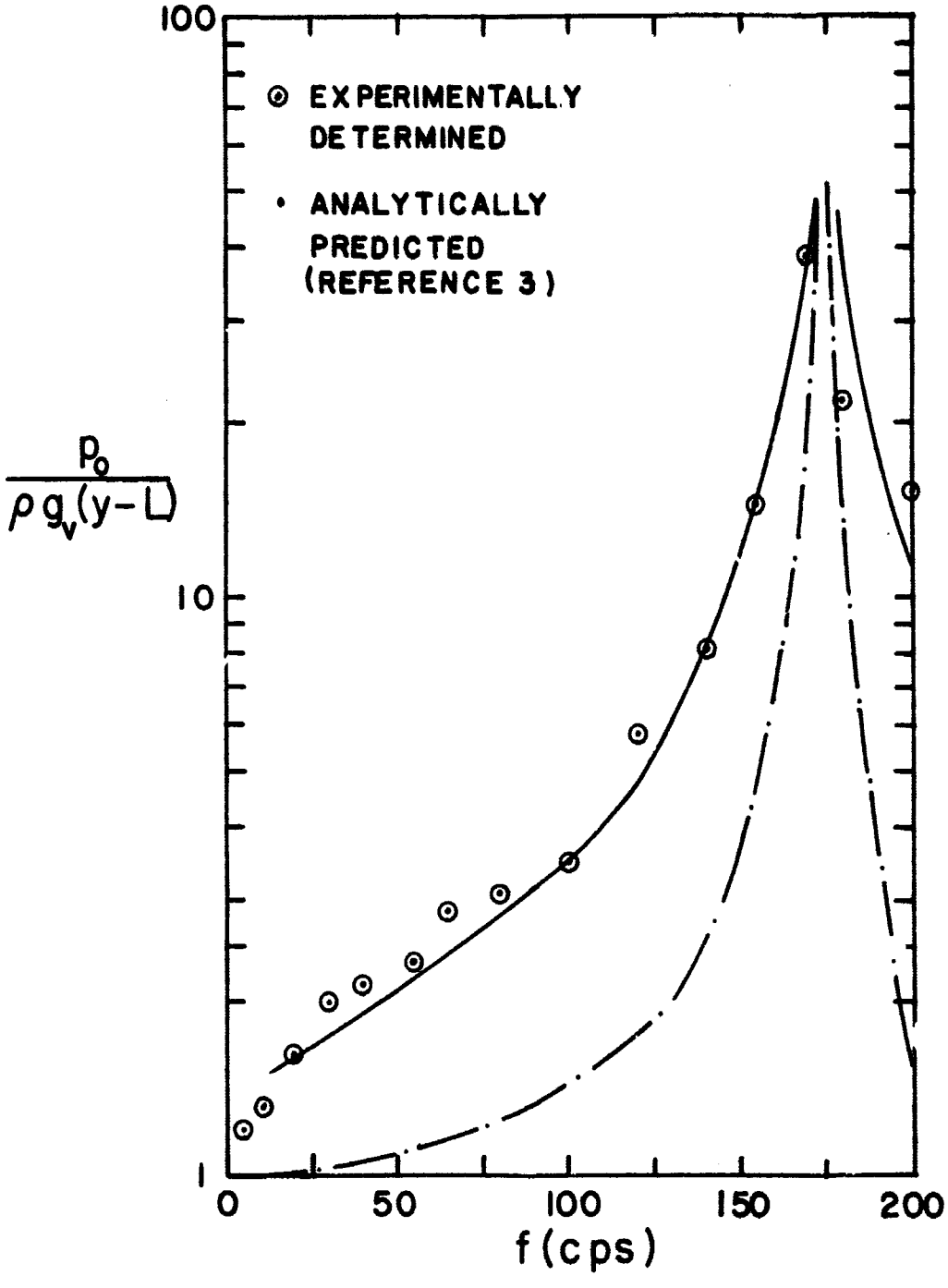

Figure 23. Comparison of Pressure Amplitude Measurements (Position 2) With Analytical Prediction

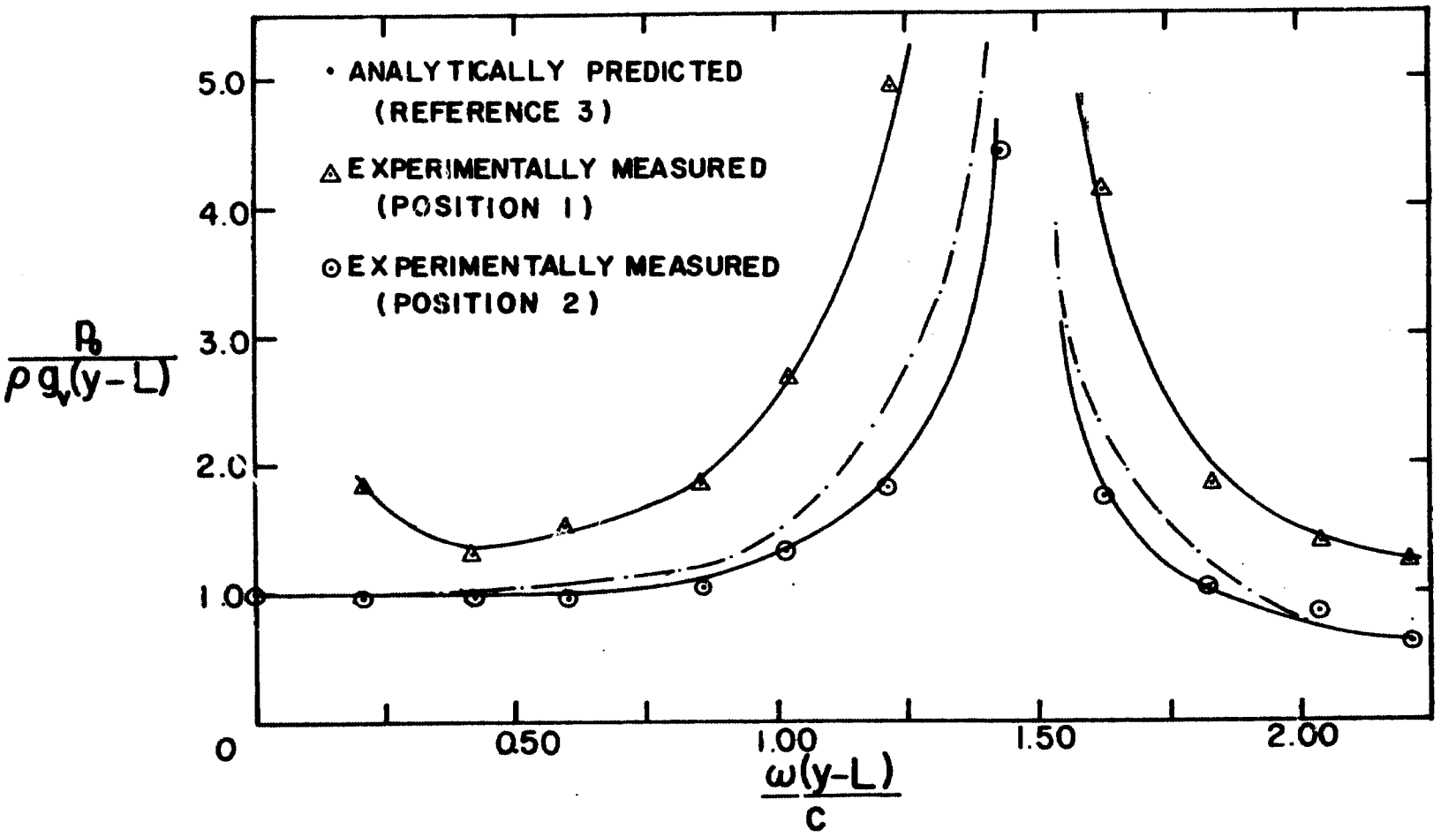

Figure 24. Comparison of Pressure Amplitude Measurements With Analytical Prediction

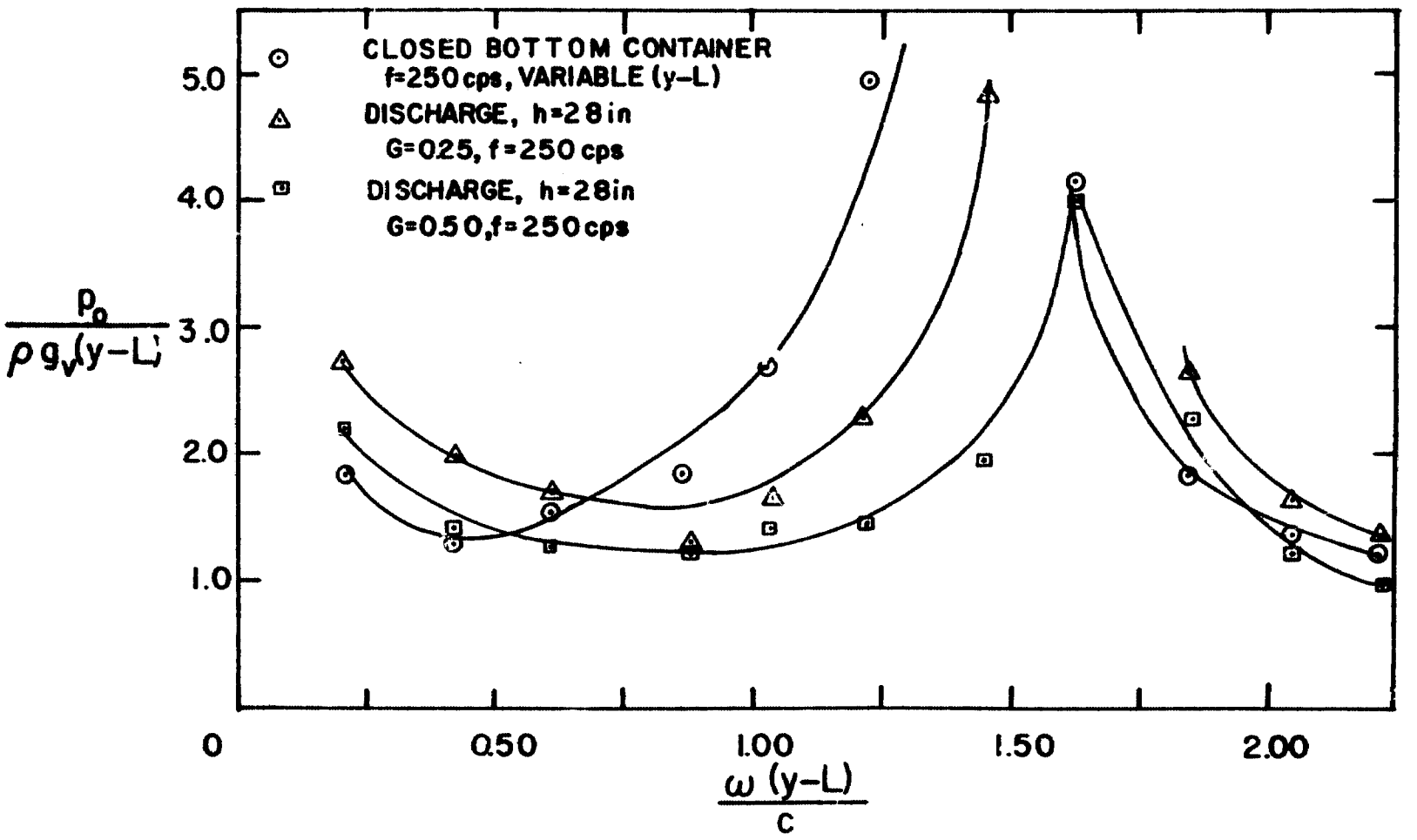

Figure 25. Measurements of Pressure Amplitudes (Position 1) For A Container With A Closed Discharge Tube and For A Discharging Container

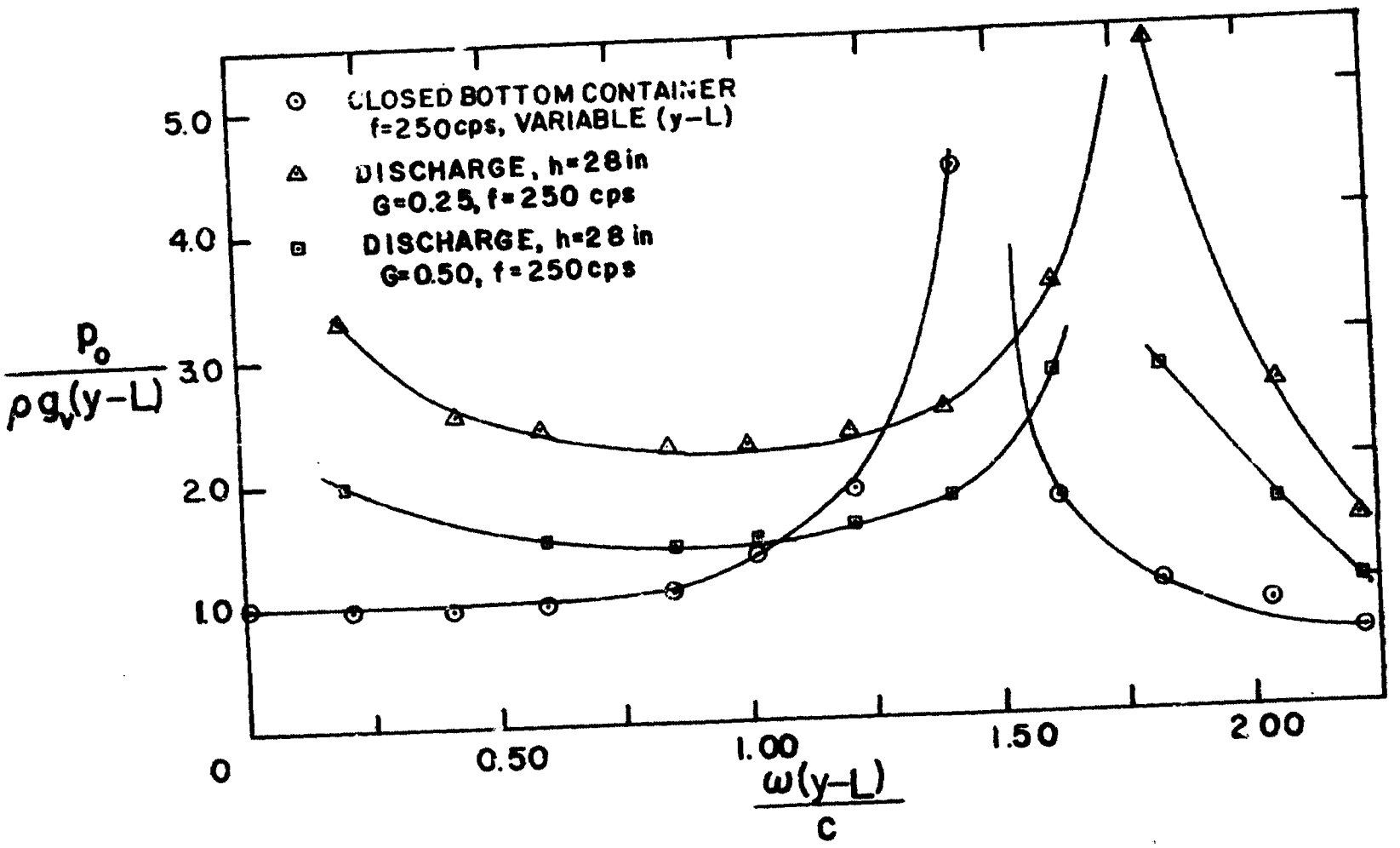

Figure 26. Measurements of Pressure Amplitude (Position 2) For A Container With A Closed Discharge Tube And For A Discharging Container

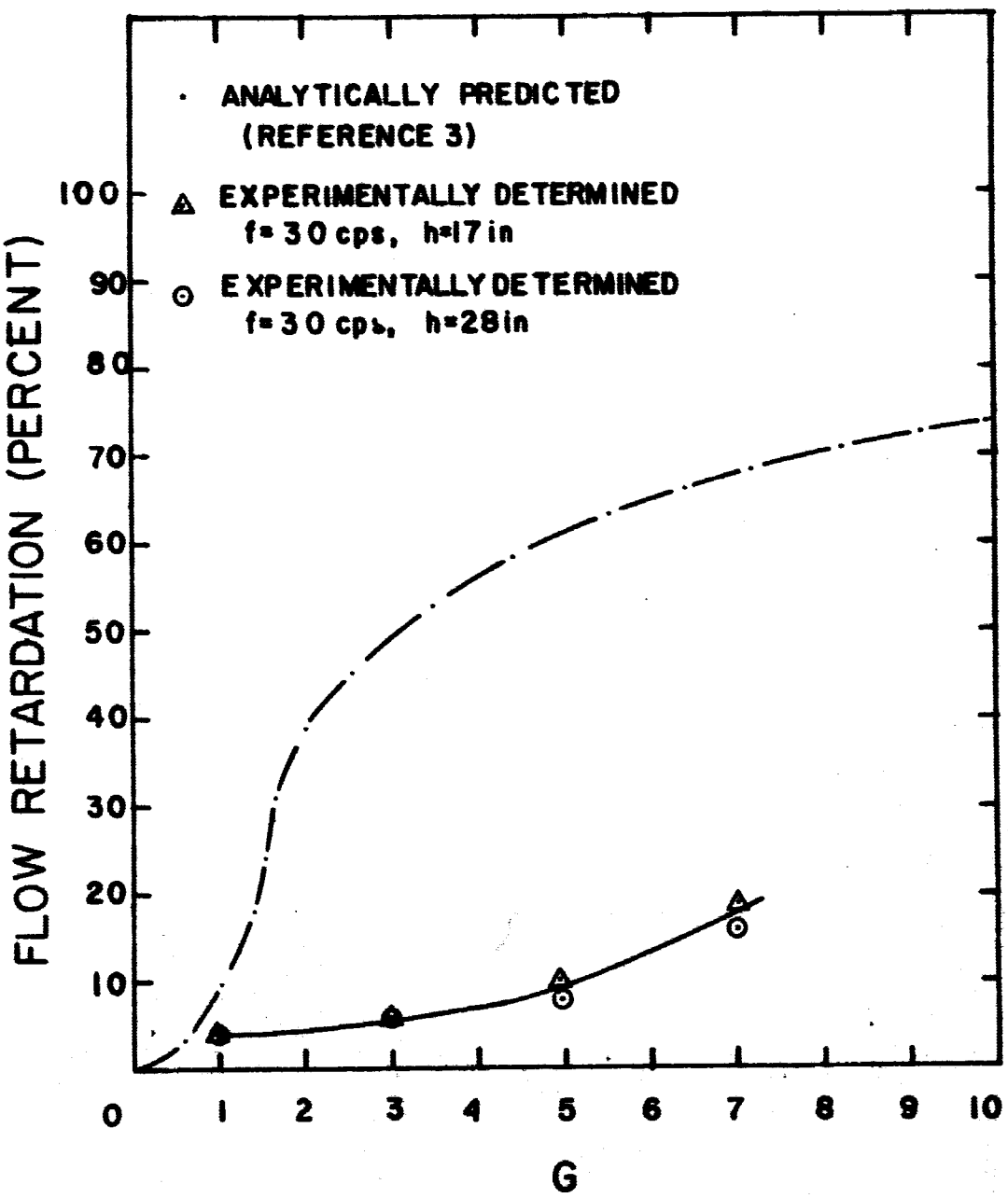

Figure 28. Comparison of Measured Flow Retardation At Higher Frequencies With Low Frequency Analytical Prediction

6.5 Time Averaged Pressure Measurements in the Discharge Tube Inlet

In this section measurements of the time averaged pressures in the discharge tube entrance (position 2) are presented as a function of time for both vibratory and non-vibratory discharge. Figures 29 through 32 illustrate the effect of increasing G-level on the time averaged pressure in the tube inlet. Figure 33 illustrates the effect of increasing frequency on the time averaged pressure. In all cases through out the discharge process the time averaged pressure in the presence of vibration is less than the corresponding pressure in the absence of vibration. For discharge at constant frequency, it can be seen that the pressure decrease becomes more pronounced as the G-level increases. For discharge at a specified G-level, the pressure decrease is attenuated by increasing frequency.

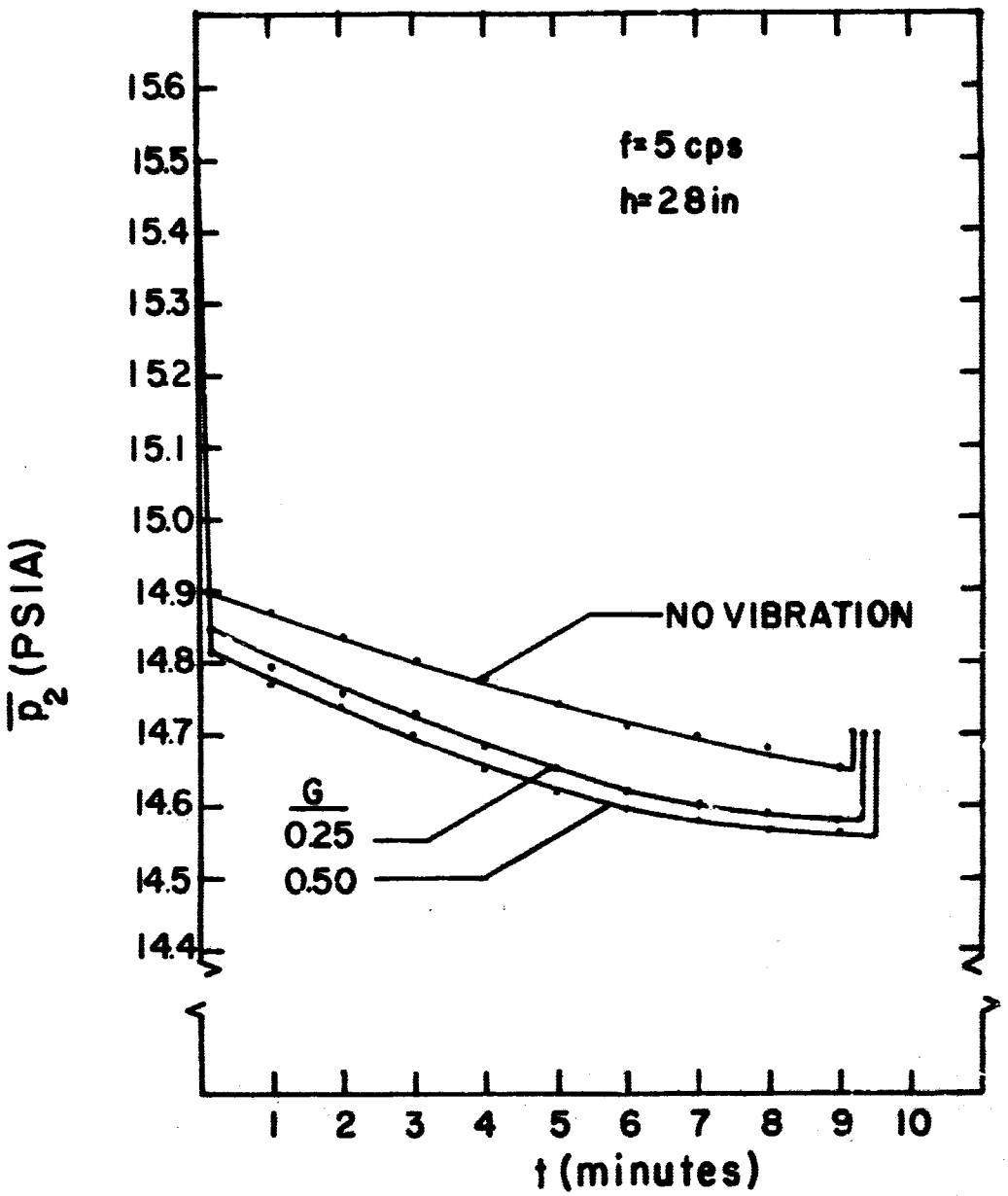

Figure 29. Variation of Time Averaged Pressure in Discharge Tube Inlet Measured During Discharge

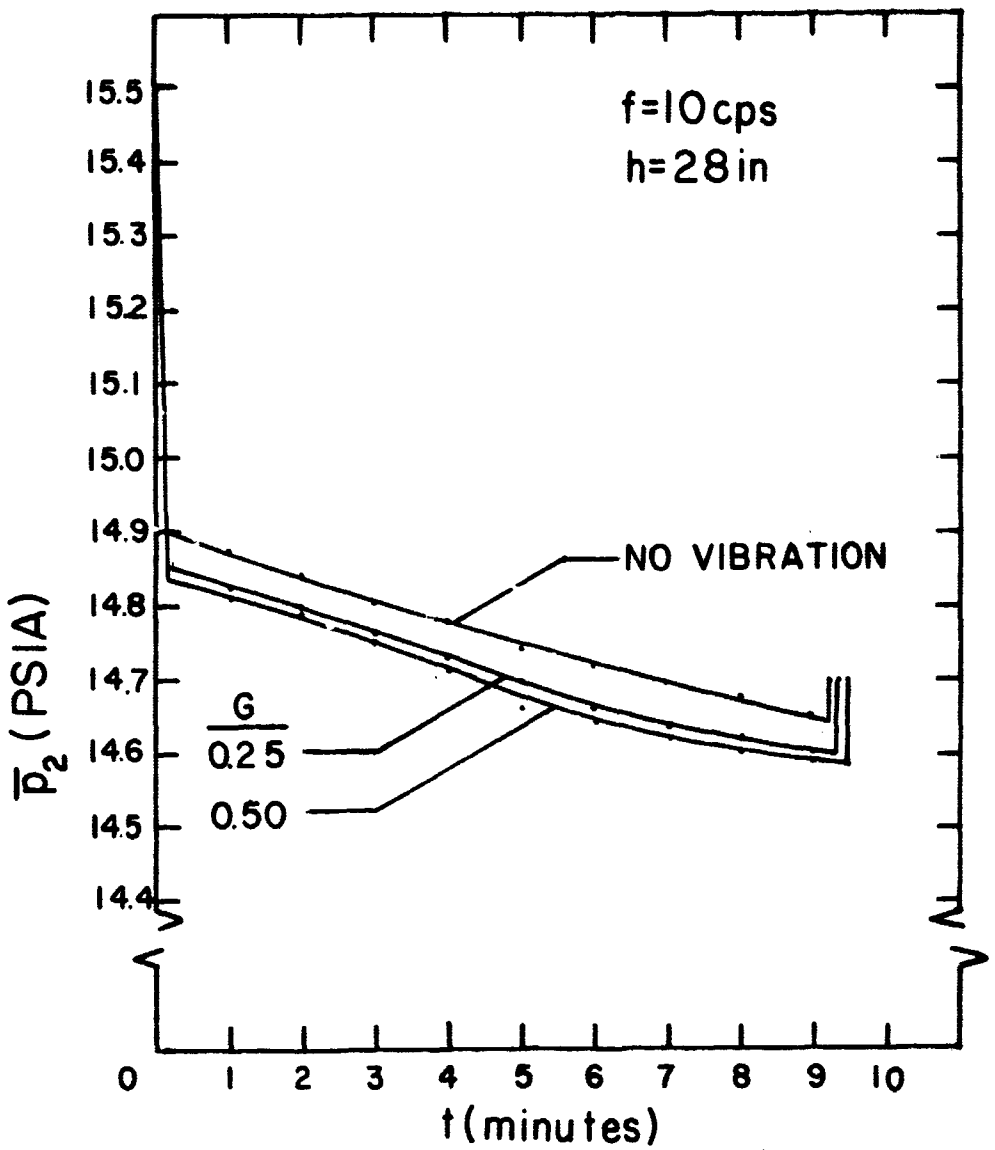

Figure 30. Variation of Time Averaged Pressure In Discharge Tube Inlet Measured During Discharge

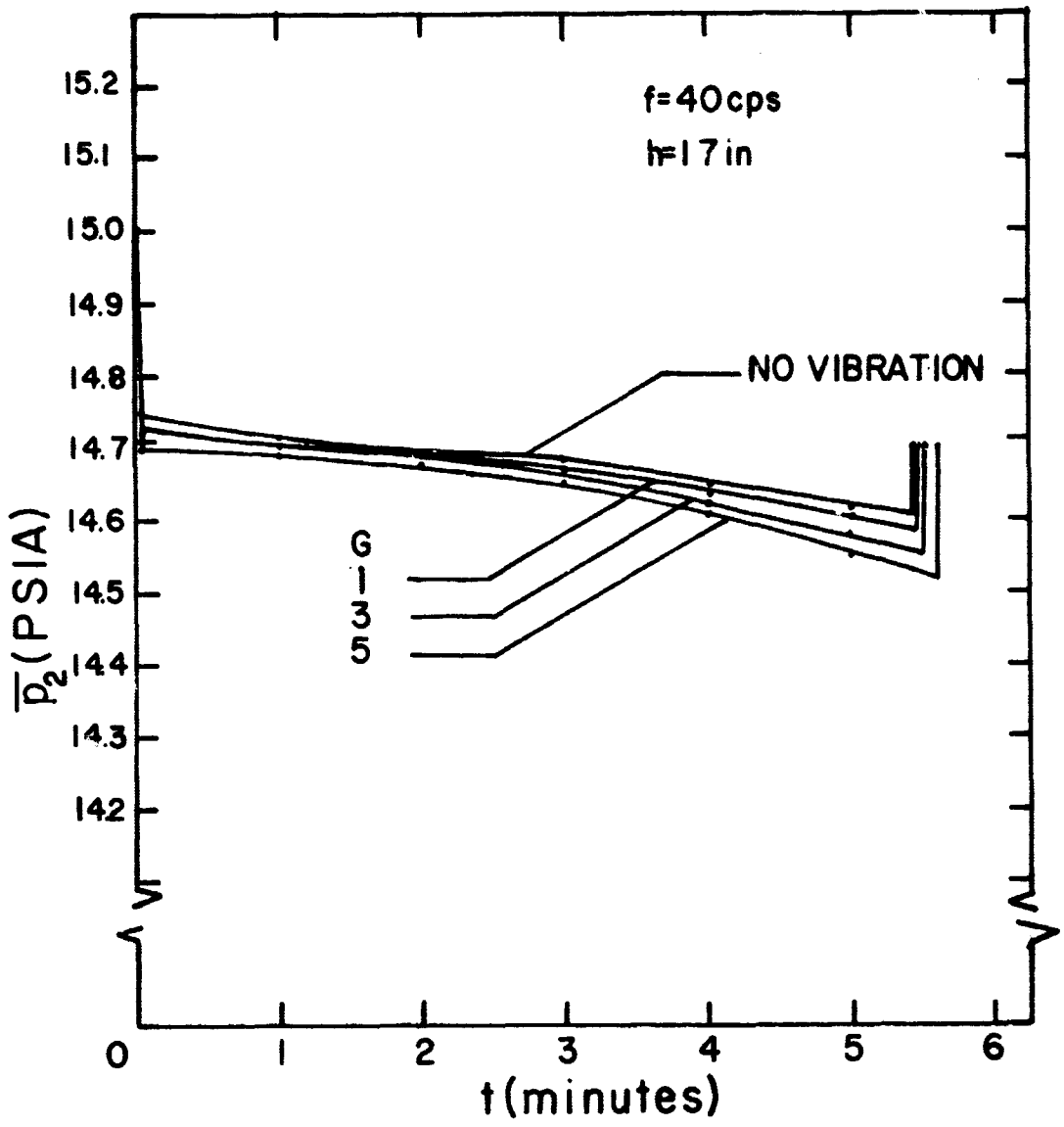

Figure 31. Variation of Time Averaged Pressure In Discharge Tube Inlet Measured During Discharge

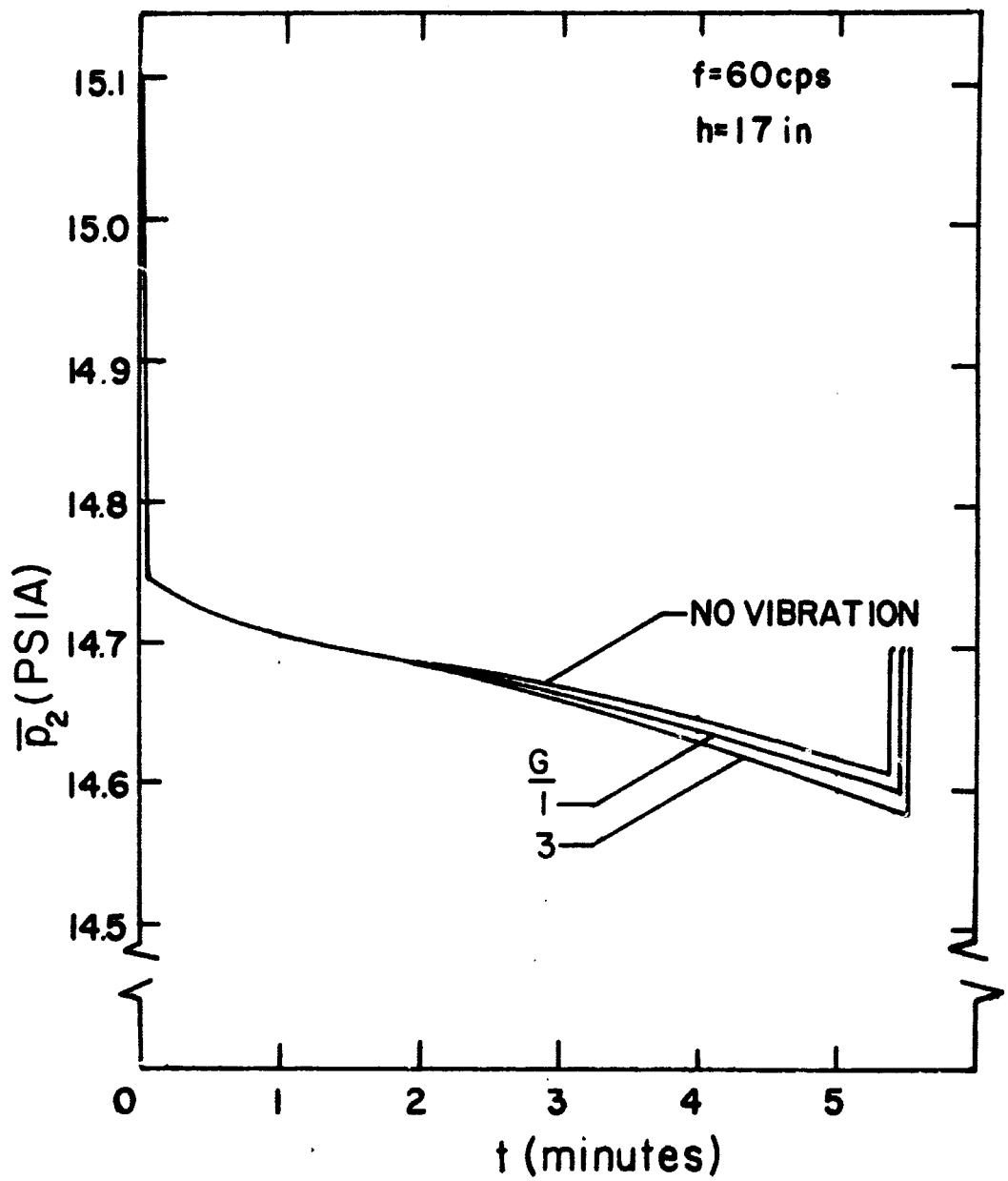

Figure 32. Variation of Time Averaged Pressure in Discharge Tube Inlet Measured During Discharge

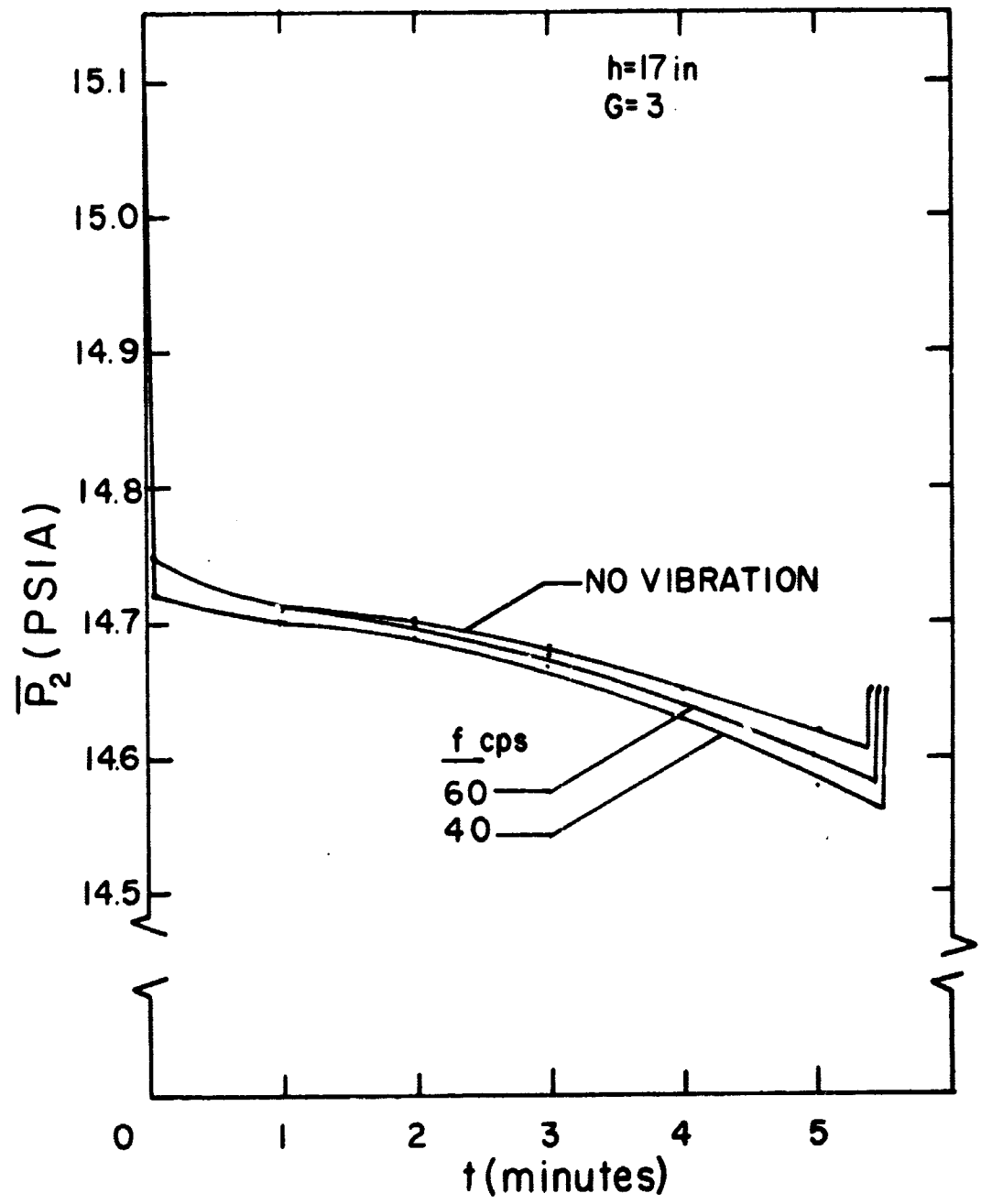

Figure 33. Variation of Time Averaged Pressure in Discharge Tube Inlet Measured During Discharge

7. CONCLUSIONS AND RECOMMENDATIONS

The discharge measurements presented in Section 6.2 agree with those given in Reference 3. The same trends were observed, a flow retardation effect which increases with increasing vibrational acceleration level and is attenuated with increasing frequency. This effect is now well established, but further experiments should be performed at high G-levels and very low frequencies.

The pressure amplitude measurements presented in Section 6.3 are in partial agreement with the analytically predicted and experimentally determined results of Reference 3, 8, 9, and 10. In Figures 22 and 23 the experimentally determined pressure amplitudes, plotted as a function of frequency, agree with the trends and orders of magnitude given by the prediction. The experimental measurements at position 2, which are illustrated in Figure 24, are in excellent agreement with the analytical prediction. The measured pressure amplitudes were only very slightly less than predicted by the exact solution. This slight deviation is understandable in view of the presence of some energy dissipation. During discharge the fluid container is open at the bottom, thus providing a direct path for pressure release. As pointed out by Schoenhals, Winter and Griggs (3),

this leads to the expectation that the pressure amplitude at the discharge tube inlet should be less than that for a container with a closed discharge tube. This, however, is not the case as can be seen in Figures 25 and 26 which show that the amplitudes measured during discharge were larger over most of the frequency range investigated. In the case of transducer position 2, the natural frequency was shifted to a higher value than the natural frequency for the closed bottom container. The natural frequency for the latter is given by the expression, $\frac{\omega(y-L)}{c} = \frac{\pi}{2}$. As the liquid level, (y-L), decreases the natural frequency increases. For position 1 the natural frequency during discharge was also shifted to the right. Figures 24, 25, and 26 indicate that the pressure amplitudes increased for small values of dimensionless frequency. The behavior suggests that there was some error involved in the measuring technique. It appeared that the error involved in the measuring technique was significant only when the liquid height was small. In Figure 7 a diagram of the discharge tube adaptor is shown. The Kistler Pressure Transducer was mounted in the positions indicated in the figure. In order to measure the pressure pulsations at the indicated positions, it was necessary for the pressure signals to travel from the pressure taps through the drilled holes in the plexiglass adaptor to the pressure transducers. Both of these holes had right angle bends connecting the vertical and horizontal sections which

were each an inch in length (Figure 7). Even when the liquid height in the discharge tank was zero, liquid still remained in the connecting holes. The behavior of the liquid in these connecting sections during vibration was not specifically studied in the present investigation. However, the experimental results indicated that its effect was negligible during the early stages of discharge. As the liquid height in the tank became small the effect of the liquid remaining in the connecting holes became significant. The liquid in the vertical section evidently caused a pressure amplitude to be measured by the transducer even when the liquid height in the tank was zero (y-L=0). At zero liquid height in the container, a pressure amplitude of 0.04 PSI was measured at position 1 when a G-level of 0.5 and a frequency of 250 cps were imposed on the test apparatus. For the same vibratory conditions a pressure amplitude of 0.05 PSI was observed at position 2. It appears, then, that the most feasible explanation for the increasing dimensionless pressure amplitude observed at low dimensionless frequencies is that the inertia of the residual liquid in the connecting holes induced an unwanted contribution to the pressure pulsations occurring at the transducer. It is recommended for future investigations that the transducers be mounted in direct contact with the fluid at the locations under study.

In Section 6.4 the results of actual vibratory discharge times are compared to those predicted by Schoenhals,

Winter, and Griggs (3). In Figure 27 results of experiments performed at low frequencies (5 and 10 cps) are presented. The experimentally determined results plotted in Figure 23 were obtained at higher frequencies (30 cps). In both the case of low frequency discharge and discharge at higher frequency, there is qualitative agreement between the experimentally determined results and the prediction. The magnitude of the flow retardation increased with increasing G-levels. For the experiments performed at low frequency (Figure 27), there is essentially no deviation between experiment and prediction. At low frequencies the fluid behaves in accordance with the model described in Section 5.2. The fluid responds in a quasi steady time varying manner; thus there is good agreement. This is not the case for the data presented in Figure 28. Here it can be seen that considerable discrepency exists between the experimental results and the prediction. This, however, is understandable because at higher frequencies the fluid does not respond in the manner for which the analysis was derived. The fluid fails to respond in a quasi steady manner because of its inertia. In order to have closer agreement between experimental results and the prediction a more accurate model must be developed, one that includes the effect of the response of the fluid to frequency. For complete verification of the low frequency analysis, more experiments at higher G-levels should be performed. Because of the limitations of the

experimental apparatus used, such experiments could not be carried out as part of this research.

The variation of the time averaged pressure in the discharge tube entrance for various vibratory conditions is presented in Section 6.5. The measurements are compared with the pressure at the same location for non-vibratory discharge. In each case the pressure measured during vibration was less than that measured for no vibration with all other conditions being the same. In the absence of a more sophisticated model the flow retardation effect can be understood, at least intuitively. The downward force acting at the top of the fluid column in the discharge tube is smaller under vibratory condtions than it is in the absence of vibration (Figures 29 through 33). This lower force would be expected to produce a smaller flow rate. This retardation was definitely observed in this investigation (Figures 12 through 21).

8. BIBLIOGRAPHY

1. Foshbaugh, R. H., and V. L. Streeter, "Resonance in Liquid Rocket Engine Systems," Journal of Basic Engineering, Transactions ASME, Series D, 1965, 87 (4); 1011-1017.

2. Abramson, Norman H., "Dynamic Behavior of Liquid in a Moving Container," Applied Mechanics Reviews, 1963, 16 (7), 501-506.

3. Schoenhals, R. J., E. R. F. Winter, and E. I. Griggs, "Effects of Longitudinal Vibration on Discharge of Liquids from Propellant Tanks," Proceedings of the 1967 Heat Transfer and Fluid Mechanics Institute, Stanford University Press.

4. Lehner, J. W., "An Analog Simulatior of Uprated Saturn I First Stage Propulsion System Dynamic Characteristics," American Astronautical Society, Proceedings of the Southeastern Symposium on Missile and Aerospace Vehicles Sciences, Vol. II, December 1966, Huntsville, Alabama, pages 88-1 to 88-12.

5. Ponder, C. A., D. H. Blount, and C. G. Fritz, "Bubble Coalesence in a Longitudinally Vibrated Liquid Column (Part I)," NASA TM-X-53180, George C. Marshal Space Flight Center, Huntsville, Alabama, December 1964.

6. Bleich, H. H., "Effect of Vibrations on the Motion of Small Gas Bubbles in a Liquid," Jet Propulsion, 1956, 26(1), 958-964.

7. Buchanan, R. N., G. Jameson, and D. Oedjoe, "Cyclic Migration of Bubbles in Vertically Vibrating Liquid Columns," Industrial and Engineering Chemistry Fundamentals, 1962, 1 (2), 82-86.

8. Kana, D. D., and F. T. Dodge, "Bubble Behavior in Liquids Contained in Vertically Vibrated Tanks," AIAA, Paper Number 66-86, presented at AIAA 3rd Aerospace Sciences Meeting, New York, New York, January 1966.

9. Schoenhals, R. J., and T. J. Overcamp, "Pressure Distributions and Bubble Formatior Induced by Longitudinal Vibration of a Flexible Liquid Filled Container," NASA TM-X-53353, George C. Marshal Space Flight Center, Huntsville, Alabama, September 1965.

10. Scheonhals, R. J. and T. J. Overcamp, "Pressure Distributions and Bubble Formation Induced by Longitudinal Vibration of a Flexible Liquid Filled Container," ASME Vol. 89, Series D, No. 4, December 1967, 737-747.

11. Baird, M. H., "Resonant Bubbles in a Vertically Vibrated Liquid Column," Canadian Journal of Chemical Engineering, 1963, 41 (2), 52-55.

12. Dodge, F. T., D. D. Kana, and N. H. Abramson, "Liquid Surface Oscillations in Longitudinally Excited Rigid Dylindrical Containers," AIAA Journal, 1965, 3 (4), 685-695.

13. Winter, E. R. F. and R. J. Schoenhals, "A Similarity Study of Gravity and Pressure Driven Discharge of Liquids from Propellant Tanks," Proceedings of the Southeastern Symposium on Missiles and Aerospace Vehicles Sciences, Vol. I, December 1966, Huntsville, Alabama, 48-1 to 48-13.

14. Tse, F. S., I. E. Morse, and R. T. Hinkle, "Mechanical Vibrations," Allyn and Bacon, Inc., Boston, 1966.

15. Daily, J. W. and D. R. F. Harleman, "Fluid Dynamics," Addison-Wesley Publishing Company, Inc., Reading, Massachusetts, 1966.

APPENDIX A

Frequency Response of Pace Transducer System

The effect of vibration on the performance of the Pace Transducer measuring system (Figures 6 and 7) is presented in the form of plots of dimensionless pressure amplitude as a function of frequency. For the results presented in Figure 34 the liquid height was maintained at a specified level, and the frequency was varied in increments. The pressure amplitude measurements were obtained at position 1. The normal length connecting tube was employed (Figure 6). The results indicate a natural frequency which is about one third of the actual value. The measurements given in Figure 35 were obtained at position 2. Again the normal length connecting tube was used. The results of Figure 35 again indicate a natural frequency of one third the actual value.

In order to ascertain whether or not the resonance curves were a characteristic of the transducer-connecting tube system, or of the transducer alone, similar experiments were performed with a longer connecting tube. These results are plotted in Figure 36. The natural frequency is again low, but for this case it is about one sixth the actual value. These results indicate that as the connecting tube length is increased, the natural frequency measured decreases.

Thus, the transducer should be in direct contact with the fluid at the point of measurement.

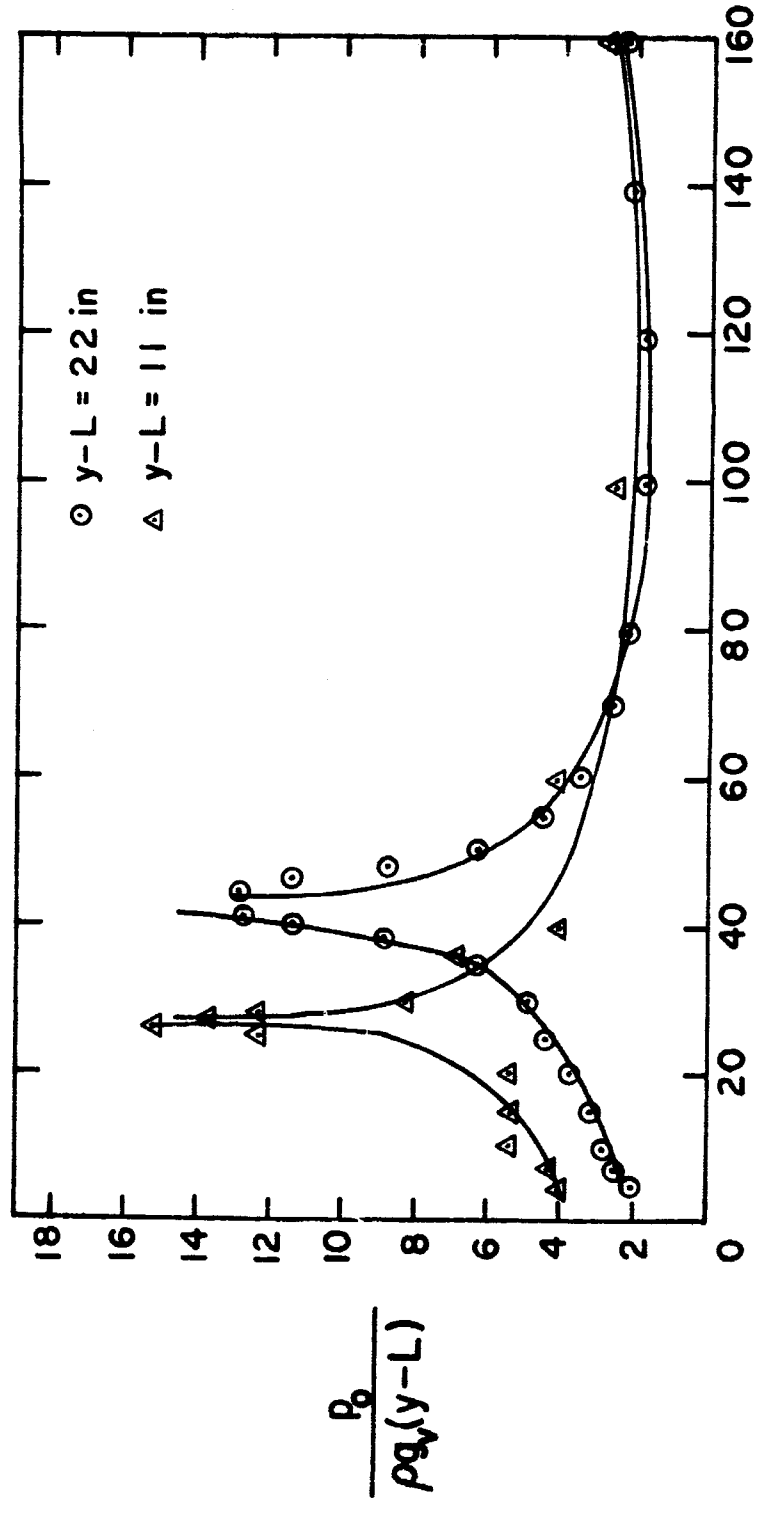

Figure 34. Measurement of Frequency Response of Pace Transducer System

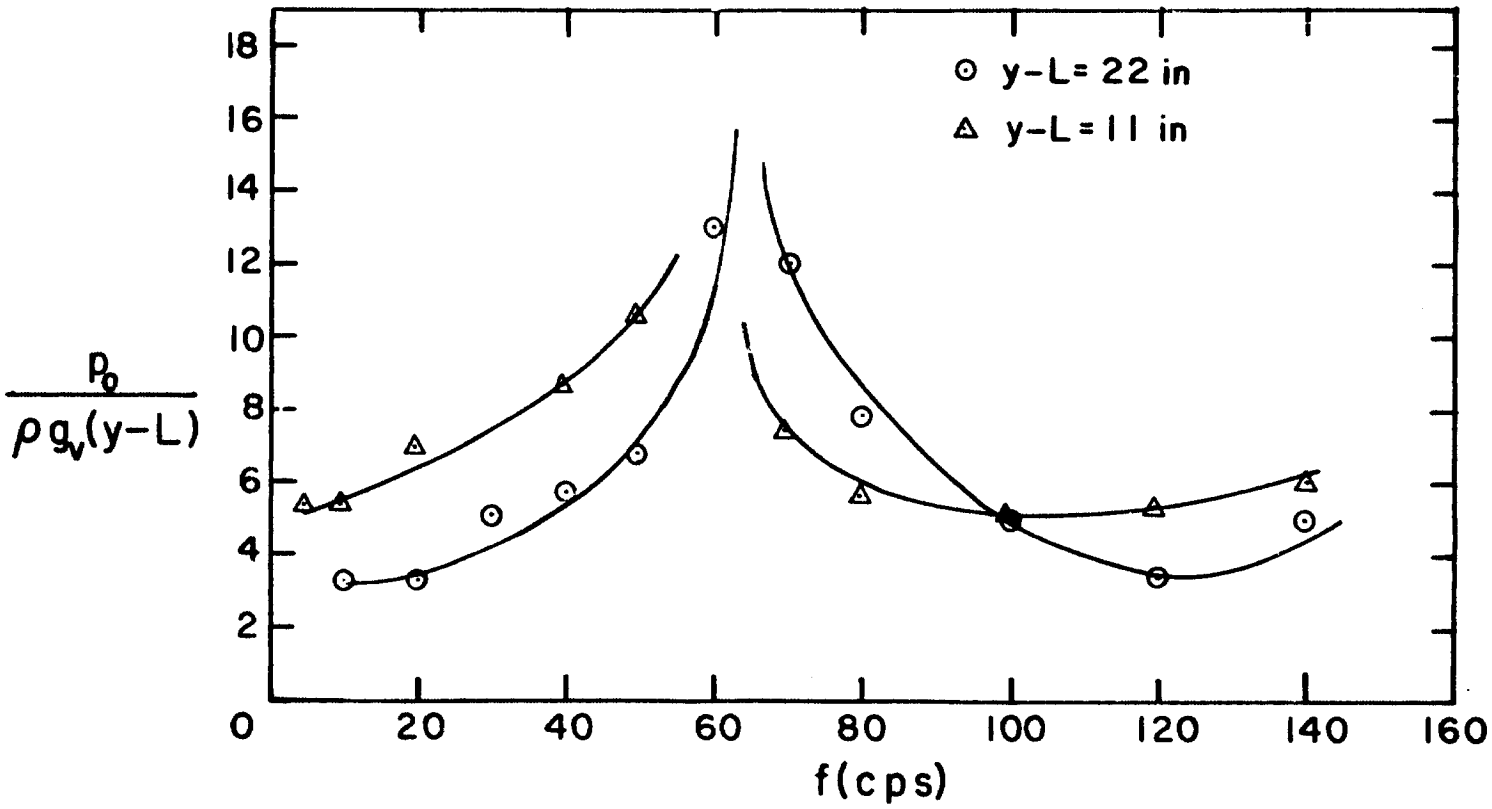

Figure 38. Measurement of Frequency Response of Pace Transducer System

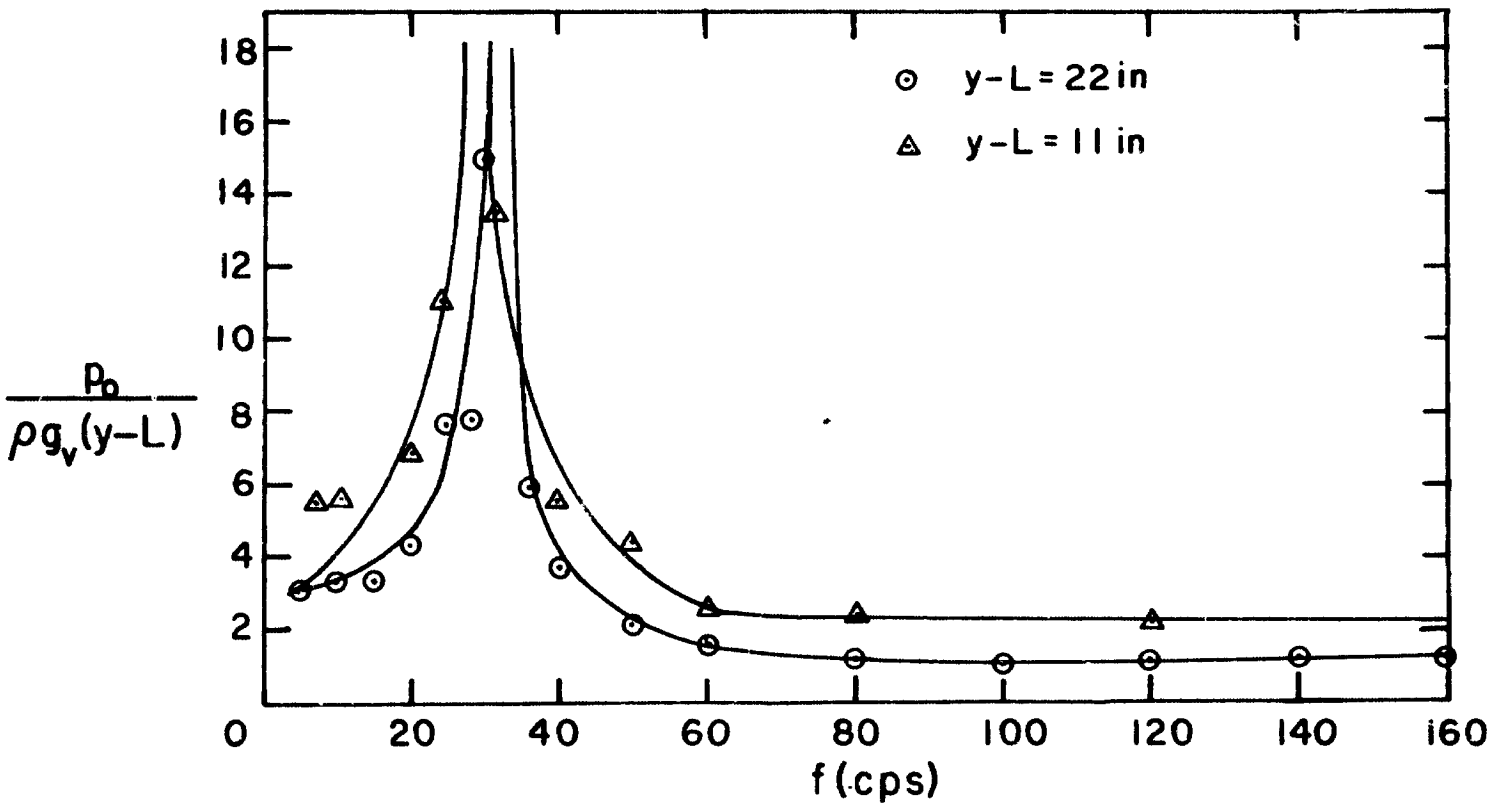

Figure 36. Measurement of Frequency Response of Pace Transducer System

APPENDIX B

Calibration of Pressure Transducers

Kistler Transducer

The Kistler Pressure Transducer was calibrated using a method suggested in the "Operating and Service Instructions" supplied with the pressure transducer and charge amplifier. The method used was essentially a dead weight method.

The transducer was mounted in a specially constructed calibration adaptor. Using this adaptor it was possible to connect the transducer to a system capable of applying pressures up to 75 PSIG. The transducer was electrically connected to the charge amplifier with a low-noise cable. The system pressure was carefully set at a specified value which was determined with a Bourdon gage. The voltage output of the charge amplifier was then measured with an oscilloscope. The results of this calibration procedure are shown in Figures 37 through 40.

Pace Transducers

The Pace Pressure Transducers used in measuring the time averaged pressure at the discharge tube inlet were calibrated using the same system as that used for the Kistler Pressure Transducer. The voltage output was

measured using an oscilloscope. These measurements are shown in Figures 41 through 44.

The Pace Transducer used in determining the height of liquid in the auxiliary tank was calibrated in a different manner. The auxiliary tank was filled with water in increments. The voltage output was recorded on a Sanborn Recorder. These results are presented in Figures 45 and 46.

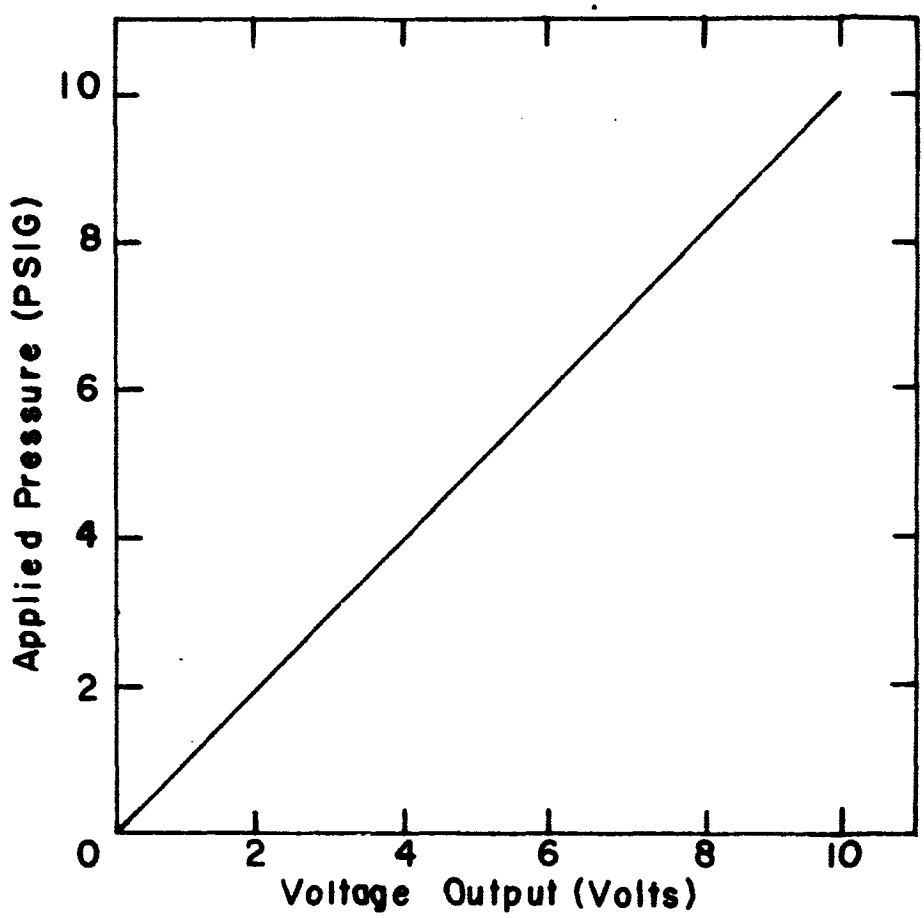

Figure 37. Calibration Curve For Kistler Pressure Transducer Charge Amplifier Range 1 PSI/VOLT

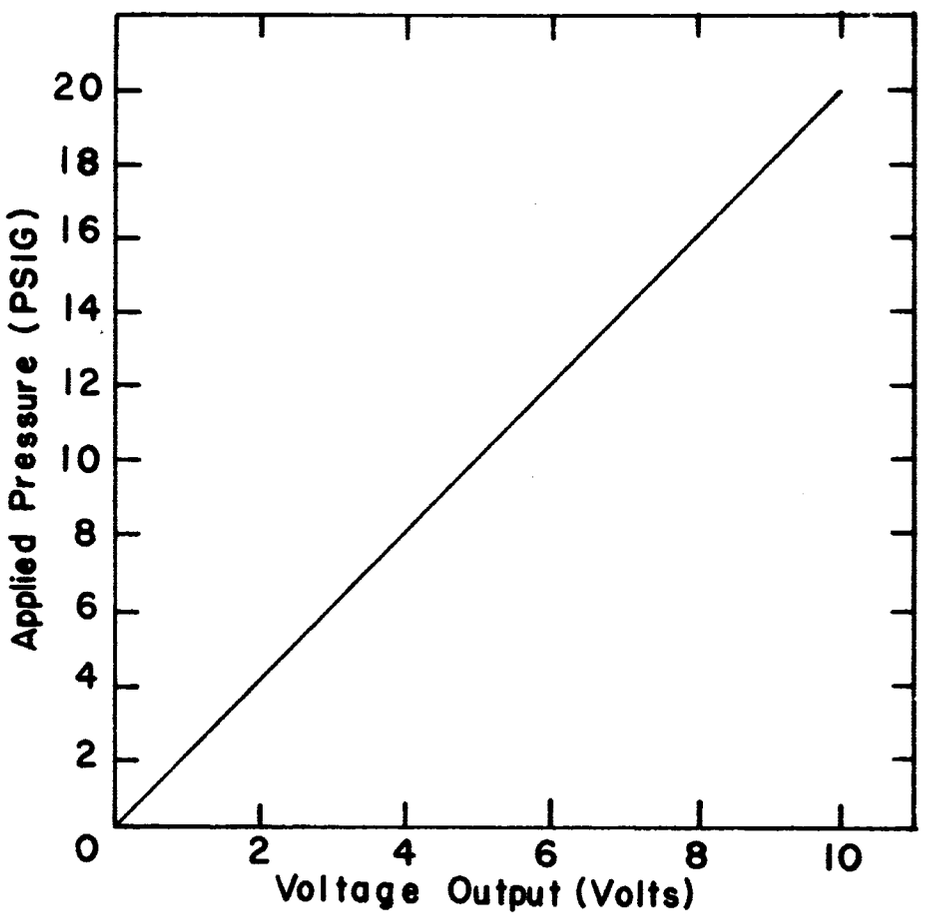

Figure 38. Calibration Curve For Kistler Pressure Transducer Charge Amplifier Range - 2 PSI/VOLT

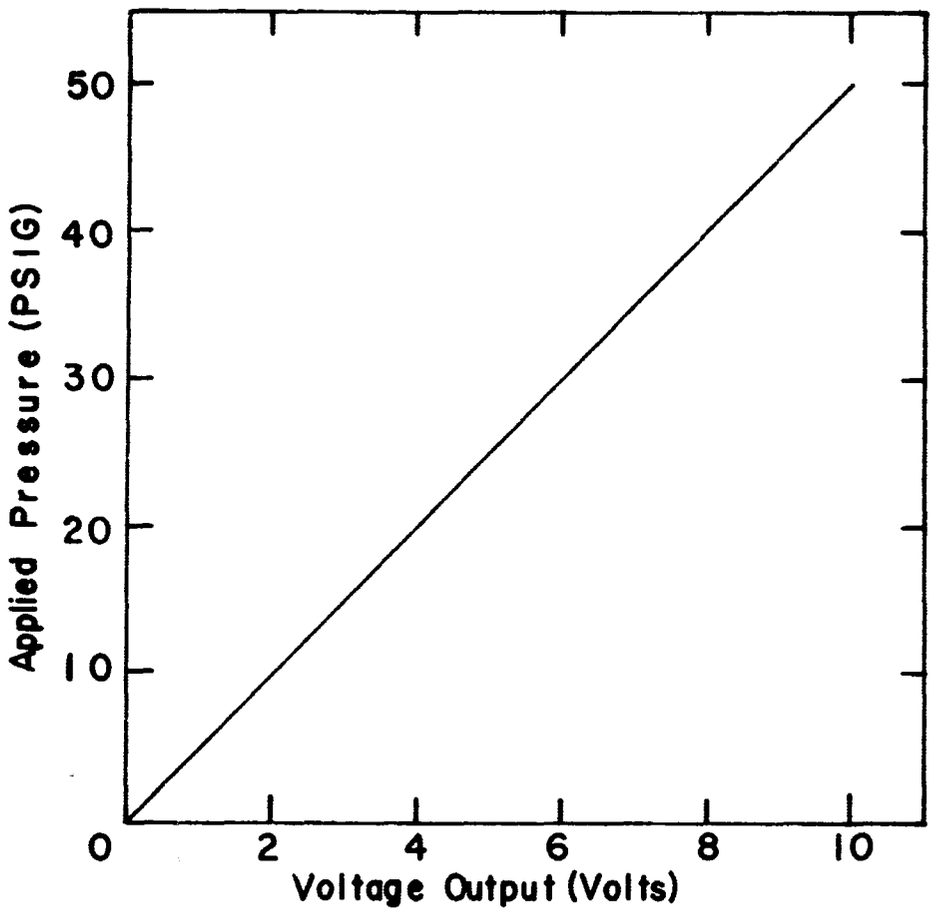

Figure 39. Calibration Curve for Kistler Pressure Transducer Charge Amplifier Range - 5 PSI/Volt

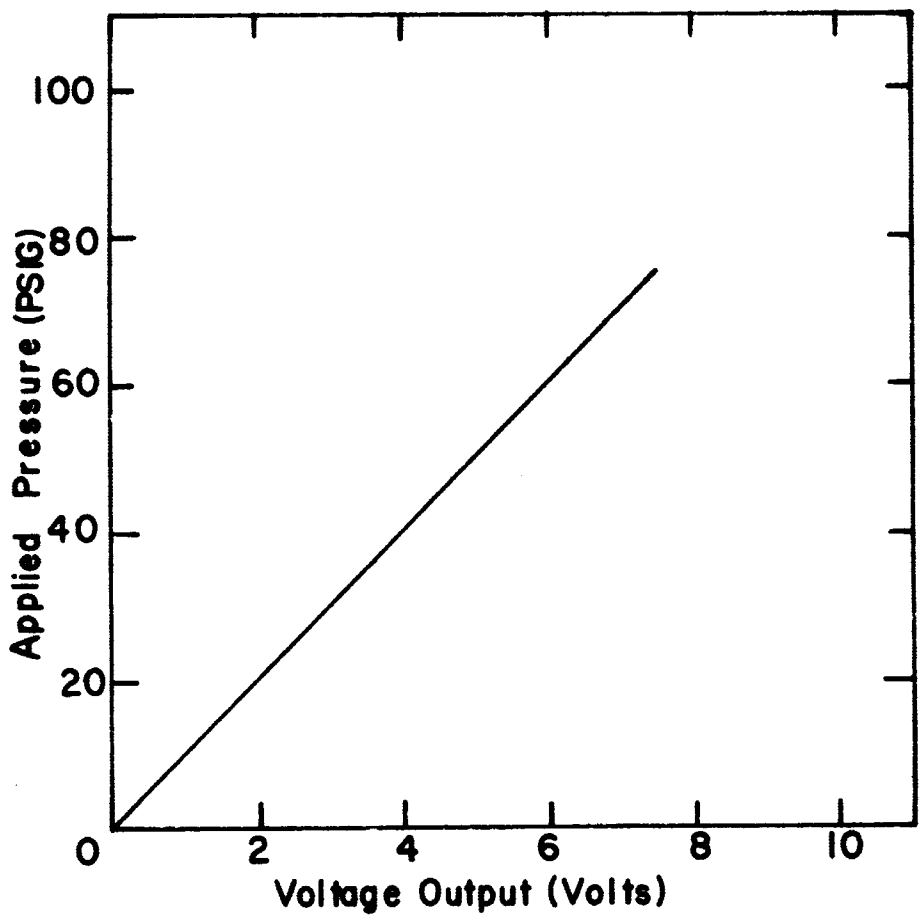

Figure 40. Calibration Curve for Kistler Transducer Charge Amplifier Range 10 PSI/Volt

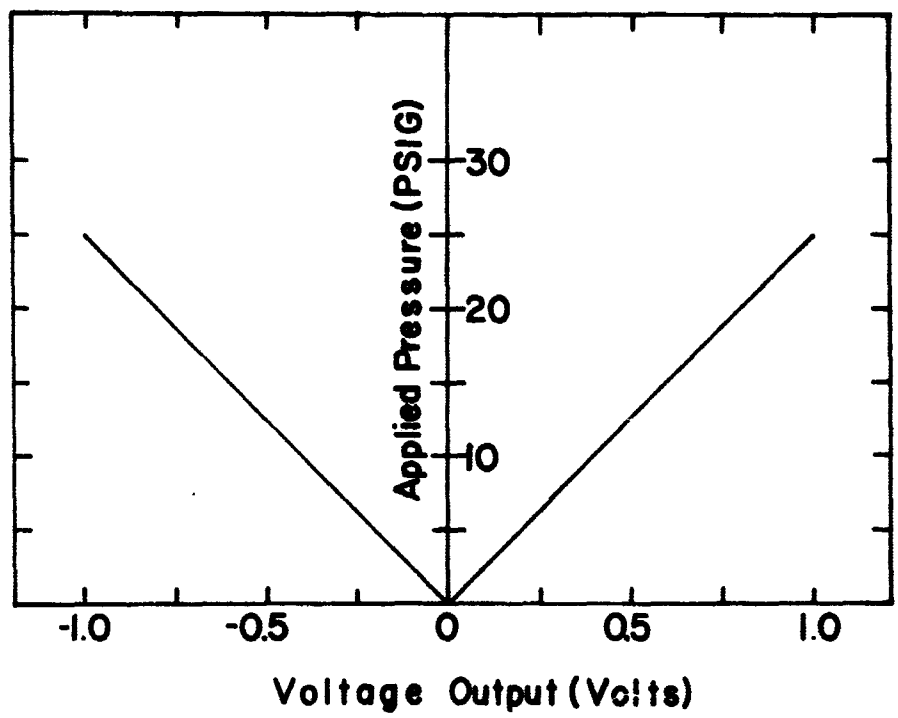

Figure 41. Calibration Curve for Pace Pressure Transducer Serial No. 20461, 25 PSI Diaphragm

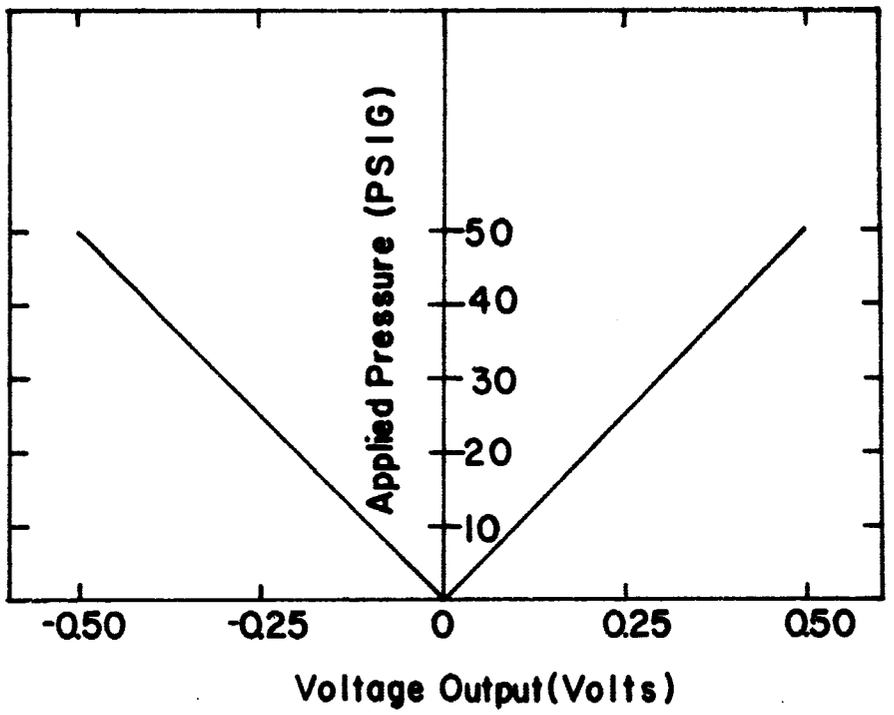

Figure 42. Calibration Curve for Pace Pressure Transducer Serial No. 20461, 50 PSI Diaphragm

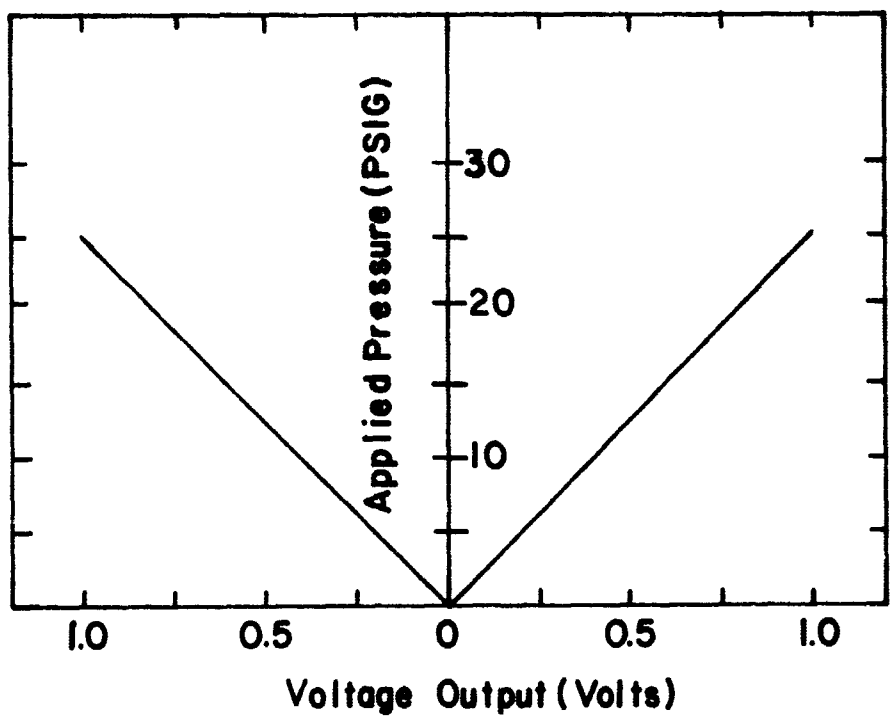

Figure 43. Calibration Curve For Pace Pressure Transducer, Serial No. 20252, 25 PSI Diaphragm

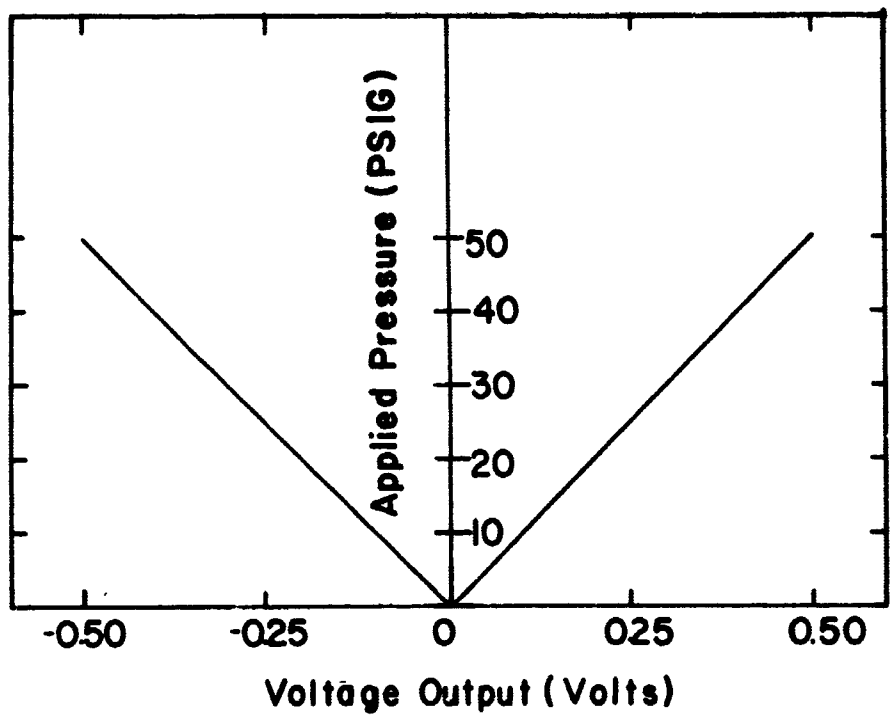

Figure 44. Calibration Curve for Pace Pressure Transducer Serial No. 20252, 50 PSI Diaphragm

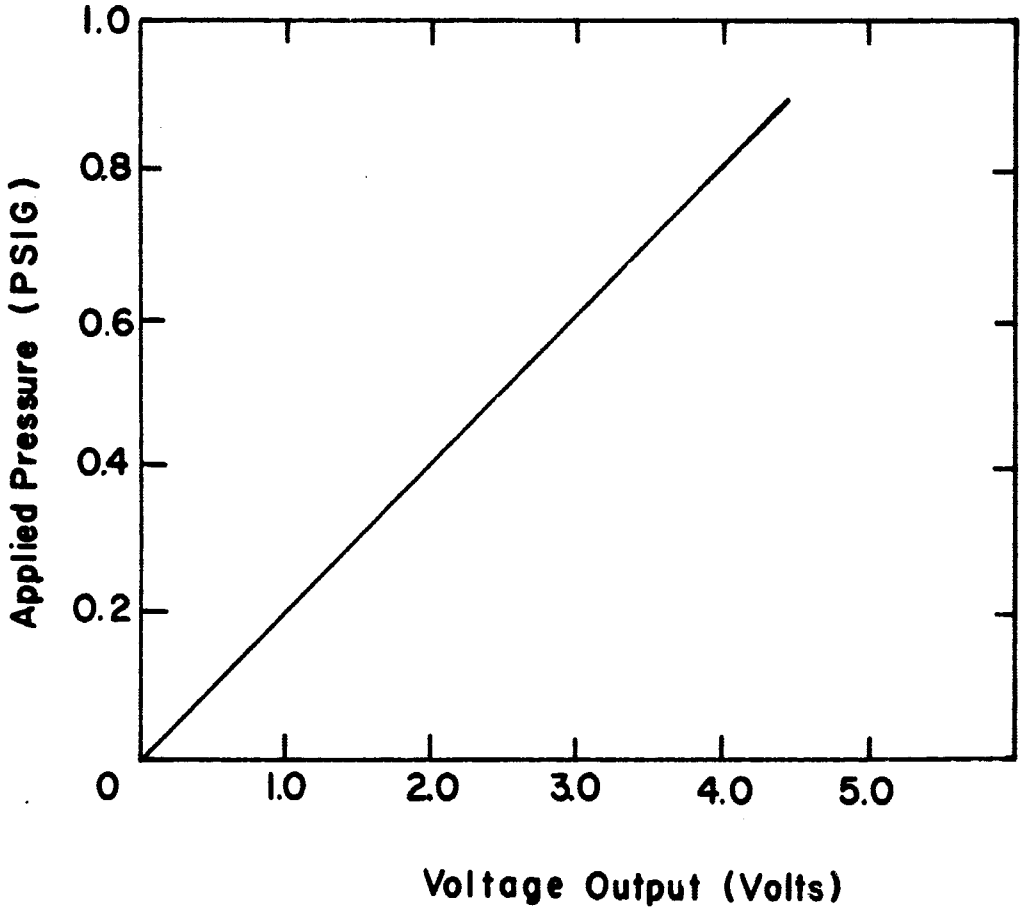

Figure 45. Calibration Curve for Pace Pressure Transducer Serial No. 20230, 1 PSI Diaphragm

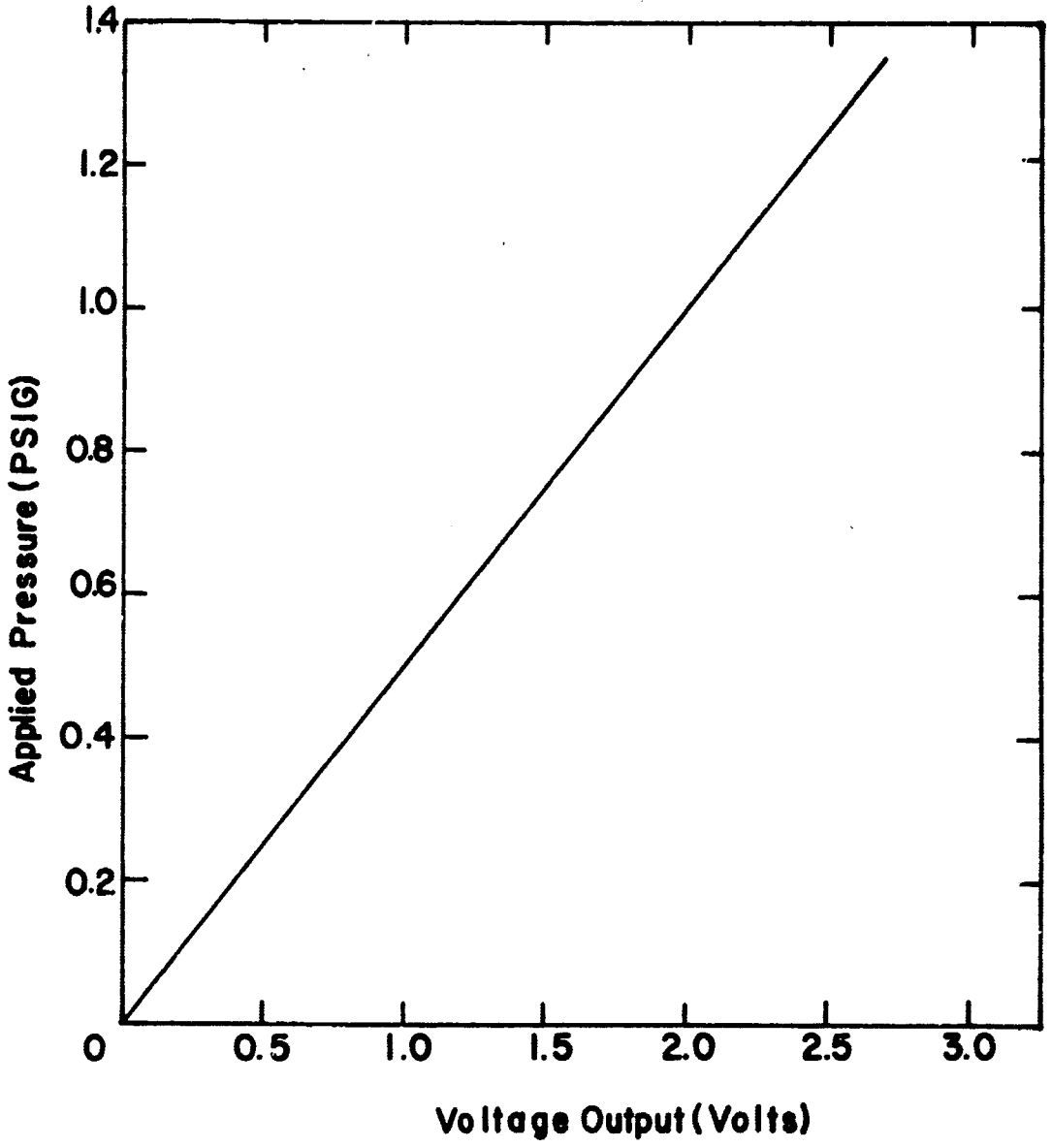

Figure 46. Calibration Curve for Pace Pressure Transducer Serial No. 20230, 10 PSI Diaphragm